

J. R. Rice, "Mathematical Analysis in the Mechanics of Fracture", Chapter 3 of Fracture: An Advanced Treatise (Vol. 2, Mathematical Fundamentals) (ed. H. Liebowitz), Academic Press, N.Y., 1968, pp. 191-311.

CHAPTER 3

MATHEMATICAL ANALYSIS IN THE MECHANICS OF FRACTURE

James R. Rice

I.	Introduction	192
II.	Preliminaries and Relevant Concepts from the Mechanics of Solids	193
	A. Stress and Strain Fields	194
	B. Elasticity	195
	C. Two-Dimensional Linear Elastic Deformation Fields	196
	D. Continuum Plasticity	200
	E. Energy Variations and Associated Methods	205
III.	Linear Elasticity in the Analysis of Deformation and Fracture	213
	A. Linear Elastic Crack Tip Stress Fields	214
	B. Some Elastic Crack Problems	218
	C. Approximate Methods for Elastic Stress Analysis of Cracks	223
	D. Energy Variations in Elastic Crack Problems	229
	E. Elastic Brittle Fracture	232
	F. Dynamic Singularities for Running Cracks	235
	G. Stress Concentrations and Energy Variations for Notches	238
IV.	Plasticity in the Analysis of Deformation and Fracture	243
	A. Small-Scale Yielding near Cracks and Notches.	243
	B. Cracks in Elastic-Plastic Antiplane Strain Fields	246
	C. Cracks in Elastic-Plastic Tensile Fields	262
	D. Elastic-Plastic Analysis of Extending Cracks and Fracture Instability	277
	E. Elastic-Plastic Strain Concentrations at Smooth-Ended Notches	288
	F. Limit Analysis of Notched Bodies	296
	G. Fracture Mechanisms in Ductile Materials	297
V.	Recommended Research	301
VI.	Summary	304
	Symbols	306
	References	308

Abstract: This chapter surveys mathematical methods and principal results in the mechanics of fracture. Primary emphasis is placed on the analysis of crack extension as treated through methods of continuum mechanics. Section II begins

with relevant concepts and basic equations from the mechanics of solids, including a survey of elasticity and plasticity, and of associated mathematical methods for boundary value problems, such as analytic function theory. Energy comparison methods and the related path-independent energy integral are introduced in this section; these novel methods of analysis prove to be widely applicable for subsequently treated notch and crack problems. Section III deals with the application of linear elasticity to fracture. Several two-dimensional crack problems are solved and approximate methods are presented for determination of stress-intensity factors with more complicated geometries. Theories of elastic-brittle fracture are reviewed and the equivalence of Griffith energy balance and cohesive forces approaches is demonstrated. In addition, dynamic running crack problems, energy rate computations, and stress concentrations at smooth-ended notches are discussed. Section IV, the longest section, deals with the elastic-plastic and fully plastic analysis of fracture. Here, the small-scale yielding approximation, for which elastic stress-intensity factors govern near tip deformation fields, is presented. Elastic-plastic crack problems in plane strain and plane stress are discussed; while these results are necessarily approximate, further insight is provided by treatment of the simpler antiplane strain case. The incremental and path-dependent nature of plastic stress-strain relations is shown to lead to a view of fracture as an instability point in a process of continuing crack advance under increasing load. Additional topics in this section include plastic strain concentrations at smooth ended notches, limit analysis of notched bodies, and a brief treatment of separation mechanisms in ductile materials.

I. Introduction

Progress in the understanding of fracture has long been inhibited by incomplete mathematical descriptions of conditions prevailing near a crack tip, particularly in ductile materials. The subject has received an increasing amount of attention from researchers in recent years, and some important advances have been made. The writer's work has centered largely on such mathematical analyses of fracture behavior, and the request by Dr. H. Liebowitz for a survey of work in this area to be included in the "Treatise on Fracture" therefore came as a particularly interesting invitation.

The plan was for a chapter describing methods of mathematical analysis and principal results in the mechanics of fracture. The presentation was to be sufficiently detailed and self-contained so that the interested reader could be introduced to the subject and learn of progress to date without extensive recourse to prior work. These guidelines have been followed in the preparation of this chapter, but it soon became apparent that a booklike length would result without some further restrictions. Thus, while mathematical methods employed are in all cases carefully introduced and derived, the presentation is, of necessity,

concise, and some familiarity with mathematical aspects of the mechanics of solids will be of assistance to the reader. The selection of topics has been influenced both by interests of the writer and by size limitations. Thus, for example, specialized methods for elastic boundary value problems, such as integral transform techniques, are not discussed, with preference given to direct analytic function theory and singular integral equation methods. The few significant results of three-dimensional analysis are simply noted without development. Also, inelastic behavior treated here is limited to time-independent plasticity, with no discussion of viscoelastic and viscoplastic behavior. A further limitation is that analyses of fracture at the dislocation and microstructural levels are given very little attention, with primary emphasis on continuum mechanics.

The chapter is divided into three main parts, the first introducing basic background material from the mechanics of solids and associated mathematical methods, the second dealing with linear elasticity in the analysis of deformation and fracture, and the third dealing with elastic-plastic and fully plastic analysis. As with most surveys, a number of results presented are original with this writing or recently obtained. This is particularly so with results based on energy comparisons and the associated path-independent energy line integral. The basic theory is outlined in Sect. II,E and applied to elastic and elastic-plastic problems of cracks and smooth-ended notches in the subsequent parts. The technique is ideally suited to problems of this type and has led to a number of exact and approximate results in nonlinear problems beyond the scope of conventional analytical methods. Another original feature is the demonstration in Sect. IV that two seemingly different approaches to the problem of elastic-plastic fracture instability are, in fact, identical.

II. Preliminaries and Relevant Concepts from the Mechanics of Solids

We begin with a brief review of concepts and basic equations from the mechanics of solids. Our concern throughout will be primarily with infinitesimal deformation, with time-independent stress-strain behavior, as in elasticity and plasticity, and with relevant mathematical methods. No claim of completeness is made. Rather, the selection of topics is dictated by needs of later sections on the analysis of models and configurations of interest in the mechanics of fracture. The first few subsections deal with relatively standard material in elasticity and plasticity including general theorems, stress-strain relations, formulations for two-dimensional problems, and analytic function theory. The last

subsection treats energy comparisons for bodies containing notches of neighboring sizes. Here, much of the material is original, and resulting methods are widely used for the treatment of strain-concentration problems in Sects. III and IV. The Cartesian tensor notation and, occasionally, a vectorialdyadic notation, is employed.

A. STRESS AND STRAIN FIELDS

Let σ_{ij} denote components of the stress tensor referred to a set of Cartesian coordinate axes x_1, x_2 , and x_3 . Then, the equations of motion (or equilibrium) are

$$\frac{\partial \sigma_{ij}}{\partial x_j} + F_i = \rho \frac{\partial^2 u_i}{\partial t^2} \quad \text{and} \quad \sigma_{ij} = \sigma_{ji} \quad (1)$$

where F_i is the body force per unit volume, u_i the displacement, and ρ the mass density. The components T_i of force per unit area acting on a plane with normal n_i are

$$T_i = \sigma_{ij} n_j \quad (2)$$

Strain ϵ_{ij} and rotation ω_{ij} components are defined in terms of displacement gradients by

$$\epsilon_{ij} = \frac{1}{2} \left(\frac{\partial u_i}{\partial x_j} + \frac{\partial u_j}{\partial x_i} \right), \quad \omega_{ij} = \frac{1}{2} \left(\frac{\partial u_i}{\partial x_j} - \frac{\partial u_j}{\partial x_i} \right) \quad (3)$$

or by other appropriate measures in cases of finite deformation (Green and Zerna, 1954). Compatibility equations

$$\frac{\partial^2 \epsilon_{ij}}{\partial x_k \partial x_l} + \frac{\partial^2 \epsilon_{kl}}{\partial x_i \partial x_j} = \frac{\partial^2 \epsilon_{ik}}{\partial x_j \partial x_l} + \frac{\partial^2 \epsilon_{jl}}{\partial x_i \partial x_k} \quad (4)$$

assure that a strain field is derivable from displacements.

The principle of virtual work provides a concise and useful statement of the equations of equilibrium and compatibility. Let σ_{ij} be any stress field in a region V in equilibrium with body forces F_i and surface forces T_i on the boundary S of V . Let u_i be any continuous and differentiable displacement field with ϵ_{ij} the associated strain field. Then, the virtual work statement

$$\int_V (\sigma_{ij} \epsilon_{ij} - F_i u_i) dV = \int_S T_i u_i dS \quad (5)$$

follows from the Green-Gauss theorem with the equilibrium and strain-displacement equations. Conversely, given the strain-displacement

equations, virtual work implies equilibrium; given the equilibrium equations, virtual work implies the strain-displacement equations.

B. ELASTICITY

We define an elastic material as one for which a strain energy density $W = W(\epsilon_{mn})$ exists as a single-valued function in strain space, where

$$W = W(\epsilon_{mn}) = \int_0^{\epsilon_{mn}} \sigma_{ij} d\epsilon_{ij} \quad (6)$$

Thus, when all strain components may be varied independently, elastic stress-strain relations are given by

$$\sigma_{ij} = \partial W / \partial \epsilon_{ij} \quad (7)$$

Linear stress-strain relations take the form

$$\sigma_{ij} = C_{ijkl} \epsilon_{kl} \quad (8)$$

where $C_{ijkl} = C_{jikl} = C_{ijlk} = C_{jilk}$ in view of symmetry of the stress tensor, and $C_{ijkl} = C_{klij}$ in view of the existence of a strain energy density. This reduces the number of independent elastic constants to 21. Symmetry considerations further reduce the number; three result for a cubic crystal and two for an isotropic solid. In the latter case,

$$\sigma_{ij} = 2G \left(\epsilon_{ij} + \frac{\nu}{1-2\nu} \delta_{ij} \epsilon_{kk} \right) \quad (9)$$

where G is the shear modulus, ν the Poisson ratio, and $E = 2(1 + \nu)G$ where E is Young's modulus.

The potential energy P of an elastic body is defined by

$$P = \int_V [W(\epsilon_{mn}) - F_i u_i] dV - \int_{S_T} T_i u_i dS \quad (10)$$

where S_T is that portion of the boundary over which tractions are prescribed. With F_i and T_i regarded as given, it is a functional of the displacement field. Presuming the elastic material of the body to exhibit stability in the small (Drucker, 1964),

$$d\sigma_{ij} d\epsilon_{ij} > 0 \quad (11)$$

for any set of strain increments and corresponding stress increments, the equilibrium displacement field minimizes the potential energy on

the class of all displacement fields satisfying prescribed displacement boundary conditions (if any) on $S - S_T$. The proof is straightforward from virtual work: let u_i^t be the true displacement field and u_i^* any kinematically admissible field. Then

$$\begin{aligned} P^* - P^t &= \int_V [W(\epsilon_{mn}^*) - W(\epsilon_{mn}^t) - F_i(u_i^* - u_i^t)] dV - \int_S T_i(u_i^* - u_i^t) dS \\ &= \int_V [\sigma_{ij}^t(\epsilon_{ij}^t - \epsilon_{ij}^*) - W(\epsilon_{mn}^t) + W(\epsilon_{mn}^*)] dV \\ &= \int_V \int_{\epsilon_{mn}^*}^{\epsilon_{mn}^t} (\sigma_{ij}^t - \sigma_{ij}) d\epsilon_{ij} dV \geq 0 \end{aligned} \quad (12)$$

The inequality of the last line, which completes the proof, follows from stability in the small and path independence. For, when the inner integral is carried over a path in strain space corresponding to a straight-line path in stress space from σ_{ij}^* to σ_{ij}^t , $d\sigma_{ij}$ has the direction of $\sigma_{ij}^t - \sigma_{ij}^*$. Uniqueness of solutions follows readily; if $P^* = P^t$, the inequality of Eq. (12) and stability in the small imply $\epsilon_{ij}^* = \epsilon_{ij}^t$.

C. TWO-DIMENSIONAL LINEAR ELASTIC DEFORMATION FIELDS

We consider here cases where all components of stress and strain depend on two Cartesian coordinates x_1 and x_2 . Further, attention is restricted to linear, homogeneous, and isotropic elastic materials.

1. *Antiplane Strain*

Assume $u_1 = u_2 = 0$ and $u_3 = u_3(x_1, x_2)$. Then only the stresses σ_{31} , σ_{32} and strains

$$\epsilon_{31} = \frac{1}{2} \frac{\partial u_3}{\partial x_1}, \quad \epsilon_{32} = \frac{1}{2} \frac{\partial u_3}{\partial x_2} \quad (13)$$

are nonzero. The relevant equilibrium equation is

$$\frac{\partial \sigma_{31}}{\partial x_1} + \frac{\partial \sigma_{32}}{\partial x_2} = 0 \quad (14)$$

and stress-strain relations are $\sigma_{3i} = 2G\epsilon_{3i}$ ($i = 1, 2$). Thus, u_3 is harmonic, $\nabla^2 u_3 = 0$. Harmonic functions of x_1 and x_2 may be represented as the real or imaginary part of an analytic function of $z = x_1 + ix_2$:

$$u_3 = G^{-1} \text{Im} [\omega(z)] \quad (15)$$

where $\omega(z)$ is analytic, as are its integrals and derivatives (Churchill, 1960). Stresses are thus representable as

$$\sigma_{32} + i\sigma_{31} = \omega'(z) \tag{16}$$

More general forms result when u_1 and u_2 are prescribed functions of x_1 and x_2 as in torsion (Sokolnikoff, 1956).

2. *Plane Strain and Generalized Plane Stress*

Assume $u_3 = 0$ and $u_1 = u_1(x_1, x_2)$, $u_2 = u_2(x_1, x_2)$. This deformation state is called plane strain, in that $\epsilon_{3i} = 0$. The equilibrium and compatibility equations reduce to

$$\begin{aligned} \frac{\partial \sigma_{ij}}{\partial x_j} &= 0 \quad (i, j = 1, 2) \\ 2 \frac{\partial^2 \epsilon_{12}}{\partial x_1 \partial x_2} &= \frac{\partial^2 \epsilon_{11}}{\partial x_2^2} + \frac{\partial^2 \epsilon_{22}}{\partial x_1^2} \end{aligned} \tag{17}$$

Equilibrium is satisfied by writing stress components in terms of the Airy stress function $U = U(x_1, x_2)$:

$$\sigma_{ij} = -\frac{\partial^2 U}{\partial x_i \partial x_j} + \delta_{ij} \nabla^2 U \quad (i, j = 1, 2) \tag{18}$$

Writing strains in terms of stresses, as appropriate for the case $\epsilon_{3i} = 0$, for satisfaction of compatibility U is biharmonic:

$$\nabla^2 \nabla^2 U = 0 \tag{19}$$

The same equations result for generalized plane stressing of thin sheets, provided one interprets σ_{ij} and ϵ_{ij} as through-the-thickness averages and assumes σ_{33} to have a negligible thickness average (Green and Zerna, 1954). Biharmonic functions are also expressible in terms of analytic functions,

$$U = \text{Re}[\bar{z}\phi(z) + \int \psi(z) dz] \tag{20}$$

where $\phi(z)$ and $\psi(z)$ are analytic and a bar denotes the complex conjugate. Stresses are then expressible as

$$\begin{aligned} \sigma_{11} + \sigma_{22} &= 4 \text{Re}[\phi'(z)] \\ \sigma_{22} - \sigma_{11} + 2i\sigma_{12} &= 2[\bar{z}\phi''(z) + \psi'(z)] \end{aligned} \tag{21}$$

Plane strain, $\sigma_{33} = \nu(\sigma_{11} + \sigma_{22})$, and plane stress, $\sigma_{33} = 0$, and resulting displacements are

$$u_1 + iu_2 = \frac{1}{2G} [\kappa\phi(z) - \overline{z\phi'(z)} - \overline{\psi(z)}] \quad (22)$$

$$\kappa = 3 - 4\nu, \quad \text{plain strain,}$$

and

$$\kappa = (3 - \nu)/(1 + \nu), \quad \text{plane stress}$$

3. Analytic Function Theory

Mathematical techniques based either directly (conformal mapping, Cauchy integrals, etc.) or indirectly (singular integral equations, Fourier transforms, etc.) on analytic function theory are of great use in static and quasistatic problems of linear elasticity. Some results pertinent to our later needs are quoted here with little development; the reader unacquainted with the subject may wish to consult specialized texts. A function is analytic in a region of the z plane if, at every point of the region, the usual limiting operation defining a derivative exists with a unique result independent of the path along which the difference in z approaches zero. A consequence of analyticity is the vanishing of any integral around a closed contour in the z plane of a function analytic on and within the contour. Integration paths for analytic functions may thus be distorted at will within the region of analyticity. The Cauchy integral formula is a related result. If $f(z)$ is analytic on and within a closed contour C ,

$$\int_C \frac{f(t)}{t-z} dt = \begin{cases} 2\pi i f(z) & \text{for } z \text{ inside } C \\ 0 & \text{for } z \text{ outside } C \end{cases} \quad (23)$$

where C is traversed in a direction such that the interior of C is to the left of the contour.

Define a function $f(z)$ by

$$f(z) = \frac{1}{2\pi i} \int_L \frac{g(t)}{t-z} dt \quad (24)$$

where L is a smooth curve or closed contour in the z plane, and the "density function" $g(t)$ is piecewise continuous on L and also satisfies a weak smoothness condition known as a Holder condition (Muskhelishvili, 1953a). Then, $f(z)$ is analytic everywhere in the z plane except on L . Letting plus (+) and minus (-) signs denote the left and right sides of L , according to the direction of traversal, limits as z

approaches a point t_0 of L from the left and right are given by the Plemelj formulas

$$\begin{aligned} f^+(t_0) - f^-(t_0) &= g(t_0) \\ f^+(t_0) + f^-(t_0) &= \frac{1}{\pi i} \int_L \frac{g(t)}{t - t_0} dt \end{aligned} \quad (25)$$

The equations apply whenever t_0 is neither a point of discontinuity of $g(t)$ nor an end of L at which $g(t_0) \neq 0$, and the integral is interpreted in the Cauchy principal value sense. Conversely, suppose $f(z)$ is analytic everywhere in some region D except along L , and that

$$f^+(t) - f^-(t) = g(t) \quad \text{on } L \quad (26)$$

Then, $f(z)$ is representable as

$$f(z) = \frac{1}{2\pi i} \int_L \frac{g(t)}{t - z} dt + f_0(z) \quad (27)$$

where $f_0(z)$ is analytic everywhere in the region D .

An important application of this last result is to singular integral equations. Suppose $h(t)$ is a piecewise continuous smooth (in the Holder sense) function defined on L , and it is desired to find a solution $g(t)$ to the equation

$$h(t_0) = \int_L \frac{g(t)}{t - t_0} dt \quad \text{on } L \quad (28)$$

Define a function $f(z)$ by Eq. (24). Then

$$f^+(t) + f^-(t) = \frac{h(t)}{\pi i} \quad \text{on } L \quad (29)$$

Suppose L denotes a single arc and let

$$\chi(z) = [(z - a)(z - b)]^{-1/2} \quad (30)$$

where a and b denote the ends of L , and choose the branch cut along L such that $\chi(z)$ behaves as $1/z$ for large $|z|$. Then it can be shown that $\chi(z)$ reverses sign in crossing L ,

$$\chi^+(t) + \chi^-(t) = 0 \quad \text{on } L \quad (31)$$

and Eq. (29) becomes

$$\left[\frac{f(t)}{\chi(t)} \right]^+ - \left[\frac{f(t)}{\chi(t)} \right]^- = \frac{h(t)}{\pi i \chi^+(t)} \quad \text{on } L \quad (32)$$

Thus, from Eqs. (26) and (27),

$$f(z) = -\frac{\chi(z)}{2\pi^2} \int_L \frac{h(t)}{\chi^+(t)(t-z)} dt + p_0(z) \chi(z) \quad (33)$$

where $p_0(z)$ is analytic in the entire z plane (and thus a polynomial). But $f(z)$ is order $1/z$ for large z , in view of its definition by Eq. (24), so that $p_0(z)$ is a constant, say $-k/2\pi i$. Then, from Eq. (25),

$$\begin{aligned} g(t_0) &= f^+(t_0) - f^-(t_0) \\ &= -\frac{\chi^+(t_0)}{\pi^2} \int_L \frac{h(t)}{\chi^+(t)(t-t_0)} dt - \frac{k}{\pi i} \chi^+(t_0) \end{aligned} \quad (34)$$

Note that there is a single infinity of solutions to the singular integral Eq. (28), depending on the value chosen for k . Also, in general, all solutions become infinite as $\chi^+(t)$ near the ends of the arc. The constant k is uniquely determined only if additional restrictions are placed on the solution $g(t)$. For example, one may choose k so that $g(t)$ is finite at one end of the arc or so that the integral of $g(t)$ along L (which equals k) has some specified value. Solutions bounded at both ends of the arc exist only for a limited class of prescribed functions $h(t)$.

D. CONTINUUM PLASTICITY

We shall deal primarily in this article with the continuum theory of plastic deformation (Hill, 1950; Prager and Hodge, 1951; Drucker, 1960), although some use will be made of the dislocation theory (Cottrell, 1953; van Bueren, 1960). The latter is, in its mathematical aspects, the elasticity analysis of line defects causing a constant displacement discontinuity which defines the Burgers vector of a dislocation, and the analysis of the generation and motion of fields of these defects. Attention is limited to continuum plasticity in this section. A yield surface is presumed to exist in a multidimensional stress space at each instant of the homogeneous deformation history of a material. Variations of stress within the yield surface cause purely elastic response. Except in the perfectly plastic case, the yield surface in stress space may translate, expand, or otherwise deform in the course of plastic deformation. In particular, the current stress state must be on the yield surface during plastic deformation. Strains ϵ_{ij} are sums of elastic ϵ_{ij}^e and plastic ϵ_{ij}^p parts, with the elastic strain given by the usual Hookian relations.

Let σ_{ij} be a stress state causing plastic deformation, and let $d\epsilon_{ij}^p$

be an increment of plastic deformation under this stress state. The basic postulate of plasticity is

$$(\sigma_{ij} - \sigma_{ij}^0) d\epsilon_{ij}^p \geq 0 \quad (35)$$

where σ_{ij}^0 is any stress state within or on the current yield surface. This inequality is, in turn, derivable from other postulates characterizing elastic-plastic materials, such as a stability postulate (Drucker, 1951), a requirement of nonnegative work in a strain cycle (Ilyushin, 1961), or a model of plastic deformation as slip on crystallographic planes under a critical resolved shear stress in the slip direction (Bishop and Hill, 1951). Normality of plastic strain increments to the yield surface in stress space is a consequence, as is also the requirement that yield surfaces be convex. Let N_{ij} be components of the outer unit normal to the current yield surface (that is, $N_{ij} d\sigma_{ij} = 0$ for all $d\sigma_{ij}$ along the yield surface, $N_{ij} = N_{ji}$, and $N_{ij}N_{ij} = 1$). Then, plastic stress-strain increment relations take the form

$$d\epsilon_{ij}^p = (d\epsilon_{kl}^p d\epsilon_{kl}^p)^{1/2} N_{ij} \quad (36)$$

when a unique normal exists at the current stress state. At corners on the yield surface, N_{ij} may be any unit tensor within the cone of limiting normals. The square root term is indeterminate for perfect plasticity. For strain hardening, it must be specified as a function of the corresponding stress increments, stress state, and prior history; its dependence on stress increments is usually taken to be linear with $N_{ij} d\sigma_{ij}$, the component normal to the yield surface. Note that plastic incompressibility ($d\epsilon_{kk}^p = 0$) and insensitivity of the yield surface to hydrostatic stress states ($N_{kk} = 0$, since $d\sigma_{ij} = d\lambda \delta_{ij}$ is along the yield surface and $N_{ij} d\sigma_{ij} = 0$) imply one another.

For plastic incompressibility, deviatoric stress components $s_{ij} = \sigma_{ij} - \delta_{ij} \sigma_{kk}/3$ alone determine yielding. A particular example for isotropic plastic behavior is the Mises yield condition $s_{ij}s_{ij} = 2\bar{\tau}^2$, where $\bar{\tau}$ is the current yield stress in shear (or equivalent shear stress). Stress-strain relations are

$$d\epsilon_{ij} = \frac{1-2\nu}{3E} \delta_{ij} d\sigma_{kk} + \frac{ds_{ij}}{2G} + \frac{d\bar{\gamma}^p}{2\bar{\tau}} s_{ij} \quad (37)$$

where $d\bar{\gamma}^p = (2 d\epsilon_{ij}^p d\epsilon_{ij}^p)^{1/2}$ is the equivalent plastic shear strain increment, and $d\bar{\gamma}^p/d\bar{\tau}$ is a specified function of $\bar{\tau}$ for strain hardening. Incremental plasticity theories are physically appropriate, but mathematical complexities often cause recourse to deformation theories for

which the current stress state depends uniquely on the current strain state. Such theories are useful when plastic deformation at each point of a material exhibits only slight deviation from a straight line path in stress or strain space (Budiansky, 1959). The deformation theory form associated with the incremental Mises relation above is

$$\epsilon_{ij} = \frac{1-2\nu}{3E} \delta_{ij} \sigma_{kk} + \frac{\gamma}{2\tau} s_{ij} \quad (38)$$

where $\gamma = [2(\epsilon_{ij} - \delta_{ij} \epsilon_{kk}/3)(\epsilon_{ij} - \delta_{ij} \epsilon_{ll}/3)]^{1/2}$ is a specified function of $\tau = (s_{ij}s_{ij}/2)^{1/2}$. Deformation plasticity theories are actually nonlinear elastic theories; for example, the above stress-strain relation is derivable from the strain energy density

$$W = \frac{E}{6(1-2\nu)} (\epsilon_{kk})^2 + \int \tau d\gamma \quad (39)$$

1. Plastic Limit Theorems

The limit theorems of perfect plasticity follow directly from the fundamental inequality, Eq. (35). Assume that there are no body forces and define the limit state as one for which deformation occurs under constant surface tractions on the boundary of the body. Then, in the limit state

$$0 = \int_S (dT_i du_i) dS = \int_V (d\sigma_{ij} d\epsilon_{ij}) dV = \int_V (d\sigma_{ij} d\epsilon_{ij}^e) dV \quad (40)$$

Virtual work and normality of plastic strain increments have been employed. The last integrand is positive definite, so that stresses and elastic strains are constant in the limit state; $d\epsilon_{ij} = d\epsilon_{ij}^p$. Let σ_{ij}^E be any stress field in equilibrium with T_i^E on the boundary and nowhere violating the yield condition. Since $(\sigma_{ij} - \sigma_{ij}^E) d\epsilon_{ij}^p \geq 0$, where σ_{ij} and $d\epsilon_{ij}^p (= d\epsilon_{ij})$ refer to the limit state,

$$\left. \begin{aligned} \int_V (\sigma_{ij} d\epsilon_{ij}) dV &\geq \int_V (\sigma_{ij}^E d\epsilon_{ij}) dV \\ \int_S (T_i du_i) dS &\geq \int_S (T_i^E du_i) dS \end{aligned} \right\} \quad (41)$$

therefore

This is the lower bound theorem. When tractions are proportional to some positive parameter P , the value at limit load exceeds any value P^E corresponding to an equilibrium stress field nowhere violating the

yield condition. Consider a strain increment field $d\epsilon_{ij}^\kappa$ derivable from a kinematically admissible displacement increment field du_i^κ (i.e., the displacement increment field satisfies any prescribed boundary conditions and incompressibility, if assumed for the material). Let σ_{ij}^κ be any stress state corresponding to a plastic strain increment $d\epsilon_{ij}^\kappa$. Since $(\sigma_{ij}^\kappa - \sigma_{ij}) d\epsilon_{ij}^\kappa \geq 0$,

therefore

$$\left. \begin{aligned} \int_V (\sigma_{ij}^\kappa d\epsilon_{ij}^\kappa) dV &\geq \int_V (\sigma_{ij} d\epsilon_{ij}^\kappa) dV \\ \int_V (\sigma_{ij}^\kappa d\epsilon_{ij}^\kappa) dV &\geq \int_S (T_i du_i^\kappa) dS \end{aligned} \right\} \quad (42)$$

This is the upper bound theorem. When tractions are proportional to some positive parameter P and du_i^κ is chosen so that the surface integral is positive, the value at limit load is less than the value P^κ defined by equality of the surface and volume integrals. Discontinuous displacement increment fields are permissible, but sliding-type discontinuities alone are admissible when incompressibility is assumed. In this case, work done on sliding displacement increments by the shear stress corresponding to a shear strain increment in the sliding direction must be included in the volume integral.

2. Plane Strain Slip-Line Theory

Consider the plane strain deformation of a perfectly plastic material with yield condition

$$\left(\frac{\sigma_{11} - \sigma_{22}}{2}\right)^2 + \sigma_{12}^2 = \tau_0^2 \quad (43)$$

the maximum resolved shear stress in the plane of deformation has a constant value τ_0 during plastic flow. Such a yield condition results for an isotropic material exhibiting plastic incompressibility (Mises and Tresca materials are special cases) when elastic strains are assumed incompressible or when plastic strains greatly exceed elastic strains (Hill, 1950). $\sigma_{33} = (\sigma_{11} + \sigma_{22})/2$ in both cases. Let α and β lines be defined so as to coincide with principal shear directions at each point of the plastic region; the α , β , and x_3 directions form a right-handed orthogonal curvilinear coordinate system and $\sigma_{\alpha\beta} = \tau_0$. Also $\sigma_{\alpha\alpha} = \sigma_{\beta\beta} = p$, say, where $p = (\sigma_{11} + \sigma_{22})/2$. Call ϕ the principal shear angle, measured positive clockwise from the x_1 to α direction and thus from the x_2 to β direction. Equilibrium equations may be put in the concise form $\nabla \cdot \sigma = 0$ where ∇ is the gradient operator and σ the stress dyadic;

$\nabla = \mathbf{i}_j \partial/\partial x_j$ and $\boldsymbol{\sigma} = \sigma_{ij} \mathbf{i}_i \mathbf{i}_j$ in Cartesian coordinates with $\mathbf{i}_1, \mathbf{i}_2, \mathbf{i}_3$ as unit vectors. Referring all quantities to the α, β system with $\partial/\partial s_\alpha, \partial/\partial s_\beta$ denoting derivatives with respect to arc length and $\mathbf{i}_\alpha, \mathbf{i}_\beta$ unit vectors, equilibrium equations in the plastic region are

$$\begin{aligned} 0 &= \left(\mathbf{i}_\alpha \cdot \frac{\partial}{\partial s_\alpha} + \mathbf{i}_\beta \cdot \frac{\partial}{\partial s_\beta} \right) [p(\mathbf{i}_\alpha \mathbf{i}_\alpha + \mathbf{i}_\beta \mathbf{i}_\beta) + \tau_0(\mathbf{i}_\alpha \mathbf{i}_\beta + \mathbf{i}_\beta \mathbf{i}_\alpha)] \\ &= \left(\frac{\partial p}{\partial s_\alpha} - 2\tau_0 \frac{\partial \phi}{\partial s_\alpha} \right) \mathbf{i}_\alpha + \left(\frac{\partial p}{\partial s_\beta} + 2\tau_0 \frac{\partial \phi}{\partial s_\beta} \right) \mathbf{i}_\beta \end{aligned} \quad (44)$$

Here, unit vectors are differentiated according to $d\mathbf{i}_\alpha = \mathbf{i}_\beta d\phi$ and $d\mathbf{i}_\beta = -\mathbf{i}_\alpha d\phi$. Integrating, the stress field is given by

$$\begin{aligned} p - 2\tau_0\phi &= \text{constant on } \alpha \text{ lines} \\ p + 2\tau_0\phi &= \text{constant on } \beta \text{ lines} \end{aligned} \quad (45)$$

Normality and the yield condition of Eq. (43) imply plastic incompressibility in the plane, $d\epsilon_{11}^p + d\epsilon_{22}^p = 0$, and correspondence of principal shear directions for the stress and plastic strain increment fields. Thus, $d\epsilon_{\alpha\alpha}^p = d\epsilon_{\beta\beta}^p = 0$. The strain dyadic $\boldsymbol{\epsilon}$ is defined as the symmetric part of $\nabla \mathbf{u}$, where \mathbf{u} is the displacement vector. When stresses are constant at a material point of the plastic region during an increment of deformation, $d\boldsymbol{\epsilon}^e = 0$ so that $d\boldsymbol{\epsilon}^p = d\boldsymbol{\epsilon} = \text{symmetric part of } \nabla d\mathbf{u}$. Thus, components du_α, du_β of the displacement increment vector along the shear directions are determined from

$$\begin{aligned} d\epsilon_{\alpha\alpha} &= \mathbf{i}_\alpha \cdot \left[\left(\mathbf{i}_\alpha \frac{\partial}{\partial s_\alpha} + \mathbf{i}_\beta \frac{\partial}{\partial s_\beta} \right) (du_\alpha \mathbf{i}_\alpha + du_\beta \mathbf{i}_\beta) \right] \cdot \mathbf{i}_\alpha \\ &= \frac{\partial(du_\alpha)}{\partial s_\alpha} - (du_\beta) \frac{\partial \phi}{\partial s_\alpha} = 0 \\ d\epsilon_{\beta\beta} &= \frac{\partial(du_\beta)}{\partial s_\beta} + (du_\alpha) \frac{\partial \phi}{\partial s_\beta} = 0 \end{aligned} \quad (46)$$

3. Antiplane Strain

The yield condition for antiplane deformation of an isotropic material is

$$\sigma_{31}^2 + \sigma_{32}^2 = \tau_0^2 \quad (47)$$

the magnitude of the shear stress vector on the x_3 face is constant in the plastic region. Introduce again α and β lines in the x_1x_2 plane such that the β direction is the principal shear direction and the α, β , and x_3 directions form a right-handed system; then, $\sigma_{3\alpha} = 0$ and $\sigma_{3\beta} = \tau_0$.

Let ϕ be the principal shear angle, measured clockwise from the x_1 to the α direction, and thus from the x_2 to principal shear direction β . The relevant equilibrium equation may be written as $\nabla \cdot \sigma_3 = 0$ where σ_3 is the stress vector on the x_3 face. Then

$$0 = \left(\mathbf{i}_\alpha \cdot \frac{\partial}{\partial s_\alpha} + \mathbf{i}_\beta \cdot \frac{\partial}{\partial s_\beta} \right) (\tau_0 \mathbf{i}_\beta) = \tau_0 \frac{\partial \phi}{\partial s_\alpha} \tag{48}$$

Thus, ϕ is constant on α lines and, since ϕ is the slope, all α lines are straight. The principal shear stress has constant direction at all points along an α line perpendicular to the stress vector at any one point of the plastic region. Normality of plastic strain increments leads to $d\epsilon_{3\alpha}^p = 0$, so that if the stress is constant $d\epsilon_{3\alpha} = 0$ and

$$du_3 = \text{constant on } \alpha \text{ lines} \tag{49}$$

Somewhat more general forms result when du_1 and du_2 are nonzero as in torsion (Prager and Hodge, 1951).

E. ENERGY VARIATIONS AND ASSOCIATED METHODS

Methods of analysis based on energy variations will play an important role in this article. We consider two bodies of linear or nonlinear elastic material, each containing a notch or void (Figs. 1a and 1b). Each is subjected to the same system of loads, consisting of tractions and/or displacements prescribed on the boundary. The two bodies are identical in composition, overall geometrical shape, and in every other feature but one—the notches differ in size. In fact, the body of Fig. 1b may be thought of as created from that of Fig. 1a by removal of material from load-free portions of the boundary. Assume loadings are by surface tractions T_i^0 on a portion of boundary S_T common to both bodies, and by imposed displacements u_i^0 on a common portion of boundary S_U . Let ΔV denote the region of material removed in forming the body of Fig. 1b from that of Fig. 1a, and let ΔS denote the newly created tractionfree surface. If $\sigma_{ij}^0, \epsilon_{ij}^0$ denotes the deformation state for Fig. 1a, the potential energy is

$$P^0 = \int_V W(\epsilon_{mn}^0) dV - \int_{S_T} T_i^0 u_i^0 dS \tag{50}$$

Letting $\sigma_{ij}^0 + \Delta\sigma_{ij}, \epsilon_{ij}^0 + \Delta\epsilon_{ij}$ denote the deformation state for Fig. 1b, and ΔP the increase in potential energy,

$$P^0 + \Delta P = \int_{V-\Delta V} W(\epsilon_{mn}^0 + \Delta\epsilon_{mn}) dV - \int_{S_T} T_i^0 (u_i^0 + \Delta u_i) dS \tag{51}$$

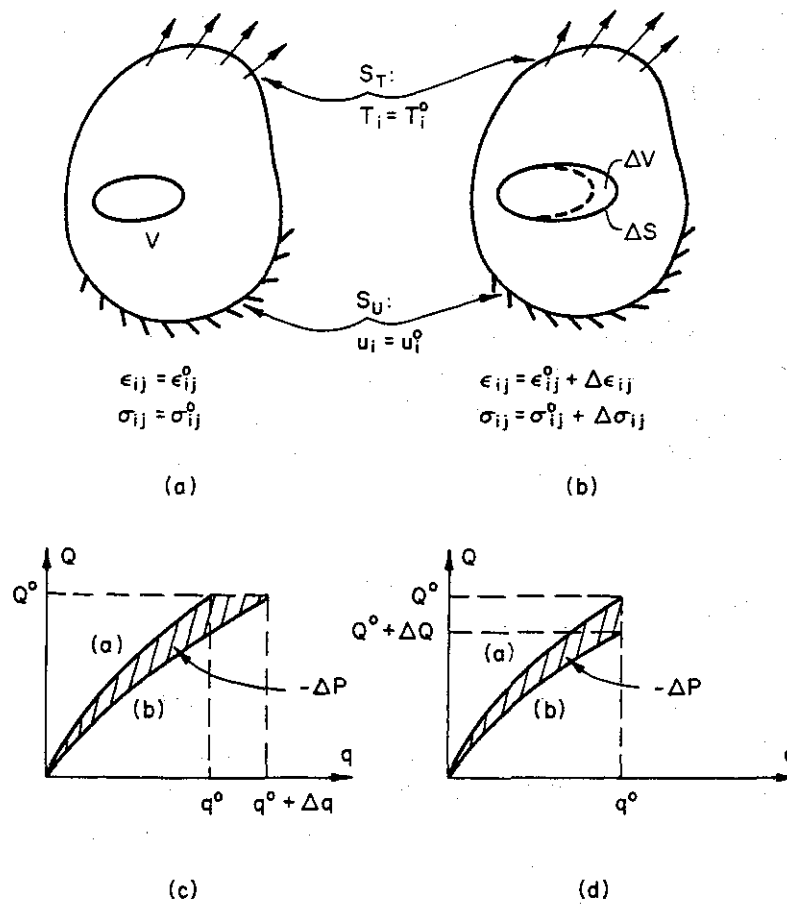


FIG. 1. (a) and (b) Comparison of two notched elastic bodies of identical shape, composition, and loading, except that the notch of body (b) is larger by an amount ΔV and has surface ΔS not common to body (a).

(c) and (d) Difference between potential energies of (b) and (a) is representable as area between force-displacement curves when loading is by forces alone (c) or by displacements alone (d).

We shall solve for the potential energy difference ΔP . First, note that this difference is expressible in terms of the difference in overall load-deflection curves for the two bodies. Suppose the loading is entirely by prescribed surface tractions proportional to a generalized force Q , and let q be the corresponding work-absorbing generalized displacement. Then, a straightforward application of virtual work in the above equations shows the potential energy decrease, $-\Delta P$, to equal the area between load-deflection curves for the two bodies (as indicated by the shaded area in Fig. 1c). Similarly, when loading is entirely by displacements proportional to q , the potential energy decrease is the shaded area in Fig. 1d.

Observe that the integral of $T_i^0 \Delta u_i$ over S_T equals the integral of

$(T_i^0 + \Delta T_i) \Delta u_i$ over the entire surface of the body of Fig. 1b. This is because $\Delta T_i = 0$ on S_T , $\Delta u_i = 0$ on S_U , and $T_i^0 + \Delta T_i = 0$ on the newly created surface ΔS . Thus, by virtual work

$$\int_{S_T} T_i^0 \Delta u_i dS = \int_{V-\Delta V} (\sigma_{ij}^0 + \Delta \sigma_{ij}) \Delta \epsilon_{ij} dV \quad (52)$$

The potential energy decrease is now expressible as (Rice and Drucker, 1967)

$$\begin{aligned} -\Delta P &= \int_{\Delta V} W(\epsilon_{mn}^0) dV \\ &+ \int_{V-\Delta V} \{(\sigma_{ij}^0 + \Delta \sigma_{ij}) \Delta \epsilon_{ij} - [W(\epsilon_{mn}^0 + \Delta \epsilon_{mn}) - W(\epsilon_{mn}^0)]\} dV \\ &= \int_{\Delta V} W(\epsilon_{mn}^0) dV \\ &+ \int_{V-\Delta V} \left\{ \int_{\epsilon_{mn}^0}^{\epsilon_{mn}^0 + \Delta \epsilon_{mn}} (\sigma_{ij}^0 + \Delta \sigma_{ij} - \sigma_{ij}) d\epsilon_{ij} \right\} dV \end{aligned} \quad (53)$$

This result is more readily interpreted after a further transformation. Note that the strain integral appearing in the volume integral is path independent. We therefore choose a useful path. First, load the body of Fig. 1b with tractions T_i^0 on S_T , displacements u_i^0 on S_U , and tractions $T_i^0 = \sigma_{ij}^0 n_j$ on the new surface ΔS ; the deformation state is $\sigma_{ij}^0, \epsilon_{ij}^0$, identical to that for the body of Fig. 1a. Now, holding the loadings on S_T and S_U fixed, reduce the tractions on ΔS to zero so that the actual deformation state $\sigma_{ij}^0 + \Delta \sigma_{ij}, \epsilon_{ij}^0 + \Delta \epsilon_{ij}$ of Fig. 1b results. Let T_i^*, u_i^* denote tractions and displacements on ΔS during this special path from ϵ_{ij}^0 to $\epsilon_{ij}^0 + \Delta \epsilon_{ij}$. Then, an application of virtual work to the volume integral above leads to

$$-\Delta P = \int_{\Delta V} W(\epsilon_{mn}^0) dV - \int_{\Delta S} \left\{ \int_{u_i^* = u_i^0, T_i^* = T_i^0}^{u_i^* = u_i^0 + \Delta u_i, T_i^* = 0} T_i^* du_i^* \right\} dS \quad (54)$$

for the potential energy reduction. The interpretation is clear; the net energy reduction is the strain energy of the material removed minus the (negative) work done in freeing the new surface of tractions. $\Delta P \leq 0$.

A simple formula results in the special case of linear elastic behavior. The strain integral in Eq. (53) is $\Delta \sigma_{ij} \Delta \epsilon_{ij}/2$, and a virtual work transformation leads to

$$-\Delta P = \frac{1}{2} \int_{\Delta V} \sigma_{ij}^0 \epsilon_{ij}^0 dV - \frac{1}{2} \int_{\Delta S} T_i^0 \Delta u_i dS \quad (55)$$

since $\Delta T_i = -T_i^0$ on the void surface. Note in this case that overall load-deflection curves (Figs. 1c and 1d) are linear and $-\Delta P = Q_0 \Delta q/2$ when boundary tractions are prescribed as in Fig. 1c. As shown by the last two equations, the general calculation involves both volume and surface integrals. Only the surface integral contributes when the notch under consideration is a crack for $\Delta V = 0$. Only the volume integral contributes for a class of smooth voids when infinitesimal geometry changes are considered, as discussed below. We shall see, however, that this discontinuity in the calculation method for limiting cases is only apparent.

The utility of a study of energy variations will be seen through the many applications in the following sections. The potential energy rate of decrease is expressible directly in terms of the concentrated stresses and strains on a notch surface or in the vicinity of a crack tip. On the other hand, this energy variation may be independently obtained, either exactly or approximately, for a wide variety of notched configurations. These independent estimates are obtainable in a simple way sometimes by inspection, by "strength of materials" style calculations, by overall load-deflection experiments, by use of the many known linear elastic solutions for notches, or by use of approximate calculations which describe salient gross features of nonlinear behavior. Consequently, some information on notch strain concentrations may be obtained without recourse to the detailed solution of boundary value problems. This method, in a somewhat less general form than presented here, has recently been applied to the analysis of several two-dimensional strain concentration problems (Rice, 1967a).

1. Infinitesimally Neighboring Smooth-Surfaced Notches

Consider voids or notches having smooth surfaces with continuously turning tangents, at least over the portion where material is removed in creating Fig. 1b from Fig. 1a. Presuming stability in the small, $d\sigma_{ij} d\epsilon_{ij} \geq 0$, carrying out the strain integral of Eq. (53) over a straight-line path in stress space leads to

$$0 \leq \int_{\epsilon_{mn}^0}^{\epsilon_{mn}^0 + \Delta\epsilon_{mn}} (\sigma_{ij}^0 + \Delta\sigma_{ij} - \sigma_{ij}) d\epsilon_{ij} \leq \Delta\sigma_{ij} \Delta\epsilon_{ij} \quad (56)$$

The same inequalities apply to all paths because of path independence. Upon a virtual work transformation of Eq. (53), we have the inequalities

$$0 \leq (-\Delta P) - \int_{\Delta V} W(\epsilon_{mn}^0) dV \leq \int_{\Delta S} \Delta T_i \Delta u_i dS \quad (57)$$

Now suppose the two notches being compared differ in size by an infinitesimal amount. Points on the notch boundary of Fig. 1a are obtainable by proceeding a distance dn normal to the boundary of Fig. 1b over the region where material is removed. For dn a sufficiently smooth function of position on the notch surface, as assumed, both $\Delta T_i = (\Delta \sigma_{ij})n_j$ and Δu_i are first-order quantities, so that the upper bound of Eq. (57) is second order. Since the integral over ΔV is first order, the upper bound is zero when dealing with an infinitesimal smooth change in geometry of the notch. Thus, representing volume elements of removed material by $dS dn$, the potential energy decrease is

$$-dP = \int_{dV} W(\epsilon_{mn}^0) dV = \int_{\Delta S} [W(\epsilon_{mn}^0) dn] dS \quad (58)$$

Note that in infinitesimal (or rate with respect to geometrical size) form, the energy variation depends only on the strain energy of the material removed.

As a special type of smooth notch, consider a flat-surfaced notch in a two-dimensional deformation field (Fig. 2). All stresses are presumed to depend only on two Cartesian coordinates, x_1 and x_2 . The notch has surfaces parallel to the x_1 direction and a smooth curved tip denoted by the arc Γ_t . Let l denote notch length, and compare the potential energy with that of a notch of length $(l + dl)$ having a geometrically identical tip so that the only change is an extension of the flat-surfaced portion by dl . Redefining P as the potential energy per unit thickness in the x_3 direction and noting that volume elements of the material removed may be represented as $dl dx_2 dx_3$, the rate of decrease of potential energy per unit thickness with respect to notch size is

$$-dP/dl = \int_{\Gamma} W(\epsilon_{mn}) dx_2 \quad (59)$$

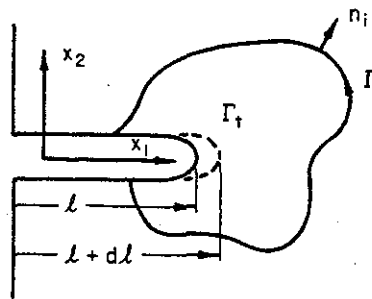


FIG. 2. Flat surface notch in two-dimensional deformation field. Γ_t denotes curved notch tip; Γ denotes any curve surrounding the tip.

Here, we have dropped the superscript "0" appearing in Eq. (58). An especially useful result follows from representing this energy rate as a path-independent line integral taken around the notch tip (Rice, 1967a), in the case when the material under consideration is homogeneous, at least in the x_1 direction. Toward this end, define an integral J such that

$$J = \int_{\Gamma} [W dx_2 - \mathbf{T} \cdot \partial \mathbf{u} / \partial x_1 ds] \quad (60)$$

Here, Γ is a curve which surrounds the tip, starting from the lower flat notch surface and ending on the upper flat notch surface, as in Fig. 2, the curve is traversed in the counterclockwise sense, s is arc length, and $\mathbf{T} = \boldsymbol{\sigma} \cdot \mathbf{n}$ is the traction vector on Γ according to an outward unit vector \mathbf{n} normal to the curve. Note that when $\Gamma = \Gamma_t$, $J = -dP/dl$, since $\mathbf{T} = 0$ on the notch surface.

We now show that the integral J is path-independent, so that J is the energy decrease rate for any choice of a curve Γ . Consider two curves Γ_1 and Γ_2 , suppose Γ_2 to enclose Γ_1 , and let J_1 and J_2 be the associated values of the integral. Then, $J_2 - J_1$ is the integral counterclockwise of $[W dx_2 - \mathbf{T} \cdot (\partial \mathbf{u} / \partial x_1) ds]$ around the boundary of the area $A(\Gamma_2, \Gamma_1)$ enclosed by the curves and the notch surfaces, since both terms of the integrand vanish on the flat surfaces. Transforming to an area integral and employing Cartesian coordinates

$$J_2 - J_1 = \int_{A(\Gamma_2, \Gamma_1)} \left[\frac{\partial W}{\partial x_1} - \sigma_{ij} \frac{\partial \epsilon_{ij}}{\partial x_1} \right] dx_1 dx_2 = 0$$

since

$$\frac{\partial W}{\partial x_1} = \frac{\partial}{\partial x_1} \int \sigma_{ij} d\epsilon_{ij} = \sigma_{ij} \frac{\partial \epsilon_{ij}}{\partial x_1} \quad (61)$$

Thus, the integral J is path independent (assuming, of course, that the region between Γ_1 and Γ_2 is simply connected and free of singularities) and

$$J = -dP/dl \quad (62)$$

We have assumed the body of Fig. 1b to be obtainable from that of Fig. 1a by removal of material. The same formulas apply for addition of material. Thus, the rate form for dP of Eq. (58) is generally valid with dn positive over that portion of the void surface where material is removed, and negative where material is added.

2. Cracks in Two-Dimensional Deformation Fields

In view of the representation of the energy variation rate as a path-independent integral taken around the tip of a flat surface notch, one would expect the same result to hold in the limiting case of a straight crack in a two-dimensional deformation field. This is so, but an independent derivation is desirable in view of the discontinuity in the limiting process noted above. Let l denote crack length and again consider P as the potential energy per unit thickness in the x_3 direction. Then, the two-dimensional version of Eq. (53) is, in the limit for an energy comparison when the difference in crack length approaches zero,

$$-\frac{dP}{dl} = \lim_{\Delta l \rightarrow 0} \frac{1}{\Delta l} \int_{A^*} \{(\sigma_{ij}^0 + \Delta\sigma_{ij}) \Delta\epsilon_{ij} - [W(\epsilon_{mn}^0 + \Delta\epsilon_{mn}) - W(\epsilon_{mn}^0)]\} dx_1 dx_2 \quad (63)$$

Here, A^* should be taken as the total area of the two-dimensional body to strictly copy Eq. (53). But the integrand is second order in Δl (by Eq. (56) at all distances from the crack tip large compared to Δl). Thus, for the limit calculation, it suffices to take A^* as any finite region in which the crack tip is imbedded. Such a region is shown in Fig. 3a; we call Γ the outward boundary of A^* .

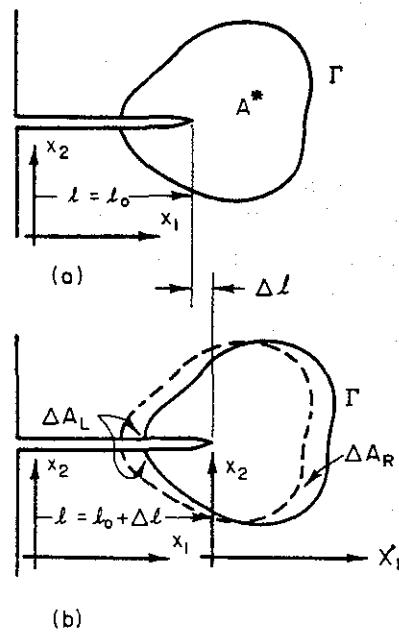


FIG. 3. Energy computation for crack advance. X_1, x_2 coordinate system, area A^* , and bounding curve Γ move with the crack tip in extension from $l = l_0$, (a), to $l = l_0 + \Delta l$, (b).

It is convenient to introduce a moving coordinate system X_1, x_2 , as shown in Fig. 3b, with $X_1 = x_1 - l$ so that $X_1 = 0$ at the crack tip, regardless of the crack length. Consider all quantities involved in the energy computation as functions of X_1, x_2 , and l . Thus

$$\begin{aligned}\sigma_{ij}^0 &= \sigma_{ij}(X_1, x_2, l_0), & \sigma_{ij}^0 + \Delta\sigma_{ij} &= \sigma_{ij}(X_1, x_2, l_0 + \Delta l), \\ u_i^0 &= u_i(X_1, x_2, l_0), & \text{etc.}\end{aligned}$$

Let d/dl be the total derivative with respect to crack length. Then

$$\frac{d}{dl} = \frac{\partial}{\partial l} + \frac{\partial X_1}{\partial l} \frac{\partial}{\partial X_1} = \frac{\partial}{\partial l} - \frac{\partial}{\partial X_1} = \frac{\partial}{\partial l} - \frac{\partial}{\partial x_1} \quad (64)$$

since $\partial X_1/\partial l = -1$ and $\partial/\partial X_1 = \partial/\partial x_1$. By a virtual work transformation, the first term of Eq. (63) becomes

$$\begin{aligned}\lim_{\Delta l \rightarrow 0} \frac{1}{\Delta l} \int_{A^*} (\sigma_{ij}^0 + \Delta\sigma_{ij}) \Delta\epsilon_{ij} dx_1 dx_2 \\ &= \lim_{\Delta l \rightarrow 0} \frac{1}{\Delta l} \int_{\Gamma} (T_i^0 + \Delta T_i) \Delta u_i ds \\ &= \int_{\Gamma} T_i(X_1, x_2, l_0) \frac{\partial u_i(X_1, x_2, l_0)}{\partial l} ds \\ &\quad - \int_{\Gamma} T_i(x_1, x_2, l_0) \frac{\partial u_i(x_1, x_2, l_0)}{\partial x_1} ds\end{aligned} \quad (65)$$

To evaluate the strain energy difference term of Eq. (63), consider A^* and Γ as a fixed area and bounding curve in the $X_1 x_2$ plane so that these move with the crack tip, as shown in Fig. 3b. The areas on the left and right between the curves Γ for $l = l_0$ and for $l = l_0 + \Delta l$ are denoted by ΔA_L and ΔA_R , respectively, as shown. Thus

$$\begin{aligned}\lim_{\Delta l \rightarrow 0} \frac{1}{\Delta l} \int_{A^*} [W(\epsilon_{mn}^0 + \Delta\epsilon_{mn}) - W(\epsilon_{mn}^0)] dx_1 dx_2 \\ &= \lim_{\Delta l \rightarrow 0} \frac{1}{\Delta l} \left\{ \int_{A^* + \Delta A_L - \Delta A_R} W(X_1, x_2, l_0 + \Delta l) dX_1 dx_2 \right. \\ &\quad \left. - \int_{A^*} W(X_1, x_2, l_0) dX_1 dx_2 \right\} \\ &= - \int_{\Gamma} W(x_1, x_2, l_0) dx_2 + \int_{A^*} \frac{\partial W(X_1, x_2, l_0)}{\partial l} dX_1 dx_2\end{aligned} \quad (66)$$

But it is a simple application of virtual work to show that

$$\int_{\Gamma} T_i(X_1, x_2, l) \frac{\partial u_i(X_1, x_2, l)}{\partial l} ds = \int_{A^*} \frac{\partial W(X_1, x_2, l)}{\partial l} dX_1 dx_2 \quad (67)$$

Now, employing the last three equations, the energy variation with respect to crack length becomes

$$-dP/dl = \int_{\Gamma} [W dx_2 - \mathbf{T} \cdot \partial \mathbf{u} / \partial x_1 ds] \equiv J \quad (68)$$

We arrive at the same result as for the flat-surfaced notch with a smooth tip, as expected physically, in spite of the very different starting points (compare Eqs. (58) and (63), both special cases of the general Eq. (53).

Results given in Eqs. (58), (59), and (68) show that, for two notched bodies differing in geometry by an infinitesimal amount, the potential energy difference (or energy decrease rate) is directly expressible in terms of the concentrated deformation field in the vicinity of the notch tip. Since energy rates are often independently obtainable, these equations will be of great use for the analysis of strain concentration problems in the mechanics of fracture. Also, we shall find the feature of path independence of the integral J useful in itself.

3. Inelastic Behavior

It is important to remember that all the above results on energy variations are strictly true for elastic behavior only. Our main applications will, however, be to elastic-plastic problems. We are thus forced to employ a deformation plasticity formulation rather than the physically appropriate incremental formulation. This is a regrettable situation, but no success has been met in attempts to formulate similar general results for incremental plasticity. Also, energy variation methods permit the treatment of several nonlinear problems presently well beyond the reach of more conventional analytical methods, either of the deformation or incremental type.

III. Linear Elasticity in the Analysis of Deformation and Fracture

Except in extreme cases of brittle behavior, fracture is normally accompanied by significant inelastic deformation, either on a gross scale or confined to the vicinity of stress concentrators such as notches and cracks. Elastic calculations are of little utility in the former case. They do, however, form a useful first step in the analysis of "low stress"

fractures originating at high-stress-concentration points when the region of inelastic deformation is small compared to notch or crack size and other characteristic lengths. Functions of the applied loadings and geometry of a notched body are then determined (stress-concentration factors, stress-intensity factors, etc.) which serve to characterize the severity of local deformations. Such parameters are useful in the analysis and prediction of fracture behavior, for they indicate when two different notched or cracked configurations have similar local deformation fields and thus may be expected to exhibit similar fracture behavior. Inelastic analyses remain desirable for a more complete characterization of stresses and deformations, either for comparative purposes similar to the utilization of elastic stress analyses, or for the direct connection of continuum level solutions with separation mechanisms on the microscale. We shall see the usefulness of elastic solutions for setting asymptotic boundary conditions on inelastic analyses in the small-scale yielding range.

A. LINEAR ELASTIC CRACK TIP STRESS FIELDS

The important features of crack tip stress distributions may be understood through the development of the general functional form of solutions in two-dimensional deformation fields. Consider a crack along a portion of the negative x_1 axis with a tip at the origin of the x_1, x_2 coordinate system. Let R denote a small region of the x_1x_2 plane enclosing only the tip at the origin and no other singularities of the problem, and in which the stress functions of Sect. II,C are analytic (except along the crack line), as in Fig. 4. Inplane stress components entering the tractionfree crack boundary condition may be expressed from Eqs. (21) as

$$\sigma_{22} - i\sigma_{12} = \phi'(z) + \overline{\Omega'(z)} + (z - \bar{z})\overline{\phi''(z)} \quad (69)$$

where the new function Ω is defined as

$$\Omega(z) = z\phi'(z) + \psi(z) \quad (70)$$

We understand the notation $\bar{F}(z)$ to denote the complex conjugate of $F(\bar{z})$, where F is any analytic function defined at \bar{z} ; $\bar{F}(z)$ is analytic. The plus (+) and minus (−) signs denote limits of the analytic functions as the crack line is approached from the regions $x_2 > 0$ and $x_2 < 0$, respectively. Points on the crack line are denoted by $z = t$, t being real and negative. Then the requirement of stressfree crack surfaces, $\sigma_{j2}^+ = \sigma_{j2}^- = 0$, leads to

$$\phi'(t)^+ + \bar{\Omega}'(t)^- = 0, \quad \phi'(t)^- + \bar{\Omega}'(t)^+ = 0 \quad (71)$$

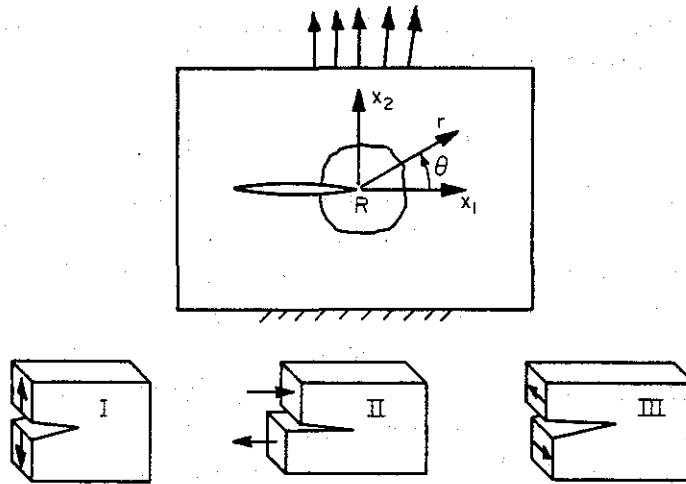


FIG. 4. Small region near crack tip in which general form of linear elastic stress field may be established. Three modes of near tip deformations shown.

Subtracting the second equation from the first

$$[\phi'(t) - \bar{\Omega}'(t)]^+ = [\phi'(t) - \bar{\Omega}'(t)]^- \tag{72}$$

Thus

$$\phi'(z) - \bar{\Omega}'(z) = 2g(z) \tag{73}$$

where $g(z)$ analytic in R . An addition yields the Hilbert equation

$$[\phi'(t) + \bar{\Omega}'(t)]^+ + [\phi'(t) + \bar{\Omega}'(t)]^- = 0 \tag{74}$$

A solution is clearly $z^{-1/2}$, since $(t^{-1/2})^+ + (t^{-1/2})^- = 0$ when the branch cut is chosen along the crack line. Since all solutions, excepting those with higher order singularities ruled out by the requirement of finite displacements, may be expressed as $z^{-1/2}$ multiplying a function analytic in R (Muskhelishvili, 1953a),

$$\phi'(z) + \bar{\Omega}'(z) = 2z^{-1/2}f(z) \tag{75}$$

where $f(z)$ analytic in R .

These equations and Eqs. (21) lead to the general expression of near crack tip inplane stresses as

$$\begin{aligned} \sigma_{11} + \sigma_{22} &= 4 \operatorname{Re}[z^{-1/2}f(z) + g(z)] \\ \sigma_{22} - \sigma_{11} + 2i\sigma_{12} &= -4iz^{-1/2} \operatorname{Im}[f(z)] - 4 \operatorname{Re}[g(z)] \\ &\quad - 4ix_2 \frac{d}{dz} [z^{-1/2}f(z) + g(z)] \end{aligned} \tag{76}$$

where $f(z)$ and $g(z)$ are analytic in the vicinity of the crack tip. A similar development shows the antiplane stresses to be given by Eq. (16) in the form

$$\sigma_{32} + i\sigma_{31} = z^{-1/2}h(z) + ik(z) \quad (77)$$

where both $h(z)$ and $k(z)$ are analytic in the vicinity of the crack tip and real on the x_1 axis. It is seen that all crack tip stress fields exhibit inverse square root singularities. The strength of the singularity is determined for inplane stresses by the value of $f(z)$ at the origin and for antiplane stresses by the value of $h(z)$ at the origin. It is convenient to follow Irwin (1960) in classifying three distinct singular stress fields, according to whether resulting displacements contribute to the opening (mode I), inplane sliding (mode II), or antiplane sliding (mode III) modes of relative displacement of the crack surfaces. For the opening mode, $f(0)$ is real. Take its value as $f(0) = K_I/2(2\pi)^{1/2}$, where the constant K_I is a mode I stress-intensity factor. Then the near crack tip singular stress field is expressed from Eqs. (76) as

$$\begin{pmatrix} \sigma_{11} \\ \sigma_{12} \\ \sigma_{22} \end{pmatrix} = \frac{K_I}{(2\pi r)^{1/2}} \cos(\theta/2) \begin{pmatrix} 1 - \sin(\theta/2) \sin(3\theta/2) \\ \sin(\theta/2) \cos(3\theta/2) \\ 1 + \sin(\theta/2) \sin(3\theta/2) \end{pmatrix} \quad (78)$$

where polar coordinates are employed as in Fig. 4. Associated displacements are

$$\begin{pmatrix} u_1 \\ u_2 \end{pmatrix} = \frac{K_I}{2G} \left(\frac{r}{2\pi}\right)^{1/2} \begin{pmatrix} \cos(\theta/2) [\kappa - 1 + 2 \sin^2(\theta/2)] \\ \sin(\theta/2) [\kappa + 1 - 2 \cos^2(\theta/2)] \end{pmatrix} \quad (79)$$

where $\kappa = (3 - 4\nu)$ for plane strain and $\kappa = (3 - \nu)/(1 + \nu)$ for generalized plane stress. The function $f(0)$ is purely imaginary for the inplane sliding mode. Taking its value as $f(0) = -iK_{II}/2(2\pi)^{1/2}$, where K_{II} is a mode II stress intensity factor, Eqs. (76) lead to the singular stress state

$$\begin{pmatrix} \sigma_{11} \\ \sigma_{12} \\ \sigma_{22} \end{pmatrix} = \frac{K_{II}}{(2\pi r)^{1/2}} \begin{pmatrix} -\sin(\theta/2) [2 + \cos(\theta/2) \cos(3\theta/2)] \\ \cos(\theta/2) [1 - \sin(\theta/2) \sin(3\theta/2)] \\ \sin(\theta/2) \cos(\theta/2) \cos(3\theta/2) \end{pmatrix} \quad (80)$$

and associated displacements

$$\begin{pmatrix} u_1 \\ u_2 \end{pmatrix} = \frac{K_{II}}{2G} \left(\frac{r}{2\pi}\right)^{1/2} \begin{pmatrix} \sin(\theta/2) [\kappa + 1 + 2 \cos^2(\theta/2)] \\ -\cos(\theta/2) [\kappa - 1 - 2 \sin^2(\theta/2)] \end{pmatrix} \quad (81)$$

Antiplane stresses σ_{13} , σ_{23} are nonsingular in the first two modes; σ_{33} is zero for generalized plane stress (which is hardly a valid approxima-

tion with such a severe stress gradient), and $\sigma_{33} = \nu(\sigma_{11} + \sigma_{22})$ for plane strain. The antiplane sliding mode singular stress distribution is obtained by taking $h(0) = K_{III}/(2\pi)^{1/2}$ in Eq. (77). Resulting stresses are

$$\begin{Bmatrix} \sigma_{13} \\ \sigma_{23} \end{Bmatrix} = \frac{K_{III}}{(2\pi r)^{1/2}} \begin{Bmatrix} -\sin(\theta/2) \\ \cos(\theta/2) \end{Bmatrix} \quad (82)$$

with all other stress components being nonsingular. The associated antiplane displacement is

$$u_3 = 2 \frac{K_{III}}{G} \left(\frac{r}{2\pi} \right)^{1/2} \sin(\theta/2) \quad (83)$$

We shall discuss methods for determining stress-intensity factors below. Resulting from linear elastic boundary value problems, they are linear in applied loads and have dimensions of stress times the square root of some characteristic length. A complete survey of available solutions is contained in a paper by Paris and Sih (1965).

Small-Scale Yielding and Elastic Fracture Mechanics

The utility of elastic stress analyses lies in the similarity of near crack tip stress distributions for all configurations. Presuming deviations from linearity to occur only over a region that is small compared to geometrical dimensions (small-scale yielding), the elastic stress-intensity factor controls the local deformation field. This is in the sense that two bodies with cracks of different size and with different manners of load application, but which are otherwise identical, will have identical near crack tip deformation fields if the stress-intensity factors are equal. Thus, the stress-intensity factor uniquely characterizes the load sensed at the crack tip in situations of small-scale yielding, and criteria governing crack extension for a given local load rate, temperature, environment, sheet thickness (when plane stress fracture modes are possible), and history of prior deformation may be expressed in terms of stress-intensity factors. It is essential to note that stress-intensity factors provide solely a convenient measure of load applied to the crack tip region. The elastic analysis of fracture contains no information on the response of the material to this load; this point has been unfortunately obscured in the literature due to the early development of elastic fracture mechanics as an extension of the Griffith theory (Griffith, 1920; Orowan, 1952; Irwin, 1958), a viewpoint now recognized as limiting and unnecessary. While the limitations of elastic fracture mechanics are evident, its progress in the organization and analysis of low stress level (small-scale yielding) crack extension behavior has been remarkable. Examples are

given by the work of Irwin (1958) and Srawley and Brown (1965) on fracture, by Paris (1964) on fatigue, and by Johnson and Willner (1965) on stress corrosion.

B. SOME ELASTIC CRACK PROBLEMS

The mathematical solutions of some elastic crack problems are outlined in this subsection. The number of useful problems which can be solved in closed form is, of course, limited, and one must usually resort to approximate methods, as discussed in the next two subsections.

1. *Two-Dimensional Problems of Isolated Cracks and Collinear Crack Arrays in Infinite Bodies*

Suppose the crack or cracks considered lie on the x_1 axis of the infinite x_1x_2 plane. Denote by L the crack line or union of all crack lines. It suffices to consider only the case of forces prescribed on the crack surfaces, for other methods of loading may be reduced to this case by superposition. One first solves the problem without cracks and determines the stresses $\sigma_{2i}(x_1, 0)$ on the prospective crack line(s). Then the crack problem is solved with the reverse of these stresses acting on L . Let the prescribed stresses be given by

$$\sigma_{2i}(x_1, 0) = -p_i(x_1) \quad \text{on } L, \quad i = 1, 2, 3 \quad (84)$$

It is assumed that the same stresses act on both crack surfaces. Employing the notation of the last section, boundary conditions for the inplane stress components become

$$\begin{aligned} -p_2(t) + ip_1(t) &= [\phi'(t)]^+ + [\bar{\Omega}'(t)]^- \\ -p_2(t) + ip_1(t) &= [\phi'(t)]^- + [\bar{\Omega}'(t)]^+ \quad \text{on } L \end{aligned} \quad (85)$$

Subtraction leads, as in Eq. (72), to the conclusion that

$$[\phi'(t) - \bar{\Omega}'(t)]^+ = [\phi'(t) - \bar{\Omega}'(t)]^- \quad \text{on } L \quad (86)$$

Thus, $\phi'(z) - \bar{\Omega}'(z)$ is analytic along the crack line(s) and, therefore, in the entire z plane. But both functions vanish at infinity for zero remote stress and rotation. Thus

$$\bar{\Omega}'(z) = \phi'(z) \quad (87)$$

and both of Eqs. (85) reduce to

$$-p_2(t) + ip_1(t) = [\phi'(t)]^+ + [\phi'(t)]^- \quad \text{on } L \quad (88)$$

Suppose there are n finite cracks with left and right ends at a_1, a_2, \dots, a_n and b_1, b_2, \dots, b_n , respectively, on the x_1 axis. Following the methods of Muskhelishvili (1953a, 1953b), define

$$\chi(z) = \prod_{j=1}^n (z - a_j)^{-1/2} (z - b_j)^{-1/2} \quad (89)$$

Then, $[\chi(t)]^+ + [\chi(t)]^- = 0$ on L when branch cuts are chosen along the crack lines so that each set of terms in the product behaves as $1/z$ for large z . Equation (88) becomes

$$-\frac{p_2(t) - ip_1(t)}{[\chi(t)]^+} = \left[\frac{\phi'(t)}{\chi(t)} \right]^+ - \left[\frac{\phi'(t)}{\chi(t)} \right]^- \quad \text{on } L \quad (90)$$

Thus, from Sect. II,C, the solution is

$$\phi'(z) = -\frac{\chi(z)}{2\pi i} \int_L \frac{p_2(t) - ip_1(t)}{[\chi(t)]^+ (t - z)} dt + P(z) \chi(z) \quad (91)$$

where $P(z)$ is analytic in the entire plane and thus a polynomial. Since $\chi(z)$ is order $1/z^n$ for large z , the vanishing of stresses at infinity requires $P(z)$ to be of order z^{n-1} :

$$P(z) = A_0 + A_1 z + A_2 z^2 + \dots + A_{n-1} z^{n-1} \quad (92)$$

The solution is completed except for the determination of n complex constants, A_i . These are found by specifying the net Burgers vector for each of the n cracks (that is, the total dislocational displacement discontinuity that occurs when $\partial(u_1 + iu_2)/\partial s$ is integrated on a circuit surrounding each of the cracks). We shall consider dislocation pileup problems in the next part for which these discontinuities are nonzero. The net Burgers vector is taken as zero, implying no residual stress field in the absence of load, for the solutions which follow.

A similar analysis may be carried out for the antiplane strain loading, $\sigma_{23} = -p_3$ on L . The resulting stress function of Eq. (16) is

$$\omega'(z) = -\frac{\chi(z)}{\pi i} \int_L \frac{p_3(t)}{[\chi(t)]^+ (t - z)} dt + Q(z) \chi(z) \quad (93)$$

Here $Q(z)$ is a polynomial of order z^{n-1} with real coefficients, determined by specifying the net Burgers vector in the x_3 direction for each of the n cracks.

2. Finite Crack of Length $2a$

Consider a single crack extending from $-a$ to $+a$ on the x_1 axis. The then constant polynomials P and Q vanish for single-valued displacements and

$$\begin{aligned}\phi'(z) &= -\frac{(z^2 - a^2)^{-1/2}}{2\pi} \int_{-a}^{+a} [p_2(t) - ip_1(t)] (a^2 - t^2)^{1/2} \frac{dt}{t - z} \\ \omega'(z) &= -\frac{(z^2 - a^2)^{-1/2}}{\pi} \int_{-a}^{+a} p_3(t) (a^2 - t^2)^{1/2} \frac{dt}{t - z}\end{aligned}\quad (94)$$

Upon comparing resulting crack tip stresses fields with Eqs. (78), (80), and (82), resulting stress-intensity factors for the crack tip at $x_1 = a$ are

$$\begin{aligned}K_I - iK_{II} &= \frac{1}{(\pi a)^{1/2}} \int_{-a}^{+a} [p_2(t) - ip_1(t)] \left(\frac{a+t}{a-t}\right)^{1/2} dt \\ K_{III} &= \frac{1}{(\pi a)^{1/2}} \int_{-a}^{+a} p_3(t) \left(\frac{a+t}{a-t}\right)^{1/2} dt\end{aligned}\quad (95)$$

A uniform remote stress state (Fig. 5) induces constant tractions in

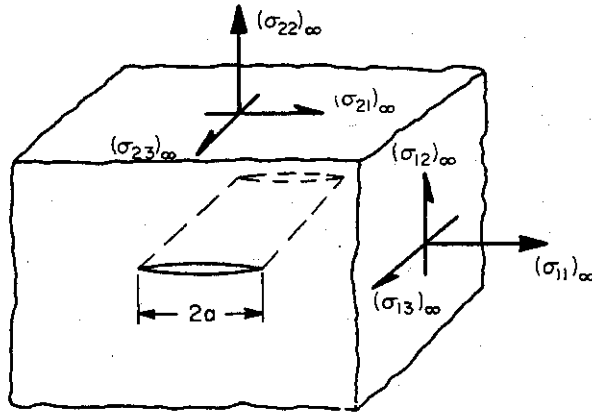


FIG. 5. Crack of length $2a$ in an infinite body subjected to a uniform remote stress state $(\sigma_{ij})_\infty$.

the superposition problem, $p_i(t) = (\sigma_{2i})_\infty$, where $(\sigma_{ji})_\infty$ is the remote stress state. Resulting stress functions from Eqs. (94) are

$$\begin{aligned}\phi'(z) &= \frac{1}{2} [(\sigma_{22})_\infty - i(\sigma_{21})_\infty] [z(z^2 - a^2)^{-1/2} - 1] \\ \omega'(z) &= (\sigma_{23})_\infty [z(z^2 - a^2)^{-1/2} - 1]\end{aligned}\quad (96)$$

The uniform stress field $(\sigma_{ij})_\infty$ must be added to this stress field to solve the problem of Fig. 5. Stress-intensity factors are

$$K_I = (\sigma_{22})_\infty (\pi a)^{1/2}, \quad K_{II} = (\sigma_{21})_\infty (\pi a)^{1/2}, \quad K_{III} = (\sigma_{23})_\infty (\pi a)^{1/2} \quad (97)$$

3. Semi-Infinite Crack

Consider a crack extending from $x_1 = -\infty$ to $x_1 = 0$. The general solution of Eqs. (91) and (93) still apply, except that $\chi(z)$ must be defined as $z^{-1/2}$ (with branch cut on the crack line) and the polynomials taken as zero. Then

$$\phi'(z) = -\frac{z^{-1/2}}{2\pi} \int_{-\infty}^0 [p_2(t) - ip_1(t)] (-t)^{1/2} \frac{dt}{t-z} \quad (98)$$

$$K_I - iK_{II} = \left(\frac{2}{\pi}\right)^{1/2} \int_{-\infty}^0 [p_2(t) - ip_1(t)] \frac{dt}{(-t)^{1/2}}$$

for the inplane modes.

4. Periodic Array of Cracks

Consider an infinite periodic array of cracks of length $2a$ on the x_1 axis, with a center-to-center spacing of $2b$ as shown in Fig. 6, and subjected

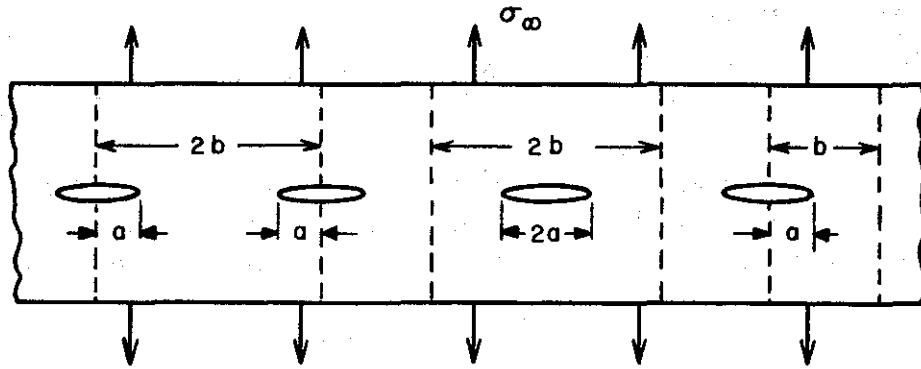


FIG. 6. The periodic array of collinear cracks provides an approximation to the double edge, central, and single edge crack configurations.

to a uniform remote stress state. Following Koiter (1959), the solution of Eq. (91) may be expressed in terms of trigonometric functions after certain identities involving infinite products:

$$\phi'(z) = \frac{1}{2} [(\sigma_{22})_\infty - i(\sigma_{21})_\infty] \{ \sin(\pi z/2b) [\sin^2(\pi z/2b) - \sin^2(\pi a/2b)]^{-1/2} - 1 \} \quad (99)$$

The same result applies for $\omega'(z)$, but with $(\sigma_{23})_\infty$ appearing as in Eqs. (96). The opening mode stress-intensity factor is

$$K_I = (\sigma_{22})_\infty (\pi a)^{1/2} [(2b/\pi a) \tan(\pi a/2b)]^{1/2} \quad (100)$$

and the same factor applies to the isolated crack results of Eqs. (97) for the inplane and antiplane sliding modes. This result forms a useful approximation to the central crack, double edge crack, and single edge crack configurations shown by the dashed line boundaries in Fig. 6. The result is exact for antiplane loadings; the single edge crack in tension provides the worst approximation due to the presence of bending effects. Paris and Sih (1965) compare this result with more exact solutions.

5. Edge Crack in a Half Plane

The effect of a free surface may be seen with reference to an edge crack of depth a along the x_1 axis of a half plane $x_1 > 0$ subjected to a uniform remote stress $(\sigma_{22})_\infty$. The integral formulation above does not apply to this problem, but an exact solution has been given by Koiter (1965) in terms of an integral which, when evaluated numerically, leads to

$$K_I = 1.12(\sigma_{22})_\infty (\pi a)^{1/2} \quad (101)$$

a correction of 12% on the result for the crack of length $2a$ in an infinite body.

6. Penny-Shaped Crack

The axially symmetric problem of a circular crack of radius a in an infinite body has been considered by Sneddon (1946) and, in general form, by Green and Zerna (1954). Near crack tip stresses and displacements are identical to the plane strain results of Eqs. (78) and (79). If the crack is opened with normal tractions $p(r)$ depending only on radial distance from the crack center, the stress-intensity factor is

$$K_I = \frac{2}{(\pi a)^{1/2}} \int_0^a \frac{r p(r)}{(a^2 - r^2)^{1/2}} dr \quad (102)$$

$p(r) = \sigma_\infty$ in the superposition problem for a penny-shaped crack in a remote uniform tensile stress field σ_∞ , and

$$K_I = (2/\pi) \sigma_\infty (\pi a)^{1/2} \quad (103)$$

7. Other Elastic Crack Problems

Irwin (1962) and Kassir and Sih (1966) have discussed the elliptical-shaped crack in a uniform stress field and have given formulas for the variation of K_I with position on the elliptical crack boundary. Plane problems of cracks in rectilinearly anisotropic materials are discussed by Paris and Sih (1965); again, characteristic inverse square

root singularities develop with the dependence of stresses on orientation angle depending on the ratios of elastic constants. Rice and Sih (1965) discuss problems of cracks along the bond line of two different elastic materials. Williams (1961) has shown characteristic inverse square root singularities to result also in thin plate bending problems, and some solutions are given by Sih *et al.* (1962). The further analysis of bending singularities on the basis of a refined plate theory including edge effects is discussed by Knowles and Wang (1960) and Williams (1962).

C. APPROXIMATE METHODS FOR ELASTIC STRESS ANALYSIS OF CRACKS

1. *Boundary Collocation of Stress Functions*

We have seen the general form for inplane stress functions in Eqs. (73) and (75); these equations may be summarized as

$$\phi'(z) = z^{-1/2}f(z) + g(z), \quad \Omega'(z) = z^{-1/2}\bar{f}(z) - \bar{g}(z) \quad (104)$$

where $\Omega(z)$ is defined in Eq. (70) and stresses are given in terms of the complex stress functions by Eqs. (21). Recall that $f(z)$ and $g(z)$ are analytic in the neighborhood of the crack tip. Now consider a finite body containing a straight edge crack; suppose the crack surfaces are free of tractions and that loadings are by prescribed tractions on the remaining portion of the boundary. The most general form for the stress functions then is Eq. (104) above, where $f(z)$ and $g(z)$ are analytic everywhere within the body, including points along the crack line. Any choice of f and g leaves the crack surfaces stressfree, so these functions need be chosen to satisfy boundary conditions on the uncracked portion of boundary only. In a similar way, a slight modification of the approach of the last subsection shows that, for a straight internal crack of length $2a$ in a finite body,

$$\begin{aligned} \phi'(z) &= (z^2 - a^2)^{-1/2}f(z) + g(z), \\ \Omega'(z) &= (z^2 - a^2)^{-1/2}\bar{f}(z) - \bar{g}(z). \end{aligned} \quad (105)$$

Again, f and g are analytic everywhere within the body, including points along the crack line, and any choice for f and g leaves the crack surfaces stress free. Thus, the functions are chosen to satisfy prescribed conditions on the external boundary (and also to result in no net Burgers vector on a circuit surrounding the crack). No general exact methods are available for determination of f and g , but the method of boundary

collocation provides a useful numerical method. Here, one assumes forms for f and g , usually of the polynomial type

$$\begin{aligned} f(z) &= F_0 + F_1 z + \cdots + F_N z^N \\ g(z) &= G_0 + G_1 z + \cdots + G_M z^M \end{aligned} \quad (106)$$

and determines the unknown constants F_i and G_i by matching prescribed stresses at an appropriate number of discrete points on the boundary.

This procedure has been employed by Gross *et al.* (1964) and Gross and Srawley (1965a, 1965b) in the analysis of several fracture testing specimens containing single edge cracks, including the finite width cracked strip subjected to bending and tension. These authors employ a representation of the stress field based on the eigenvalue expansion of Williams (1957), which is equivalent to the complex variable Eqs. (104). While the Williams expansion is not suitable for treating internal cracks, the complex variable form is readily extended to this case, as in Eqs. (105), and has been employed by Kobayashi *et al.* (1964) for the problem of a central crack in a finite width strip. No careful studies on numerical convergence have been carried out, and accuracy must be judged largely by insensitivity of results to the inclusion of more terms and by experience with other configurations.

2. Conformal Mapping

It is well known that any simply connected region can be mapped conformally into a unit circle, and that the plane elasticity problems may be reduced to the solution of a finite set of simultaneous equations, provided the mapping function is expressible as a ratio of polynomials (Muskhelishvili, 1953b; Sokolnikoff, 1956). The difficulties lie in finding a mapping function and in approximating the function by a ratio of polynomials. The procedure of solution is as follows: In the case where tractions are prescribed on the boundary, an integration of the stress Eqs. (21) leads to the boundary condition

$$\phi(z) + z\overline{\phi'(z)} + \overline{\psi(z)} = \int_0^s [iT_1(s) - T_2(s)] ds \quad (107)$$

where T_i are surface tractions, s denotes arc length (increasing in a direction so that the material lies to left of the boundary) and the zero point in the integration may be chosen arbitrarily. Let $z = z_1(\xi)$ map the region into the interior of a unit circle in the ξ plane, and introduce $\phi_1(\xi) = \phi(z)$, $\psi_1(\xi) = \psi(z)$. The boundary condition above then becomes

$$\phi_1(\xi) + \frac{z_1(\xi)}{z_1'(\xi)} \overline{\phi_1'(\xi)} + \overline{\psi_1(\xi)} = \int_0^s [iT_1(s) - T_2(s)] ds \quad (108)$$

Let σ denote boundary values of ξ and call $F(\sigma)$ the integral of surface tractions appearing on the right. Since $\bar{\xi} = 1/\sigma$ on the boundary,

$$\phi_1(\sigma) + \frac{z_1(\sigma)}{\bar{z}_1'(1/\sigma)} \bar{\phi}_1'(1/\sigma) + \bar{\psi}_1(1/\sigma) = F(\sigma) \quad (109)$$

Since $\bar{\psi}_1(1/\xi)$ is analytic outside the unit circle, and $\bar{\psi}_1(0)$ may be chosen to vanish without altering the stress field, an application of the Cauchy integral formula (Eq. (23)) leads to

$$\phi_1(\xi) + \frac{1}{2\pi i} \oint \frac{z_1(\sigma)}{\bar{z}_1'(1/\sigma)} \bar{\phi}_1'(1/\sigma) \frac{d\sigma}{\sigma - \xi} = \frac{1}{2\pi i} \oint F(\sigma) \frac{d\sigma}{\sigma - \xi} \quad (110)$$

Recognizing that $\phi_1(\xi)$ is expressible in a power series form for ξ within the unit circle, the integral on the left side of this equation results in a finite order polynomial in ξ with coefficients depending linearly on a finite number of the coefficients in the power series expansion of $\bar{\phi}_1(\xi)$, when the mapping function $z_1(\xi)$ is a polynomial in ξ . Both sides of Eq. (110) may be expanded in powers of ξ and upon matching coefficients, the first few coefficients in the power series for $\phi_1(\xi)$ are obtained by solving a set of linear simultaneous equations, with remaining coefficients being determined directly. Once $\phi_1(\xi)$ is known, $\psi_1(\xi)$ is obtained directly by applying the Cauchy integral formula to the equation resulting upon equating the complex conjugates of both sides of Eq. (109). A similar but more involved procedure may be employed when the mapping function is a ratio of polynomials (Muskhelishvili, 1953b).

The mapping procedure applies also to the infinite region containing a single interior void, where now the mapping function carries the exterior of the void boundary onto the interior of a unit circle. If stresses are applied at infinity, or if unbalanced forces act on the void surface, or if the Burgers vector for the hole is nonzero, then the functions ϕ_1 and ψ_1 are not analytic within the unit circle. However, these functions can be split into analytic and singular parts; the latter involve the terms $\log \xi$ and $1/\xi$, and their coefficients may be expressed directly in terms of the remote stresses, unbalanced force, and Burgers vector (Sokolnikoff, 1956). The known singular parts may be included into the definition of $F(\sigma)$ in Eq. (109), and the same procedure of solution discussed above applies for the analytic parts. Several problems in plane elasticity, solved through conformal mapping, are discussed in the books by Sokolnikoff (1956), Muskhelishvili (1953b), and Savin (1961). Bowie (1956, 1964) has developed polynomial approximations to actual mapping functions for several crack problems, and has employed methods

discussed here for analysis of a finite strip with symmetric edge cracks and for an edge crack emanating from the boundary of a circular hole in an infinite body. A special feature of his method is that the sharpness of the crack tip is retained in the approximate mapping so that the same inverse square root singularity results.

3. Continuous Dislocation Arrays and Singular Integral Equations

A powerful method of analysis is based on the representation of a crack by a continuous distribution of dislocation singularities. Consider first an isolated straight dislocation line in the x_3 direction and let b_i be the Burgers vector (b_i is the integral of $\partial u_i/\partial s$ taken counterclockwise around the dislocation line). Suppose the dislocation line is at the point t on the x_1 axis. For an infinite body, the solution is found by writing the complex stress functions ϕ , Ω , and ω in the form of constants times $\log(z - t)$, and determining the constants so that displacement discontinuities are correctly given and no net force or moment acts on a region enclosing the dislocation. There results

$$\begin{aligned}\phi'(z) &= \frac{G(b_1 + ib_2)}{i\pi(\kappa + 1)} \frac{1}{z - t} \\ \Omega'(z) &= -\frac{G(b_1 - ib_2)}{i\pi(\kappa + 1)} \frac{1}{z - t} \\ \omega'(z) &= \frac{Gb_3}{2\pi} \frac{1}{z - t}\end{aligned}\quad (111)$$

For a physical dislocation, the plane strain value of $\kappa = 3 - 4\nu$ should be chosen for the inplane (edge dislocation) components b_1 and b_2 . Stresses acting along the x_1 axis are, from Eqs. (16), (21), and (70),

$$\begin{aligned}\sigma_{21}(x_1, 0) &= \frac{2Gb_1}{\pi(\kappa + 1)} \frac{1}{x_1 - t} \\ \sigma_{22}(x_1, 0) &= \frac{2Gb_2}{\pi(\kappa + 1)} \frac{1}{x_1 - t} \\ \sigma_{23}(x_1, 0) &= \frac{Gb_3}{2\pi} \frac{1}{x_1 - t}\end{aligned}\quad (112)$$

To simulate the crack(s) lying along a portion L of the x_1 axis in an infinite body, we introduce a continuous array of dislocations with density functions $\mu_i(t)$, so that $\mu_i(t) dt$ represents the infinitesimal Burgers vector of a dislocation at t . Thus, for example, the continuous

array of dislocations with Burgers vectors in the x_2 direction, as suitable for the mode I tensile case, results in

$$\begin{aligned} \phi'(z) = \Omega'(z) &= \frac{G}{\pi(\kappa + 1)} \int_L \frac{\mu_2(t)}{z - t} dt \\ \sigma_{22}(x_1, 0) &= \frac{2G}{\pi(\kappa + 1)} \int_L \frac{\mu_2(t)}{x_1 - t} dt \\ \sigma_{21}(x_1, 0) = \sigma_{23}(x_1, 0) &= 0 \end{aligned} \tag{113}$$

The last integral is interpreted in the Cauchy principal value sense. Now consider a crack of length $2a$, as in the last subsection, with stresses $\sigma_{22}(x_1, 0) = -p_2(x_1)$ applied to its surface. We solve the problem by choosing $\mu_2(t)$ to satisfy the singular integral equation

$$p_2(t_0) = \frac{2G}{\pi(\kappa + 1)} \int_{-a}^{+a} \frac{\mu_2(t)}{t - t_0} dt, \quad |t_0| < a \tag{114}$$

and the condition of single valued displacements requires that the net Burgers vector be zero

$$\int_{-a}^{+a} \mu_2(t) dt = 0 \tag{115}$$

We have outlined the solution of such integral equations in Sect. II,C. Following that development from Eq. (28)–(34), it is clear that the auxiliary analytic function $f(z)$ introduced there is simply $\phi'(z)/\pi i$, and, on comparing Eq. (33) with the solution to the crack problem given by Eq. (94), it is clear that the singular integral equation leads to the same solution.

Now consider the practical problem of a crack in a body with boundaries a finite distances from the crack line. Let us presume that the solution for the problem of an isolated dislocation in the same body with no crack is known. This solution will contain the singular terms of Eqs. (111) and additional nonsingular terms which are required to satisfy boundary conditions. Note that the nonsingular solution may be obtained by standard techniques such as conformal mapping, where, in order to free the boundaries of stresses, tractions corresponding to the negative of those given by the singular terms are prescribed. Stresses created by the isolated dislocation will contain the singular terms of Eqs. (112) plus nonsingular terms. Limiting attention to symmetrical cases for which an edge dislocation with Burgers vector

in the x_2 direction creates no shear stress on the x_1 axis (the prospective crack line), the stress will have the form

$$\sigma_{22}(x_1, 0) = \frac{2Gb_2}{\pi(\kappa + 1)} \left[\frac{1}{x_1 - t} + \lambda(x_1, t) \right], \quad \sigma_{21} = \sigma_{23} = 0 \quad (116)$$

Thus, for the internal crack of length $2a$ on the x_1 axis subjected to stresses $\sigma_{22}(x_1, 0) = -p_2(x_1)$, the governing integral equation for the dislocation density is

$$p_2(t_0) = \frac{2G}{\pi(\kappa + 1)} \int_{-a}^{+a} \mu_2(t) \left[\frac{1}{t - t_0} - \lambda(t_0, t) \right] dt, \quad |t_0| < a \quad (117)$$

We now follow Muskhelishvili (1953a) in reducing this equation to a regular Fredholm integral equation which may be solved by standard numerical techniques. Temporarily regarding

$$p_2(t_0) + \frac{2G}{\pi(\kappa + 1)} \int_{-a}^{+a} \mu_2(t) \lambda(t_0, t) dt$$

as the prescribed function in the standard form of Eq. (28), $\mu_2(t)$ may be expressed by adopting the general solution of Eq. (34) to the present case (for which $\chi(z) = (z^2 - a^2)^{-1/2}$):

$$\begin{aligned} \frac{2G}{\pi(\kappa + 1)} \mu_2(t_0) = & - \frac{1}{\pi^2(a^2 - t_0^2)^{1/2}} \int_{-a}^{+a} \frac{(a^2 - t^2)^{1/2}}{t - t_0} \left[p_2(t) \right. \\ & \left. + \frac{2G}{\pi(\kappa + 1)} \int_{-a}^{+a} \mu_2(s) \lambda(t, s) ds \right] dt \end{aligned} \quad (118)$$

Here, the constant k of Eq. (34) has been set equal to zero in correspondence with the single valued displacement condition of Eq. (115). Now let

$$r(t) = \frac{2G}{\kappa + 1} \left(\frac{\pi}{a} \right)^{1/2} \mu_2(t) (a^2 - t^2)^{1/2} \quad (119)$$

On comparing the singular crack tip stress field resulting from an inverse square root singularity in dislocation density with Eqs. (78), we find that this function has the special feature of equaling the stress-intensity factor at $x_1 = a$:

$$r(a) = K_I \quad (120)$$

The function $r(t)$ may now be entered as the unknown in the integral equation and there results the Fredholm form

$$r(t_0) + \int_{-a}^{+a} \frac{r(s) \Gamma(t_0, s)}{(a^2 - s^2)^{1/2}} ds = \frac{1}{(\pi a)^{1/2}} \int_{-a}^{+a} \frac{(a^2 - t^2)^{1/2}}{t_0 - t} p_2(t) dt \quad (121)$$

The kernel is obtained by changing the order of integration in Eq. (118) and

$$\Gamma(t_0, s) = \frac{1}{\pi^2} \int_{-a}^{+a} \frac{(a^2 - t^2)^{1/2}}{t - t_0} \lambda(t, s) dt \quad (122)$$

For $\lambda(a, s)$ and $\lambda(-a, s)$ bounded (as must be the case for an internal crack) the kernel Γ is a well-behaved function of t_0 . The singularity in s poses no problem in numerical evaluation, for the substitution $s = a \sin \theta$ results in bounded terms in the integrand. The integral equation may be solved numerically by replacing the integral by a sum based on unknown values of $r(s)$ at discrete points of the integration interval, resulting in a system of linear simultaneous equations, and solutions to any degree of accuracy may be pursued. Thus, we see that the solution of internal crack problems may be made to depend on the solution of the considerably simpler problem of an isolated dislocation, which determines the nonsingular contribution $\lambda(t, s)$ of the dislocation stress field. Methods equivalent to this procedure have been employed by Greif and Sanders (1965) in the analysis of the effect of a reinforcing stringer attached to a cracked sheet and by Bueckner (1960) in discussing several crack problems, including the edge-notched strip in bending.

4. Other Numerical Methods

The methods discussed in this section are sufficient for handling most two-dimensional crack problems of practical interest and, indeed, a large number of solutions are available to date, as indicated by the references. Unfortunately, no methods of comparable usefulness are available for three-dimensional problems. Perhaps the finite element method of structural analysis summarized recently by Argyris (1965) will prove useful for these problems, as the method has been notably successful in dealing with singularities, cases for which finite difference methods are usually inaccurate.

D. ENERGY VARIATIONS IN ELASTIC CRACK PROBLEMS

The computation of the potential energy difference for two otherwise identical elastic bodies with notches of different sizes is discussed in Sect. II,E. The general result is given by Eq. (54), which leads to Eq. (55) in the special case of linear behavior. In both of these formulas, only the traction removal integral over the newly created surfaces contributes for the special case of cracks. Considering the two-dimen-

sional case of a crack along the x_1 axis and calling P the potential energy per unit thickness, Eq. (55) for linear behavior leads to

$$-\frac{dP}{dl} = \lim_{\Delta l \rightarrow 0} \frac{1}{2\Delta l} \int_l^{l+\Delta l} \sigma_{2i}(x_1, 0, l)[u_i^+(x_1, 0, l + \Delta l) - u_i^-(x_1, 0, l + \Delta l)] dx_1 \quad (123)$$

as the limiting form for an energy comparison of a crack of length l with one of length $(l + \Delta l)$. The superscripts plus (+) and minus (−) denote upper and lower crack surfaces. Only the singular terms of Eqs. (78)–(83) contribute in the limit, and there results

$$-\frac{dP}{dl} = \mathcal{G} = \frac{1 - \nu^2}{E} (K_I^2 + K_{II}^2) + \frac{1}{2G} K_{III}^2 \quad (124)$$

Here, we have employed the plane strain value $\kappa = 3 - 4\nu$ in Eqs. (79) and (81); the $1 - \nu^2$ factor should be removed for the plane stress approximation. The symbol \mathcal{G} was introduced by Irwin (1957, 1960), who first derived this formula; we shall use it subsequently to denote the special linear elastic value of $-dP/dl$ above, when discussing nonlinear behavior. This computation has also been discussed by Bueckner (1958) and Sanders (1960). It was shown in Eq. (68) that the energy variation rate could alternately be expressed as the path-independent integral J which for linear behavior has the form

$$J = \int_{\Gamma} (\frac{1}{2}\sigma_{ij}\epsilon_{ij} dx_2 - T_i \partial u_i / \partial x_1 ds) \quad (125)$$

Γ may be chosen as any path surrounding the crack tip. If we take it to be a circle of radius r and let $r \rightarrow 0$, it is clear that only the singular terms of Eqs. (78)–(83) contribute. An explicit calculation based on these singular terms leads to

$$J = \mathcal{G} = \frac{1 - \nu^2}{E} (K_I^2 + K_{II}^2) + \frac{1}{2G} K_{III}^2 \quad (126)$$

and verifies the general proof of equality between J and $-dP/dl$ in Sect. II,E.

The existence of inverse square root singularities in elastic crack problems is understood through energy comparisons. Note that for Γ a circular path in Eq. (125), $dx_2 = r \cos \theta d\theta$ and $ds = r d\theta$. By path independence, J is independent of r . Thus, the coefficient of r in the integrand must be order r^{-1} . But, for a stress singularity of order r^{-n} , this coefficient is order r^{-2n} , so that n must equal $\frac{1}{2}$.

Compliance Methods

We have noted that energy variations are expressible in terms of the change in load deflection curves with increasing notch size, and that, for linear behavior,

$$-\frac{dP}{dl} = \frac{1}{2}Q \frac{\partial q(Q, l)}{\partial l} = -\frac{1}{2}q \frac{\partial Q(q, l)}{\partial l} \quad (127)$$

where Q and q are a generalized force and displacement pair, as in Fig. 1. Since these quantities may be measured experimentally and since the rate of energy decrease is directly related to stress-intensity factors, an experimental method (called the compliance test) may be employed to find the intensity of the crack tip elastic singularity. This method has been discussed by Irwin (1960). Srawley *et al.* (1964) report the results of compliance testing on a single edge-notched tension specimen. The dependence of stress-intensity factors on load-deflection curves also permits approximate strength of materials style calculations. Consider the split rectangular beam of Fig. 7a subjected to end forces Q per unit thickness. Simple beam theory gives

$$q = 8Ql^3/Eh^3 \quad (128)$$

for the separation of the beam arms when the ends at the crack tip are considered clamped.

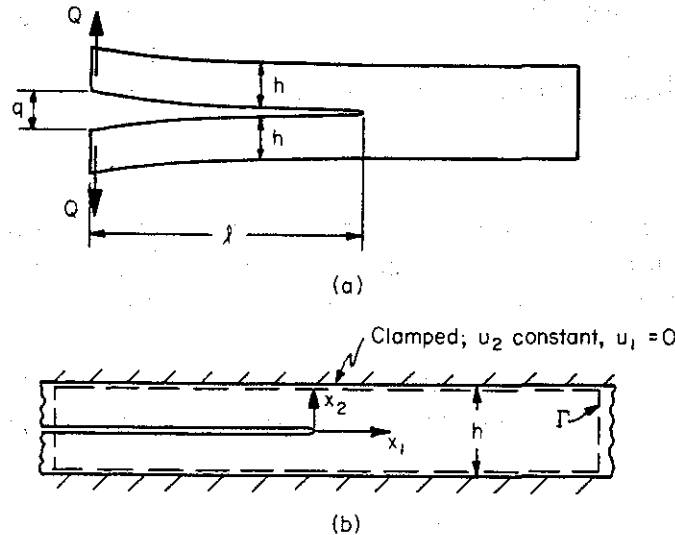


FIG. 7. Near tip stress fields may be determined through energy methods (a) by approximate strength of materials computations as for wedging open a cracked beam, (b) by inspection or application of the path-independent integral, as for the clamped strip with a long crack, and by experimental compliance measurements.

Thus, from Eqs. (124) and (127) with the $(1 - \nu^2)$ dropped, since simple beam theory is plane stress,

$$K_I = 2\sqrt{3}Ql/h^{3/2} \quad (129)$$

Another simple example is afforded by the infinitely long cracked strip with clamped boundaries given constant vertical displacements. Here, it is instructive to employ the path-independent integral J of Eq. (125) evaluated on the dashed-line contour Γ shown. Since dx_2 and $\partial u_i/\partial x_i$ vanish on the clamped boundary and since σ_{ij} and T_i vanish at $x_1 = -\infty$, the entire contribution comes from the portion of Γ at $x_1 = +\infty$. But $\partial u_i/\partial x_1$ vanishes at $x_1 = +\infty$, so that

$$J = \frac{1}{2}(\sigma_{22}\epsilon_{22})_\infty h = \frac{Eh}{2(1 - \nu^2)} (\epsilon_{22})_\infty^2 = \frac{K_I^2}{E} \quad (\text{for plane stress}). \quad (130)$$

E. ELASTIC BRITTLE FRACTURE

We consider here two seemingly different approaches to elastic brittle fracture, the Griffith (1920) theory and an atomic or molecular cohesive force theory as discussed by Barenblatt (1962). By elastic brittle behavior we understand an idealized case in which behavior is elastic up to separation.

1. Griffith Energy Balance

Consider a two-dimensional straight crack configuration and let l be a measure of crack length. We call P_T the total potential energy of the cracked body and follow Griffith in writing this as

$$P_T = P + 2Sl \quad (131)$$

Here, P is the usual potential energy (per unit thickness) of the loaded elastic body and includes both strain energy and the potential of applied loads. The term $2Sl$ is an energy ascribed to the newly created crack faces, where S is the surface energy, so that $2S$ is the work required in the quasistatic direct normal separation of two unit area surfaces. An equilibrium crack length corresponds to a stationary value of the potential energy

$$dP_T/dl = 0, \quad \text{or} \quad -dP/dl = 2S \quad (132)$$

The interpretation of this equation relies on further postulates on the nature of crack extension. If crack extension is considered as fully reversible, one finds that the most common loadings result in the

equilibrium crack length being unstable; cracks could then not exist unless some mechanism is postulated to keep them open under zero load. The more usual interpretation relies on the postulate of preexisting cracks which cannot rebond and shorten in length when loads are removed. In this case, extension may occur when $-dP/dl$ evaluated at the preexisting crack length is sufficiently elevated by increasing load to the critical value of $2S$. Subsequent crack extension may be either stable, in the sense that growth occurs quasistatically under increasing load, or unstable. The equilibrium crack length is unstable and results in a running crack (since shortening is ruled out) when

$$-d^2P_T/dl^2 = -d^2P/dl^2 \geq 0 \quad (133)$$

Presuming loadings are by the tensile mode only, these equations may be expressed in terms of stress-intensity factors through Eq. (124). The critical intensity is

$$K_I = [2ES/(1 - \nu^2)]^{1/2} \quad (134)$$

and the crack extension is unstable if

$$\partial K_I/\partial l \geq 0 \quad (135)$$

An example of an unstable configuration is the crack of length l in a remote tensile field σ_∞ . Then $K_I = \sigma_\infty(\pi l/2)^{1/2}$ and $\partial K_I/\partial l > 0$. Wedge forces P per unit thickness at distance l from the tip of a long crack afford an example of stable extension, for then, from Eq. (98), $K_I = P(2/\pi l)^{1/2}$ and $\partial K_I/\partial l < 0$.

2. Cohesive Forces Model

The Griffith theory ignores the unrealistic prediction of singular stresses at a crack tip and employs an energy balance to obtain a fracture criterion. Another approach to the problem of elastic brittle fracture has been originated in work by Barenblatt (1962). Prospective fracture surfaces ahead of a crack are permitted to separate under loading, with the separation opposed by atomic or molecular cohesive forces. Figure 8 shows a crack with a zone of cohesive forces ahead. The total separation distance between upper and lower crack surfaces is called $\delta = \delta(x_1) = u_2^+(x_1, 0) - u_2^-(x_1, 0)$, and the cohesive restraining stress $\sigma(\delta)$ is shown as a function of δ . The total cohesive zone size is determined from a boundedness condition, so that the positive stress singularity at the outer edge of the cohesive zone is just canceled by the negative singularity due to the cohesive stresses $\sigma(\delta)$ acting in the zone. Consequently, the crack tip closes smoothly and stresses are

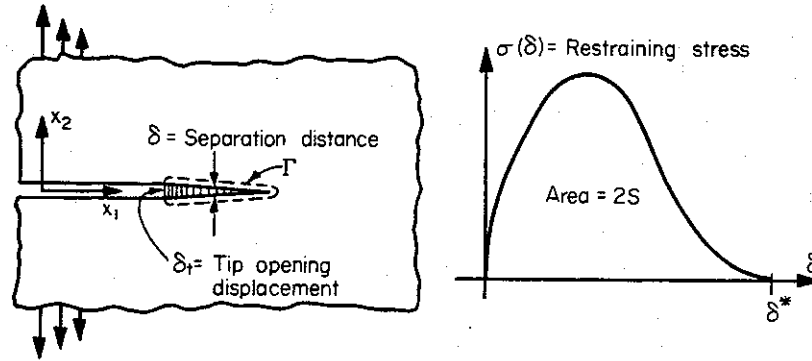


FIG. 8. Cohesive force approach to elastic brittle fracture; area under cohesive stress versus separation distance curve is twice the surface energy.

bounded. Barenblatt (1962) treats the problem through a special postulate on the shape of the deformed surfaces. However, a recent analysis (Rice, 1967a) of the problem employing the path-independent integral J (Eq. (60)) removes this artificial restriction. First note that the proof of path independence in Sect. II,E applies for any group of contours Γ surrounding the crack tip and not passing through the cohesive zone. We therefore make the convenient choice, shown in Fig. 8, of shrinking Γ down to the upper and lower surfaces of the cohesive zone. Since $dx_2 = 0$ for this choice of Γ ,

$$\begin{aligned}
 J &= - \int_{\Gamma} T_i \frac{\partial u_i}{\partial x_1} ds = - \int_{\text{c.z.}} \sigma_{22} \frac{\partial}{\partial x_1} (u_2^+ - u_2^-) dx_1 \\
 &= - \int_{\text{c.z.}} \sigma \frac{\partial \delta}{\partial x_1} dx_1 = - \int_{\text{c.z.}} \frac{\partial}{\partial x_1} \left[\int_0^{\delta} \sigma(\delta) d\delta \right] dx_1 \\
 &= \int_0^{\delta_t} \sigma(\delta) d\delta
 \end{aligned} \tag{136}$$

Here, c.z. stands for the cohesive zone and δ_t is the separation distance at the crack tip. Now let δ^* be the separation distance when the surface atoms can be considered pulled out of the range of cohesive forces. Then the equilibrium condition at which crack extension is just possible corresponds to loads large enough to elevate J to a value corresponding to $\delta_t = \delta^*$:

$$J = \int_0^{\delta^*} \sigma(\delta) d\delta \tag{137}$$

Now let us suppose that the cohesive zone at extension is very small compared to other geometric dimensions of the problem. The integral J

being path independent, we can choose Γ to lie at large distances from the cohesive zone, where the deformation field is indiscernible from the usual elastic solution, which does not consider cohesive forces. Thus, by Eq. (68), J is equal to the potential energy decrease rate of the usual noncohesive elastic solution. Also, by definition of surface energy, the total area under the cohesive stress-separation distance curve is twice the surface energy. We thus see that the cohesive force theory and Griffith theory lead to identical predictions of the equilibrium crack length for small cohesive zones. Predictions of stability for the cohesive model depend on J . If J decreases with increasing crack length, further load is required to achieve $\delta_i = \delta^*$, and we have stability; if J increases, the equilibrium equation (Eq. (136)) cannot be satisfied, and we have instability. Thus, with the equality between J and the energy decrease rate of the noncohesive crack solution, stability predictions are also identical. We conclude that the Griffith and the cohesive force theories are fully identical in their prediction of fracture behavior, so long as the usual condition of a small cohesive zone is met.

F. DYNAMIC SINGULARITIES FOR RUNNING CRACKS

We consider the two-dimensional plane strain problem of a running crack in an elastic material. The displacement vector may be split into irrotational and solenoidal parts by introducing functions $\Phi(x_1, x_2, t)$, $\Psi(x_1, x_2, t)$:

$$u_1 = \frac{\partial \Phi}{\partial x_1} + \frac{\partial \Psi}{\partial x_2}, \quad u_2 = \frac{\partial \Phi}{\partial x_2} - \frac{\partial \Psi}{\partial x_1} \quad (138)$$

The stress equations of motion and isotropic stress-strain relations are satisfied if (Kolsky, 1953)

$$C_d^2 \nabla^2 \Phi = \partial^2 \Phi / \partial t^2, \quad C_s^2 \nabla^2 \Psi = \partial^2 \Psi / \partial t^2 \quad (139)$$

where C_d and C_s are the dilatation and shear wave speeds. We consider the special case of a crack with a tip propagating at constant velocity V in the x_1 direction and introduce the notations (Yoffé, 1951)

$$x = x_1 - Vt, \quad y_d = \alpha_d x_2, \quad y_s = \alpha_s x_2 \quad (140)$$

where

$$\alpha_d^2 = 1 - (V^2/C_d^2), \quad \alpha_s^2 = 1 - (V^2/C_s^2) \quad (141)$$

Then, writing $\Phi_0(x, y_d, t) = \Phi(x_1, x_2, t)$, etc., one obtains

$$\frac{\partial^2 \Phi_0}{\partial x^2} + \frac{\partial^2 \Phi_0}{\partial y_d^2} = \frac{1}{\alpha_d^2 C_d^2} \frac{\partial^2 \Phi_0}{\partial t^2}, \quad \frac{\partial^2 \Psi_0}{\partial x^2} + \frac{\partial^2 \Psi_0}{\partial y_s^2} = \frac{1}{\alpha_s^2 C_s^2} \frac{\partial^2 \Psi_0}{\partial t^2} \quad (142)$$

in the moving coordinate system.

Having compensated for the moving crack boundary, we can obtain the structure of the stress singularity by ignoring the time-derivative terms and seeking appropriate singular solutions of the Laplacian equations

$$\frac{\partial^2 \Phi_0}{\partial x^2} + \frac{\partial^2 \Phi_0}{\partial y_d^2} = 0, \quad \frac{\partial^2 \Psi_0}{\partial x^2} + \frac{\partial^2 \Psi_0}{\partial y_s^2} = 0 \quad (143)$$

These may be solved in a manner analogous to Williams' (1957) treatment of the static case. We suppose the crack tip to be at the origin of the moving coordinate systems and introduce polar coordinates r_d, θ_d and r_s, θ_s where

$$\begin{aligned} r_d e^{i\theta_d} &= x + iy_d = (x_1 - Vt) + i\alpha_d x_2 \\ r_s e^{i\theta_s} &= x + iy_s = (x_1 - Vt) + i\alpha_s x_2 \end{aligned} \quad (144)$$

Then, assuming harmonic solutions of the form

$$\Phi_0 = Ar_d^n \cos n\theta_d, \quad \Psi_0 = -Br_s^n \sin n\theta_s \quad (145)$$

(which give symmetric stresses as appropriate to the tensile mode) one finds that stressfree crack surface boundary conditions result in two linear homogeneous equations for A and B . Setting the determinant of coefficients equal to zero, one finds

$$n = \frac{3}{2}, \quad B = [2\alpha_d/(1 + \alpha_s^2)] A \quad (146)$$

The spatial constant A can only be determined by complete solutions of boundary value problems, but these equations are sufficient to determine the functional form of the near crack tip stress distribution, which is the dynamic analog of Eqs. (78). The resulting near tip field is

$$\begin{aligned} \sigma_{11} &= \frac{3}{4} GA \left[(1 + 2\alpha_d^2 - \alpha_s^2) \frac{\cos(\theta_d/2)}{r_d^{1/2}} - \frac{4\alpha_s\alpha_d}{1 + \alpha_s^2} \frac{\cos(\theta_s/2)}{r_s^{1/2}} \right] \\ \sigma_{12} &= \frac{6}{4} GA\alpha_d \left[\frac{\sin(\theta_d/2)}{r_d^{1/2}} - \frac{\sin(\theta_s/2)}{r_s^{1/2}} \right] \\ \sigma_{22} &= \frac{3}{4} GA \left[-(1 + \alpha_s^2) \frac{\cos(\theta_d/2)}{r_d^{1/2}} + \frac{4\alpha_s\alpha_d}{1 + \alpha_s^2} \frac{\cos(\theta_s/2)}{r_s^{1/2}} \right] \end{aligned} \quad (147)$$

where G is the shear modulus. A dynamic stress-intensity factor may be related to the spatial constant A by

$$K_D = \frac{3(2\pi)^{1/2} G[4\alpha_s\alpha_d - (1 + \alpha_s^2)^2]}{4(1 + \alpha_s^2)} A \quad (148)$$

so that $\sigma_{22} = K_D/(2\pi r)^{1/2}$ directly ahead of the tip, in analogy to the static zero-velocity limit.

Two general types of dynamic problems have been considered. Yoffé (1951) and Craggs (1960) dealt with similar problems, the former with a crack of constant length being opened at one end and closed at the other with constant speed, and the latter with a semi-infinite crack subjected to surface loads with points of application moving at the same speed as the crack. Broberg (1960) and Baker (1962) treat the crack as suddenly opening from zero length and symmetrically growing with constant velocity. Some features of the solutions to these two problem types have been compared by Cotterell (1964). The Yoffé-Craggs solutions result in dynamic stress-intensity factors independent of velocity and thus identical to the corresponding static problems. Employing a Griffith-type theory to predict the load required to maintain a given velocity (Craggs, 1960), their solutions indicate a steady decrease of load to zero at the Rayleigh surface wave velocity (0.91 to 0.95 C_s for typical values of Poisson's ratio). As we shall discuss subsequently, this unacceptable result is related to the neglect of an analysis of how their steady-state condition is achieved. The more realistic Broberg-Baker analysis leads to a dynamic stress-intensity factor whose ratio to the static value for the same crack length decreases to zero at the Rayleigh surface speed (Cotterell, 1964). It is not, however, the Rayleigh speed which sets the practical upper limit on crack velocity. A figure in the neighborhood of half the shear wave speed (and thus, approximately, of the Rayleigh speed) is typical for many brittle materials (Schardin, 1959). Yoffé suggested an explanation on the basis of a bifurcation of the above near crack tip dynamic stress field. She noted that, at approximately half of the shear speed, the angle at which the maximum circumferential stress ($\sigma_{\theta\theta}$ in polar coordinates) occurs shifts from the line in front of the crack to an angle of $\pm 60^\circ$ with the crack line. This observation is consistent with crack branching and the sometimes roughened fracture surface appearance near the terminal speed.

Another result of the near tip stress distribution is the decrease in stress triaxiality in front of the crack with increasing speed. Computing the ratio of principal stresses, σ_{22} perpendicular to the prospective fracture surface and σ_{11} parallel, from Eqs. (147)

$$\frac{\sigma_{22}}{\sigma_{11}} = \frac{4\alpha_s\alpha_d - (1 + \alpha_s^2)^2}{(1 + 2\alpha_d^2 - \alpha_s^2)(1 + \alpha_s^2) - 4\alpha_s\alpha_d} \quad (149)$$

This ratio falls continuously, with increasing velocity, from unity, in the static case, to zero at the Rayleigh speed (defined by the vanishing of the numerator). The drop is initially slow, however, with the ratio

lying between 0.9 and 0.7 in the terminal velocity range of 0.4 to 0.6 times the Rayleigh speed. This drop in stress triaxiality may be at least partly responsible for the increasing fracture toughness at high crack speeds in rate sensitive ductile materials which exhibit an initial embrittlement with load rates (Eftis and Krafft, 1965). Returning to the Craggs–Yoffé analysis and their predicted drop in required load with increasing velocity, it is clear that, since the dynamic stress-intensity factor is speed-independent in their solution, σ_{22} will be finite for any finite load. Since the stress ratio approaches zero at the Rayleigh speed, σ_{11} would become infinite, and any finite region near the crack tip would have an infinite strain energy (and kinetic energy). Essentially, then, their result simply says that if a cracked body has an enormous amount of energy near the tip, very little load is required to maintain the crack speed. Thus, the important point in interpreting such steady-state solutions is the question as to how the energy content was achieved. The Broberg–Baker solution provides a mechanism by starting from zero crack size in a static stress field. Indeed, the dynamic stress-intensity factor (and thus σ_{22}) drops to zero at the Rayleigh speed in their solution, as noted above.

G. STRESS CONCENTRATIONS AND ENERGY VARIATIONS FOR NOTCHES

1. *Elliptical Hole*

Consider the elliptical hole, of semiaxes a in the x_1 direction and b in the x_2 direction, in an infinite plane subjected to remote biaxial inplane tensions $(\sigma_{11})_\infty$, $(\sigma_{22})_\infty$ and antiplane shear $(\sigma_{23})_\infty$ (Fig. 9). The inplane problem is readily solved by the conformal mapping procedures of Sect. III,C, on noting (Sokolnikoff, 1956) that a transformation of the form $z(\xi) = C_1\xi + C_2/\xi$ carries the exterior of the ellipse onto the interior of a unit circle. A similar, but easier, method of solution may be developed for the antiplane problem. Resulting stresses at the end of the semiaxis of length a are

$$\begin{aligned}\sigma_{22}(a, 0) &= (\sigma_{22})_\infty [1 + 2(a/b)] - (\sigma_{11})_\infty \\ &= (\sigma_{22})_\infty [1 + 2(a/r_t)^{1/2}] - (\sigma_{11})_\infty\end{aligned}\tag{150}$$

$$\sigma_{23}(a, 0) = (\sigma_{23})_\infty [1 + (a/b)] = (\sigma_{23})_\infty [1 + (a/r_t)^{1/2}]$$

where $r_t = b^2/a$ is the root radius of curvature. Aside from the stress concentration on the notch surface, another feature of the solution is the rapid rise of σ_{11} from zero at the surface, creating a high stress triaxiality for plane strain conditions. In the limiting case of a crack,

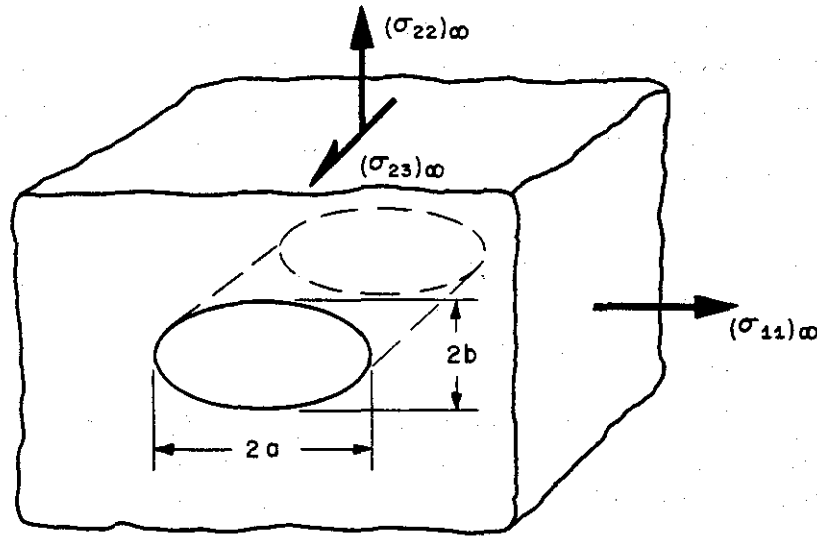


FIG. 9. Elliptical hole in an infinite body; uniform remote stresses.

Eqs. (78), $\sigma_{11} = \sigma_{22}$ directly ahead of the tip. The solution for an ellipsoidal cavity has been given by Sadowsky and Sternberg (1949) and many other notch stress concentrations are discussed in the books by Neuber (1937), Savin (1961), and Peterson (1953).

2. Energy Comparisons

The general results on energy comparisons of Sect. II,E serve as a technique for the approximate estimation of stress-concentration factors. First, we obtain estimates of how much potential energy decrease rates for notches differ from those for cracks of similar size. Consider the general case of an ellipsoidal cavity, with semiaxes a, b, c , in a uniform remote stress field $(\sigma_{ij})_{\infty}$. The linear elastic result of Eq. (55) may be employed, taking the state $\sigma_{ij}^0, \epsilon_{ij}^0$ to denote the uniform deformation field with no cavity present and the state $\sigma_{ij}^0 + \Delta\sigma_{ij}, \epsilon_{ij}^0 + \Delta\epsilon_{ij}$ to denote the field after introducing the cavity. Then T_i^0 of Eq. (55) equals $(\sigma_{ij})_{\infty} n_j$ on the cavity surface ΔS , where the unit normal points into the cavity. Now we employ a special feature of the problem of an ellipsoidal inclusion in an infinite body (the cavity being a limiting case of an inclusion with zero elastic moduli). As Eshelby (1957) has noted, strains are constant in the inclusion. Thus, surface displacements of points on the ellipsoidal boundary are given by (except for an unessential rigid body translation and rotation)

$$u_i^0 + \Delta u_i = \epsilon_{ij}^0 x_j \quad (151)$$

where the symmetric set of constants ϵ_{ij}^v are the strains in the imagined zero moduli inclusion. These may be determined in a simple way from known values of stress concentrations at the semiaxes, for the "inclusion" strains must be compatible with strains on the void boundary. Equation (55) then becomes, for the potential energy reduction due to introducing the cavity,

$$\begin{aligned} -\Delta P &= \frac{1}{2} \int_{\Delta V} (\sigma_{ij})_{\infty} (\epsilon_{ij})_{\infty} dV - \frac{1}{2} \int_{\Delta S} (\sigma_{ij})_{\infty} n_j [\epsilon_{ik}^v - (\epsilon_{ik})_{\infty}] x_k dS \\ &= \frac{1}{2} (\sigma_{ij})_{\infty} \epsilon_{ij}^v \Delta V = \frac{2}{3} \pi abc (\sigma_{ij})_{\infty} \epsilon_{ij}^v \end{aligned} \quad (152)$$

Presuming only the inplane components $(\sigma_{11})_{\infty}$, $(\sigma_{22})_{\infty}$ to act on the two-dimensional configuration of Fig. 9, matching void strains with surface strains under plane strain conditions leads to

$$\begin{aligned} \epsilon_{11}^v &= \frac{1-\nu^2}{E} \sigma_{11}(0, b), & \epsilon_{22}^v &= \frac{1-\nu^2}{E} \sigma_{22}(a, 0) \\ \epsilon_{12}^v &= \epsilon_{13}^v = \epsilon_{23}^v = 0 \end{aligned} \quad (153)$$

Now, defining P as the potential energy per unit thickness, writing the two-dimensional version of Eq. (152), and employing the stress concentration Eq. (150) for $\sigma_{22}(a, 0)$ and a similar equation for $\sigma_{11}(0, b)$, the reduction in energy due to introduction of the elliptical hole is

$$\begin{aligned} -\Delta P &= \frac{1}{2} (\sigma_{ij})_{\infty} \epsilon_{ij}^v \Delta A = \frac{1}{2} \pi ab (\sigma_{ij})_{\infty} \epsilon_{ij}^v \\ &= \frac{\pi(1-\nu^2)}{E} \{ (\sigma_{22})_{\infty}^2 a^2 + (\sigma_{11})_{\infty}^2 b^2 + \frac{1}{2} [(\sigma_{22})_{\infty} - (\sigma_{11})_{\infty}]^2 ab \} \end{aligned} \quad (154)$$

If we let $l = 2a$ denote the total length of the elliptical hole in the x_1 direction and call $-dP/dl$ the rate of energy variation with respect to notch length when the thickness b is held constant,

$$-\frac{dP}{dl} = -\frac{1}{2} \frac{\partial(\Delta P)}{\partial a} = \frac{\pi(1-\nu^2)}{E} \{ (\sigma_{22})_{\infty}^2 a + [(\sigma_{22})_{\infty} - (\sigma_{11})_{\infty}]^2 b/4 \} \quad (155)$$

Comparing with the case of a crack ($b = 0$),

$$-\frac{dP}{dl} = \frac{\pi(1-\nu^2)}{E} (\sigma_{22})_{\infty}^2 a \quad (156)$$

(which could have been independently written from Eqs. (124) and (97)), there is seen to be no effect of notch thickness when the remote stress

is equal biaxial tension. For uniaxial remote stress, the energy decrease rate is the same as for a slightly longer crack with effective half length

$$a_{\text{eff}} = a[1 + (b/4a)] \quad (157)$$

A similar slight effect of notch thickness was found by Bowie and Neal (1967). They considered a flat surfaced edge notch with semi-circular tip in a semi-infinite plane and independently derived the linear elastic version of our Eq. (59). Employing a variation of the approximate conformal mapping procedure of Sect. III,C, they found an energy release rate corresponding to the edge crack stress-intensity factor of Eq. (101), but with an effective crack depth (to within 1%).

$$a_{\text{eff}} = a(1 + 0.18r_t/a) \quad (158)$$

where r_t is root radius and a is the total notch depth. Starting from Eq. (152), a similar result could be established for the effective penny-shaped crack radius of an axially symmetric ellipsoidal void. The last two equations show that energy rates for cracks differ little from those for notches of comparable length and position, with corrections which are not large, even for circular holes, and which become negligible for narrow notches (say, a/b or $a/r_t > 4$). Thus, compliance tests to determine stress-intensity factors may accurately be carried out with machined notches (as is generally the case). Also, as suggested by Bowie and Neal, photoelastic analyses may be employed to determine the surface strain energy density of smooth ended notches, so as to compute energy rates from Eqs. (58) and (59), and thus crack tip stress-intensity factors.

3. Approximate Estimates of Stress Concentrations

We can reverse the viewpoint above and regard the energy variation rate as known for narrow notches, either from a solution of the related crack problem or from compliance methods, and use the relation between energy rate and surface strain energy to estimate stress concentrations. For example, with a narrow flat-surfaced notch in a two-dimensional plane strain deformation field, Eq. (59) and the approximation of the energy rate as the value for a similarly loaded body with a crack of the same length leads to

$$\begin{aligned} \frac{(1 - \nu^2) K_I^2}{E} &= \frac{1}{2} \frac{1 - \nu^2}{E} \int_{r_t} \sigma^2 dx_2 \\ &= \frac{1}{2} \frac{1 - \nu^2}{E} \int_{-\pi/2}^{+\pi/2} \sigma^2(\phi) r_t(\phi) \cos \phi d\phi \end{aligned} \quad (159)$$

Here, σ is the surface stress, Γ_t denotes the curved notch tip, ϕ is the tangent angle, and $r_t(\phi)$ is the radius of curvature, as in Fig. 10. Now, if an approximate form containing an unknown constant is chosen for the dependence of the surface stress on orientation angle ϕ , the equation serves to evaluate the constant and thus to estimate the maximum stress.

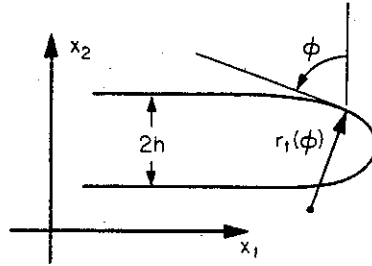


FIG. 10. Coordinates employed for description of notch surface; ϕ is tangent angle and $r_t(\phi)$ is radius of curvature.

In view of the result noted by Eshelby for ellipsoidal inclusions, it is reasonable to approximate surface strains on the notch tip as being compatible with the homogeneous deformation of an imagined zero moduli inclusion. Calling ϵ_{\max} the surface strain at $\phi = 0$, the inclusion strain is taken as $\epsilon_{22}^v = \epsilon_{\max}$, with all other components vanishing. Compatibility of strains on the notch boundary then leads to the approximation for surface strains

$$\epsilon(\phi) \approx \epsilon_{\max} \cos^2 \phi \quad (160)$$

The corresponding approximation for surface stresses, $\sigma(\phi) \approx \sigma_{\max} \cos^2 \phi$, when inserted into Eq. (159) then leads to the approximate maximum concentrated stress

$$\sigma_{\max} \approx \frac{\sqrt{2} K_I}{\left[\int_{-\pi/2}^{+\pi/2} r_t(\phi) \cos^5 \phi d\phi \right]^{1/2}} = \left(\frac{15}{8} \right)^{1/2} \frac{K_I}{r_t^{1/2}} \quad (161)$$

the later form applying to the case of a semicircular tip $r_t(\phi) = r_t$, a constant. As an example, for a narrow flat-surfaced notch of length $2a$ and semicircular tip in an infinite body subject to a remote stress $(\sigma_{22})_{\infty}$, $K_I = (\sigma_{22})_{\infty} (\pi a)^{1/2}$ from Eq. (97), and

$$\sigma_{\max} \approx \left(\frac{15\pi}{8} \right)^{1/2} (\sigma_{22})_{\infty} \left(\frac{a}{r_t} \right)^{1/2} = 2.43 (\sigma_{22})_{\infty} \left(\frac{a}{r_t} \right)^{1/2} \quad (162)$$

Equation (159) also sets an absolute lower bound on the maximum

stress arising at the tip of a narrow flat-surfaced notch, for applying the inequality $\sigma \leq \sigma_{\max}$ leads to

$$K_I^2 \leq \frac{1}{2} \sigma_{\max}^2 \int_{\Gamma_t} dx_2 = \sigma_{\max}^2 h, \quad \text{or} \quad \sigma_{\max} \geq \frac{K_I}{h^{1/2}} \quad (163)$$

where (Fig. 10) h is the half thickness of the notch. Thus, for example, with the narrow notch of length $2a$ in a remote stress field $(\sigma_{22})_{\infty}$,

$$\sigma_{\max} \geq \pi^{1/2} (\sigma_{22})_{\infty} (a/h)^{1/2} \quad (164)$$

regardless of the shape of the notch tip.

IV. Plasticity in the Analysis of Deformation and Fracture

Elastic-plastic and fully plastic analyses are required both for the better understanding of fracture at the conventional macroscopic continuum level and for the relation of macroscopic analyses to the mechanics of brittle and ductile separation processes operative on the microscale. In contrast to elastic fracture mechanics, methods of analysis in the inelastic range are much less developed. Thus, results presented in this part are, in places, tentative and incomplete. Nevertheless, some significant advances have been made and the increased understanding of fracture accompanying current and future developments will likely be great.

A. SMALL-SCALE YIELDING NEAR CRACKS AND NOTCHES

Consider a loaded elastic-plastic body containing a crack or narrow notch, as in Fig. 11a, and suppose the load level is sufficiently low so that the yielded zone at the tip is small compared to characteristic geometric dimensions such as notch length, unnotched width, etc. The situation envisioned here has been termed "small-scale yielding" and is the situation in which linear elastic stress-intensity factors form a useful measure of the intensity of the surrounding elastic field (Sect. III,A). A special boundary layer formulation is then possible for determination of the near tip elastic-plastic field (Rice, 1966b, 1967b,c). First recall that when the notch is presumed to be a sharp crack, the near tip field from a linear elastic analysis has the form, in the case of tensile mode I loadings as in Fig. 11a,

$$\sigma_{ij} = \frac{K_I}{(2\pi r)^{1/2}} f_{ij}(\theta) + \text{other terms bounded at the crack tip} \quad (165)$$

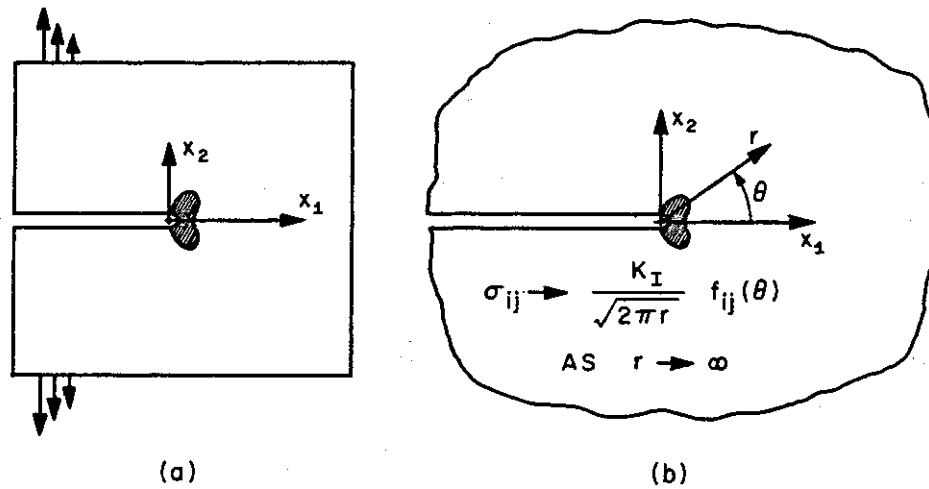


FIG. 11. (a) Small-scale yielding near a narrow notch or crack. (b) The actual configuration is replaced by a semi-infinite notch in an infinite body; actual boundary conditions are replaced by the requirement of an asymptotic approach to the linear elastic crack tip stress field.

Here, the set of functions $f_{ij}(\theta)$ are as in Eqs. (78), and are the same for all symmetrically loaded crack configurations. Now consider the material as elastic-plastic and the notch either a sharp crack or a narrow void. One anticipates that the elastic singularity governs stresses at distances from the notch tip that are large compared to the (small) yield zone and root radius dimensions, but still small compared to characteristic geometric dimensions such as notch length. Then the statement that the elastic singularity governs may be expressed in a formal way by saying that the actual configuration (Fig. 11a) may be replaced by a notch of semi-infinite length in an infinite body (Fig. 11b), and the actual boundary conditions may be replaced by the boundary-layer type requirement of an asymptotic approach to the elastic singularity stress distribution at large distances. That is,

$$\sigma_{ij} \rightarrow \frac{K_I}{(2\pi r)^{1/2}} f_{ij}(\theta) \quad \text{as } r \rightarrow \infty \quad (166)$$

where K_I is the stress-intensity factor for the associated elastic crack problem. Such small-scale yielding solutions for cracks are mathematically exact only in the limit of a vanishingly small plastic zone. But small-scale yielding solutions have been found to be highly accurate approximations to available complete solutions up to substantial fractions (typically, one-half) of general yielding loads (Rice, 1967b).

Recall that we have introduced the path-independent integral J ,

$$J = \int_{\Gamma} (W dx_2 - \mathbf{T} \cdot \partial \mathbf{u} / \partial x_1 ds) \quad (167)$$

for two-dimensional deformation fields in Sect. II,E. The proof of path independence applies strictly to paths Γ surrounding the notch tip in elastic material outside the plastic zone. Path independence results also for paths passing through the plastic zone when a deformation plasticity theory, which is really nonlinear elasticity, is employed. Let us take Γ to be a circle of radius r lying outside the plastic zone in Fig. 11b. We can let $r \rightarrow \infty$ without altering the value of the integral. Since both W and $\mathbf{T} \cdot \partial \mathbf{u} / \partial x_1$ are of quadratic order in stresses in the linear elastic portions of material, and since $dx_2 = r \cos \theta d\theta$ and $ds = r d\theta$, only the asymptotically approached inverse square-root stress distribution need be taken into account for evaluating the integral. Thus, J has the same value in the small-scale yielding solution as it has for the linear elastic crack solution, namely

$$J = (1 - \nu^2) K_I^2 / E \quad (168)$$

for plane strain tensile mode loadings (compare Eq. 126)). The more general result for small-scale yielding involving the inplane or antiplane sliding modes of loading, or for combined mode loadings, is that

$$J = \mathcal{G} \quad (169)$$

where \mathcal{G} is Irwin's linear elastic energy rate, given in terms of stress-intensity factors in Sect. III,D. We shall see that the choice of special integration paths for the integral J , along with the fact that its value is known, provides a useful tool for elastic-plastic analysis.

Employment of the path-independent integral also provides a useful technique in situations involving large-scale plastic yielding. Although its value is not then known, we can, within the approximation of a deformation theory, fall back on the physical interpretation in terms of an energy comparison for similarly loaded bodies containing notches of neighboring sizes. This interpretation justifies approximate calculations as, for example, in connection with the two configurations of Fig. 7. Highly simplified elastic-plastic models may also be suitable. For, even though the solution would then be wrong in detail, one might confidently expect accurate predictions of a gross feature of the solution such as the energy rate.

B. CRACKS IN ELASTIC-PLASTIC ANTIPLANE STRAIN FIELDS

Cracks opened by tensile mode I loadings are of primary interest in the mechanics of fracture. Mathematical difficulties have to date prevented a detailed treatment of elastic-plastic problems in this case. The same is not so for the antiplane mode III loading of cracks and a number of solutions (Hult and McClintock, 1956; Neuber, 1961; Rice, 1966b, 1967c) have been obtained for this class of problems, including both perfectly plastic and strain-hardening behavior. While the precise relevance to tensile problems is uncertain, McClintock and Irwin (1965) have pointed out that several observed features of tensile crack extension are anticipated from antiplane solutions.

1. Perfect Plasticity

We have reviewed the general construction of plastic region stress fields and the form of displacement increment relations for the antiplane straining of an isotropic perfectly plastic material in Sect. II,D. Thus, following Hult and McClintock (1956), stresses are constant along radial

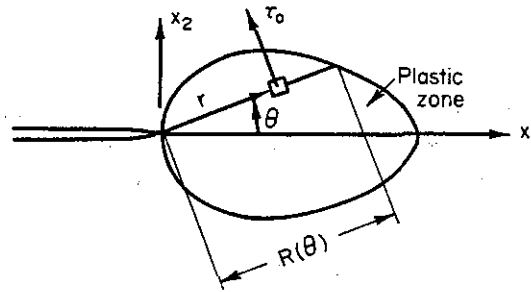


FIG. 12. Antiplane deformation of a perfectly plastic material; $\sigma_{3\theta} = \tau_0$ throughout plastic zone. $R(\theta)$ is distance to elastic-plastic boundary.

lines in a plastic zone adjacent to a crack tip, as in Fig. 12. In polar coordinates, the lines $\theta = \text{constant}$ are the α lines of Sect. II,D and

$$\sigma_{3\theta} = \tau_0, \quad \sigma_{3r} = 0 \quad (170)$$

where τ_0 is the yield stress in shear. Antiplane displacement increments du_3 in the course of loading are thus also constant along the radial lines, from Eq. (49), so that $u_3 = u_3(\theta)$ in the plastic region for monotonic loading. Introducing the "engineering" shear strains, calling $R(\theta)$ the distance to the elastic-plastic boundary as in Fig. 12, and noting that $\gamma_{3\theta} = \gamma_0 = \tau_0/G$ (the initial yield strain) on the boundary,

$$\gamma_{3\theta} = \frac{1}{r} \frac{\partial u_3}{\partial \theta} = \gamma_0 \frac{R(\theta)}{r}, \quad \gamma_{3r} = \frac{\partial u_3}{\partial r} = 0 \quad (171)$$

In terms of distance to the elastic-plastic boundary, displacements in the plastic region are thus given by

$$u_3 = u_3(\theta) = \gamma_0 \int_0^\theta R(\beta) d\beta \quad (172)$$

where we take the displacement as zero on the line ahead of the crack. Note that the displacement is discontinuous at the crack tip and a total opening displacement δ_t results where

$$\delta_t = u_3(\pi/2) - u_3(-\pi/2) = \gamma_0 \int_{-\pi/2}^{+\pi/2} R(\beta) d\beta \quad (173)$$

The plastic region solution is completed once the distance $R(\theta)$ to the boundary is known. This must be chosen in such a way that a linear elastic stress field exists, nowhere violating yield and in satisfaction of prescribed loads and certain continuity conditions (Prager and Hodge, 1951) on the elastic-plastic boundary. From Sect. II, B, stresses in the elastic region are representable in terms of an analytic function of $z = x_1 + ix_2$ as

$$\sigma_{32} + i\sigma_{31} = \omega'(z) \quad (174)$$

We may profitably change our point of view, now, and regard this equation as saying that z is an analytic function of $\sigma_{32} + i\sigma_{31}$ in the elastic region. Equivalently, $x_1 - ix_2$ is an analytic function of $\sigma_{32} - i\sigma_{31}$, which we write as

$$x_1 - ix_2 = F(\xi) \quad (175)$$

where F is analytic and the dimensionless stress ξ is

$$\xi = (\sigma_{32} - i\sigma_{31})/\tau_0 \quad (176)$$

This transformation is especially effective since the unknown elastic-plastic boundary maps into a portion of a unit circle in the ξ plane. Boundary conditions on $F(\xi)$ along the elastic-plastic boundary are obtained by noting, in reference to Fig. 12, that $\xi = e^{i\theta}$ at a point on the boundary with polar coordinate θ and that $x_1 - ix_2 = R(\theta)e^{-i\theta}$ at that point. Thus, we have

$$R(\theta) = e^{i\theta}F(e^{i\theta}) \quad (177)$$

as a formula for distance to the boundary once $F(\xi)$ is known, and, since $R(\theta)$ must be real, we have the boundary condition

$$\text{Im}\{e^{i\theta}F(e^{i\theta})\} = 0 \quad (178)$$

along the unit arc map of the elastic-plastic boundary in the ξ plane.

2. Small-Scale Yielding Solution for Perfect Plasticity

In accord with the discussion of Sect. IV,A, we obtain the small-scale yielding solution by viewing a crack as semi-infinite and by imposing asymptotic boundary conditions of an approach to the mode III elastic singularity. From Eqs. (77) and (82), the asymptotic condition becomes, with reference to Fig. 13a,

$$\sigma_{32} + i\sigma_{31} \rightarrow \frac{K_{III}}{(2\pi z)^{1/2}} \quad \text{as } |z| \rightarrow \infty \quad (179)$$

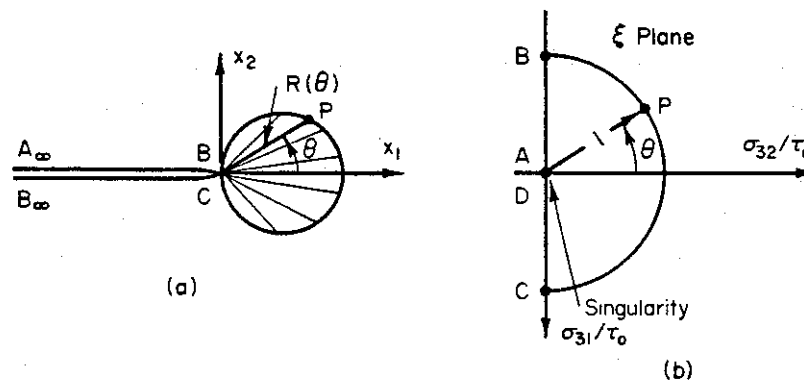


FIG. 13. Small-scale yielding solution for elastic-perfectly plastic antiplane strain. (a) Physical plane. (b) Map of elastic region of physical plane onto interior of unit semicircle in stress plane, with corresponding points as labeled.

where K_{III} is the stress-intensity factor from a linear elastic solution to the crack problem. This condition may be expressed in terms of $F(\xi)$ of Eq. (175) as

$$x_1 - ix_2 = F(\xi) \rightarrow \frac{K_{III}^2}{2\pi\tau_0^2\xi^2} \quad \text{as } |\xi| \rightarrow 0 \quad (180)$$

The map of the physical x_1x_2 plane of Fig. 13a into the ξ plane is shown in Fig. 13b. Points at infinity map into the origin of the ξ plane, the elastic-plastic boundary maps into a unit semicircle, and the crack surfaces map into the imaginary ξ axis, all as shown. Since $x_2 = 0$ on the crack surfaces, $F(\xi)$ must be real on the imaginary ξ axis. A solution satisfying this condition, as well as Eq. (178) on the elastic-plastic boundary, and which correctly gives the asymptotic behavior as required by Eq. (180), is

$$F(\xi) = \frac{K_{III}^2}{2\pi\tau_0^2} \left(1 + \frac{1}{\xi^2}\right) \quad (181)$$

The resulting distance $R(\theta)$ to the elastic-plastic boundary is obtained from Eq. (177) as

$$R(\theta) = R_0 \cos \theta, \quad \text{where } R_0 = \frac{K_{III}^2}{\pi\tau_0^2} \quad (182)$$

The plastic zone is a circle (as shown in Fig. 13a) of diameter R_0 . Resulting strains and displacements within the plastic zone and crack opening displacement are

$$\begin{aligned} \gamma_{3\theta} &= \frac{K_{III}^2}{\pi G \tau_0} \frac{\cos \theta}{r}, & \gamma_{3r} &= 0 \\ u_3 &= \frac{K_{III}^2}{\pi G \tau_0} \sin \theta, & \delta_t &= \frac{2K_{III}^2}{\pi G \tau_0} = 2\gamma_0 R_0 \end{aligned} \quad (183)$$

Solving for stresses in the elastic region, from Eqs. (175) and (181),

$$\sigma_{32} + i\sigma_{31} = K_{III} \left[2\pi \left(z - \frac{K_{III}^2}{2\pi\tau_0^2} \right) \right]^{-1/2} \quad (184)$$

and we see that the effect of yielding is to create a stress field identical to the characteristic elastic singularity field, but shifted ahead by half the plastic zone diameter as if the crack tip were at the center of the plastic zone. This interpretation was first noted by Irwin and Koskinen (1963).

3. Complete Solutions for Perfect Plasticity

The small-scale yielding approximation becomes poor at load levels inducing plastic zones comparable to characteristic geometric dimensions, and recourse must be made to complete solutions. These have been given by Hult and McClintock (1956) for an edge crack in a semi-infinite plane subjected to a uniform remote stress state, and by Rice (1966b) for an edge crack in a finite-width plane. The latter solution applies also to the antiplane versions of the double edge, internal, and periodic array crack configurations shown in Fig. 6. Employing the same notation of a for crack length and b for plane width, the mode III elastic stress-intensity factor for a uniform remote antiplane shear stress is

$$K_{III} = \tau_\infty (\pi a)^{1/2} [(2b/\pi a) \tan(\pi a/2b)]^{1/2} \quad \text{where } \tau_\infty = (\sigma_{32})_\infty \quad (185)$$

and low stress level solutions are obtained through the above small yielding results with this value of K_{III} . The method of obtaining the complete solution parallels the small-scale yielding procedure. The elastic region of the physical plane is mapped into the ξ (dimen-

sionless stress) plane. Again, the elastic-plastic boundary maps into a unit semicircle and crack surfaces map into the imaginary ξ axis, as in Fig. 13b. But now the mapping is somewhat complicated by the x_2 direction surfaces of the finite-width plane transforming into a slit extending out from the origin along the real ξ axis. Boundary conditions are set on $F(\xi) = (x_1 - ix_2)$ and the problem is reduced to a standard type which can be solved by conformal transformation of the slit semicircle onto a semicircle with no slit, the latter configuration being one for which Laplacian equations are readily solved. We shall discuss a similar procedure in connection with strain hardening below, and therefore only note results here.

For the special case of an edge crack in a semi-infinite plane ($b = \infty$), resulting expressions for the length R_0 , over which the plastic zone extends in front of the crack, and for the crack opening displacement δ_t , are (Rice, 1966b)

$$R_0 = a \left[\frac{2}{\pi} \frac{1+s^2}{1-s^2} E_2 \left(\frac{2s}{1+s^2} \right) - 1 \right] \quad (186)$$

$$\delta_t = 2\gamma_0 a \left[\frac{2}{\pi} (1+s^2) E_1(s^2) - 1 \right]$$

where $s = \tau_\infty/\tau_0$, and E_1 and E_2 are complete elliptic integrals of the first and second kind, respectively. These may be shown to reduce to the small scale yielding results at low stress levels when terms of order s^2 are negligible compared to unity. The plastic zone elongates from the circular shape at higher stress levels, much as in Fig. 12, and at the limit load the zone extends to infinity in the x_1 direction with a height in the x_2 direction which asymptotically approaches $4a/\pi$. Figures 14 and 15 show numerical results for this case as well as for finite-width planes with ratios a/b of crack length to plane width equal to 1/5 and 3/5. The graphs show the dimensionless plastic zone size and opening displacement

$$\frac{R_0}{a} \frac{(\pi a/2b) \operatorname{ctn}(\pi a/2b)}{(1-a/b)^2} \quad \text{and} \quad \frac{\delta_t}{2\gamma_0 a} \frac{(\pi a/2b) \operatorname{ctn}(\pi a/2b)}{(1-a/b)^2}$$

as a function of the ratio of net section stress to yield stress, τ_n/τ_0 , where $\tau_n = \tau_\infty(1-a/b)^{-1}$ is the average stress on the uncracked width. These particular dimensionless combinations are chosen since both equal $(\tau_n/\tau_0)^2$ for any ratio of a/b , according to the small-scale yielding solution with stress-intensity factor as given by Eq. (185). The small-scale yielding results are shown by the dashed lines in both graphs. The factor depending on the ratio of a to b in the above dimensionless

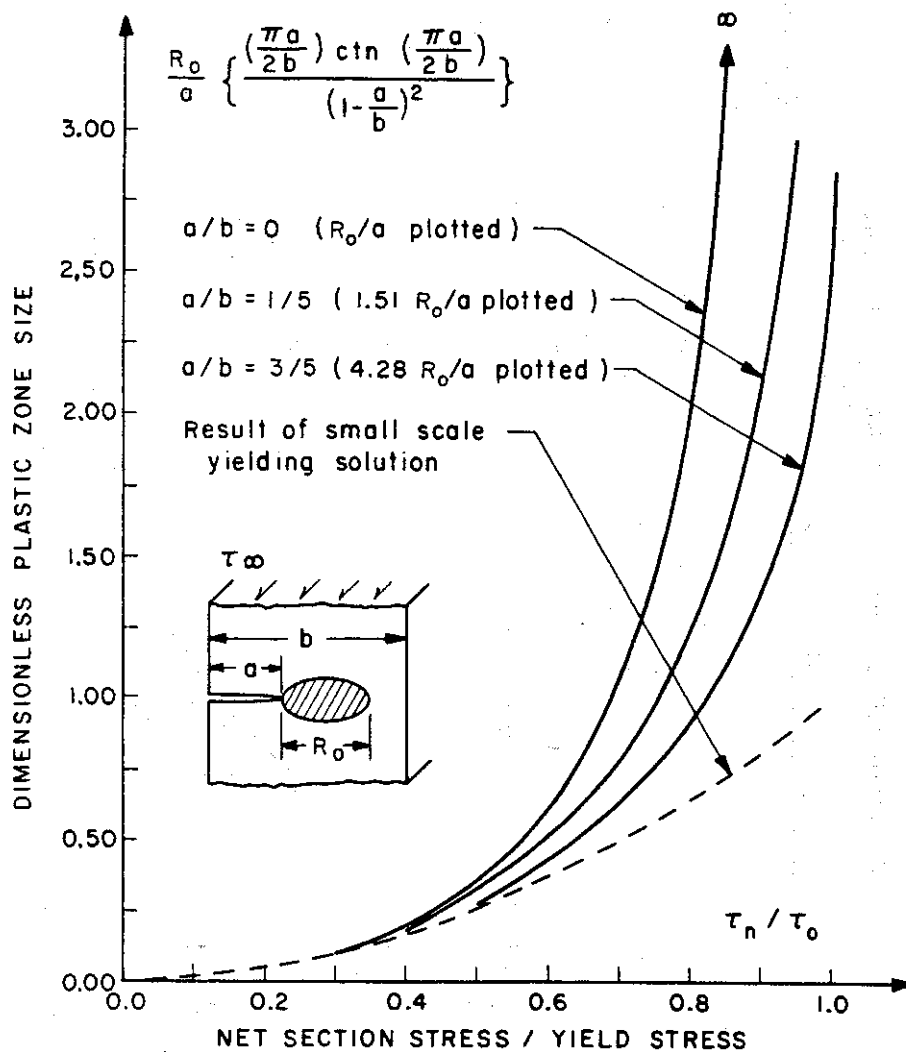


FIG. 14. Variation of plastic zone size with net section stress, for different crack-length-to-plane-width ratios. Dashed line shows small-scale yielding approximation. Antiplane strain of elastic perfectly plastic material (Rice, 1967b).

combinations has numerical value 1.00 when $a/b = 0$, 1.51 for $a/b = 1/5$, and 4.28 for $a/b = 3/5$. Deviations from the dashed-line results indicate the range of validity of the small-scale yielding approximation. Plastic zone size predictions begin to deviate significantly from 30 to 50% of the limit load in Fig. 14, with less deviation for the larger crack length-to-width ratios. Opening displacements deviate significantly from 60 to 70% of the limit load, again with less deviation for the larger ratios.

The elastic-plastic crack problem in antiplane strain may be formulated in a similar fashion for anisotropic perfectly plastic materials having arbitrary convex yield surfaces in the two-dimensional σ_{31}, σ_{32} stress

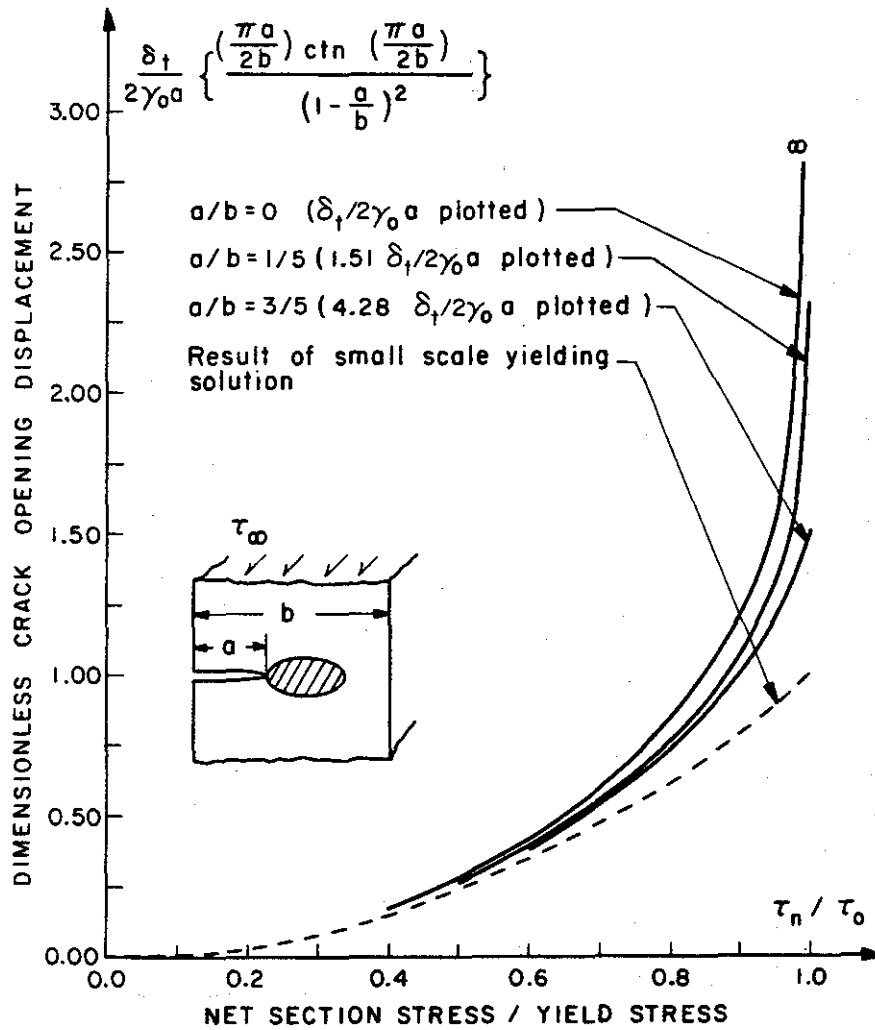


FIG. 15. Variation of crack opening displacement with net section stress, for different crack length to width ratios. Dashed line shows small-scale yielding approximation. Antiplane strain of elastic perfectly plastic material (Rice, 1967b).

space. The procedure is outlined in a survey on crack plasticity by Rice (1967b), and a membrane analogy is presented which allows effective visualization of solutions. Some small-scale yielding solutions are also given. A particular feature arising for single crystal-type yield surfaces is that plastic flow is confined to discrete slip lines emanating from the crack tip.

4. Comparison of Fracture Criteria

Some understanding of the role of plasticity in altering failure criteria of elastic fracture mechanics is obtained through choosing different criteria based on the elastic-plastic solution discussed above. First note

that the stress-intensity factor governs at low load levels and let K_{III}^f be its value at fracture in a small-scale yielding experiment. Then, from Eqs. (182) and (183), the accompanying plastic zone size and crack opening displacement are

$$R_0^f = \frac{(K_{III}^f)^2}{\pi\tau_0^2}, \quad \delta_t^f = \frac{2(K_{III}^f)^2}{\pi G\tau_0} = 2\gamma_0 R_0^f \quad (187)$$

It is now convenient to consider R_0^f , the plastic zone size at fracture in a small-scale yielding experiment, as a characteristic length describing a particular material and test condition. Then the linear elastic fracture criterion, $K_{III} = K_{III}^f$, predicts the net section stress at fracture as

$$\tau_n^f = \tau_0 \frac{[(\pi a/2b) \operatorname{ctn}(\pi a/2b)]^{1/2}}{(1 - a/b)} \left(\frac{R_0^f}{a}\right)^{1/2} \quad (188)$$

Examining the elastic-plastic solution, one might choose a fracture criterion $R_0 = R_0^f$, since the plastic zone size ahead of the crack governs the strain along the prospective plane of separation. Alternatively, one might choose a fracture criterion $\delta_t = \delta_t^f = 2\gamma_0 R_0^f$, since the crack opening displacement is an integrated effect of the highly concentrated strain near the crack tip. Both the critical zone size and critical opening displacement criteria agree with the linear elastic prediction (Eq. (188)) in the small-scale yielding range, but not at the high fracture stress levels resulting for short cracks. Figures 16 and 17 compare predicted

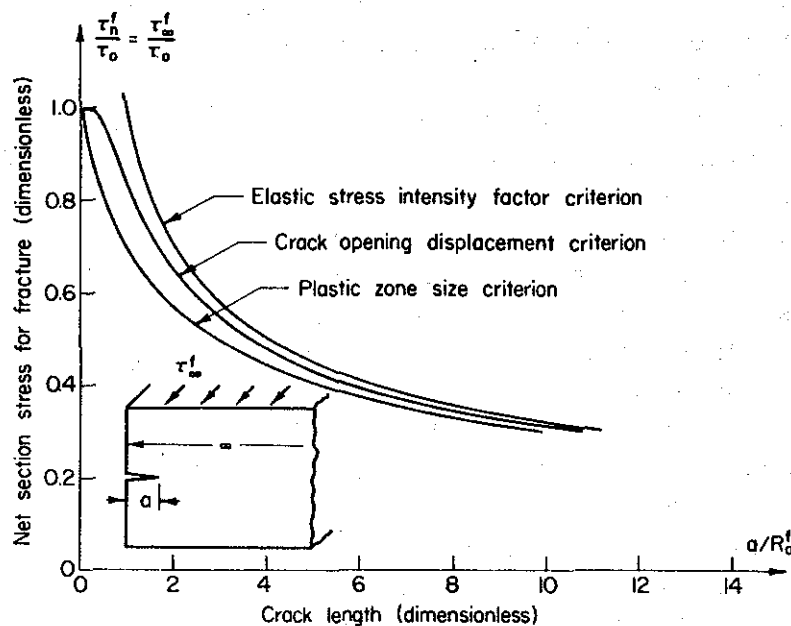


FIG. 16. Comparison of different fracture criteria, as based on perfectly plastic antiplane strain solution, for edge crack in a half plane (Rice, 1966b).

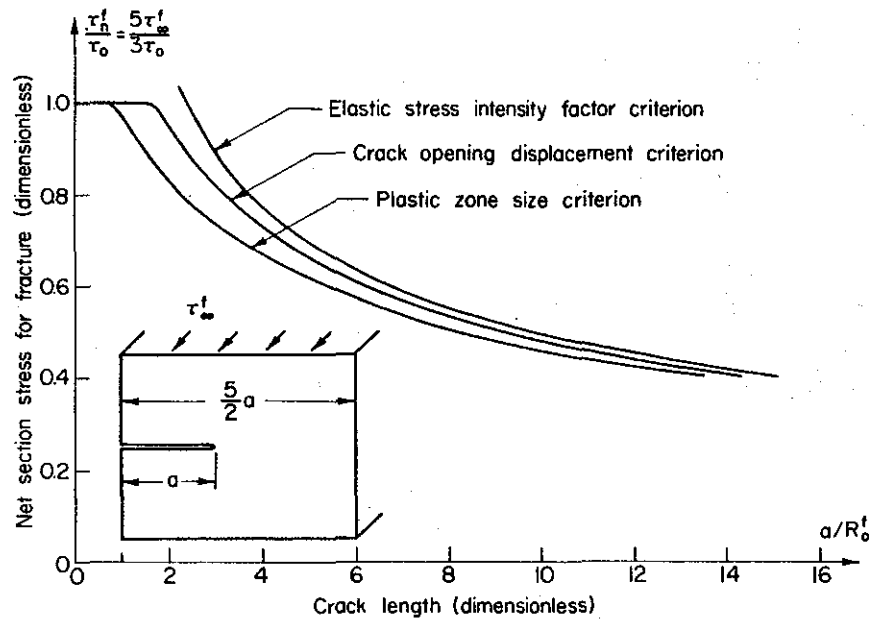


FIG. 17. Comparison of different fracture criteria, as based on perfectly plastic antiplane strain solution, for crack traversing two-fifths of plane width (Rice, 1966b).

dimensionless fracture stresses τ_n^f/τ_0 from the three criteria, showing them as a function of a/R_0^f , the ratio of crack length to plastic zone size at fracture in a small-scale yielding experiment. Figure 16 is for the case of a crack in an infinitely wide plane, whereas Fig. 17 is for a crack traversing two-fifths of the plane width. The horizontal line segments appearing for small crack lengths in the latter figure correspond to cases in which fully plastic conditions result before the zone size and opening displacement fracture criteria are met.

Aside from providing an indication of the deviation from linear elastic predictions, the curves serve to show the lack of any single parameter which may replace the stress-intensity factor in describing the intensity of local deformations in the large-scale yielding range. The two plasticity criteria differ from each other as much as the closest differs from the elastic criterion, except for very short cracks. It should be noted that current practices (ASTM, 1960) in applications of elastic fracture mechanics include semiempirical corrections to account for yielding influences on fracture size effects. The curves marked "stress-intensity factor criterion" do not include these corrections, which tend to shift predictions toward those based on the opening displacement criterion. Also, it is cautioned that the relevance of antiplane solutions to tensile problems is uncertain, and it is unknown if similarly chosen tensile criteria would lead to similar deviations in the large-scale yielding range.

5. Strain Hardening

Governing equations for elastic-plastic strain-hardening behavior in antiplane deformation have been formulated by Neuber (1961) and Rice (1967c), employing a deformation plasticity theory. Isotropic stress-strain relations relating the principal shear stress τ and strain γ , where

$$\tau = (\sigma_{31}^2 + \sigma_{32}^2)^{1/2} \quad \text{and} \quad \gamma = (\gamma_{31}^2 + \gamma_{32}^2)^{1/2} \quad (189)$$

are taken as linear behavior up to an initial yield point τ_0, γ_0 and nonlinear hardening thereafter:

$$\tau = (\tau_0/\gamma_0) \gamma \quad \text{for} \quad \gamma < \gamma_0 \quad \text{and} \quad \tau = \tau(\gamma) \quad \text{for} \quad \gamma > \gamma_0 \quad (190)$$

where $\tau(\gamma)$ is a function describing the stress-strain relation in the hardening range. Principal shear stress and strain directions are collinear, so that, in component form,

$$\sigma_{31} = [\tau(\gamma)/\gamma] \gamma_{31}, \quad \sigma_{32} = [\tau(\gamma)/\gamma] \gamma_{32} \quad (191)$$

as in Eq. (38). As in the perfectly plastic case, it is advantageous to formulate equations for physical coordinates x_1, x_2 in terms of strains γ_{31}, γ_{32} or stresses σ_{31}, σ_{32} . Then the equilibrium and compatibility equations may be transformed as follows:

$$\begin{aligned} \frac{\partial \sigma_{31}}{\partial x_1} + \frac{\partial \sigma_{32}}{\partial x_2} = 0 & \quad \text{becomes} \quad \frac{\partial x_1}{\partial \sigma_{31}} + \frac{\partial x_2}{\partial \sigma_{32}} = 0 \\ \frac{\partial \gamma_{31}}{\partial x_2} - \frac{\partial \gamma_{32}}{\partial x_1} = 0 & \quad \text{becomes} \quad \frac{\partial x_1}{\partial \gamma_{32}} - \frac{\partial x_2}{\partial \gamma_{31}} = 0 \end{aligned} \quad (192)$$

The compatibility equation is satisfied by writing

$$x_1 = \partial \psi / \partial \gamma_{31}, \quad x_2 = \partial \psi / \partial \gamma_{32} \quad (193)$$

where ψ is a function of the strain components. Substitution into the equilibrium equations and use of the stress-strain relations leads to a linear differential equation for ψ having variable coefficients. The equation takes its simplest form in a polar coordinate system in the strain plane. To this end, let ϕ be the angle between the x_2 direction and the principal shear direction, measured positive counterclockwise. Then

$$\gamma e^{i\phi} = \gamma_{32} - i\gamma_{31}, \quad \tau e^{i\phi} = \sigma_{32} - i\sigma_{31} \quad (194)$$

and when the strain plane potential function is expressed in terms of γ and ϕ , Eqs. (193) may be written in the form

$$x_1 = -\sin \phi \frac{\partial \psi}{\partial \gamma} - \frac{\cos \phi}{\gamma} \frac{\partial \psi}{\partial \phi}, \quad x_2 = \cos \phi \frac{\partial \psi}{\partial \gamma} - \frac{\sin \phi}{\gamma} \frac{\partial \psi}{\partial \phi} \quad (195)$$

The equilibrium equation of Eqs. (192) is then satisfied if

$$\frac{\tau(\gamma)}{\gamma\tau'(\gamma)} \frac{\partial^2 \psi}{\partial \gamma^2} + \frac{1}{\gamma} \frac{\partial \psi}{\partial \gamma} + \frac{1}{\gamma^2} \frac{\partial^2 \psi}{\partial \phi^2} = 0 \quad (196)$$

where $\tau'(\gamma) = d\tau/d\gamma$. Note that this becomes Laplace's equation for a linear stress-strain relation as in the elastic region of the strain plane, $\gamma < \gamma_0$. The antiplane displacement u_3 and potential function ψ are related as Legendre transforms

$$u_3 = \gamma \partial \psi / \partial \gamma - \psi, \quad \psi = r \partial u_3 / \partial r - u_3 \quad (197)$$

where r is radial distance in a polar coordinate system in the physical plane.

6. Small-Scale Yielding Solution for Strain Hardening

The strain field of the semi-infinite crack maps into the semi-infinite portion of the strain plane defined by $-\pi/2 \leq \phi \leq +\pi/2$, these limits giving the principal shear directions corresponding to the lower and upper crack surfaces, respectively. Since $x_2 = 0$ on the crack surfaces, Eqs. (195) require $\partial \psi / \partial \phi = 0$ at $\phi = \pm \pi/2$. The strain singularity at the crack tip maps it into points at infinity in the strain plane, and thus the derivatives of ψ vanish at infinity, since $x_1 = x_2 = 0$ at the tip. The requirement of an asymptotic approach to the elastic singularity leads, as in Eqs. (179) and (180), to a singularity at the origin of the strain plane, which is the map of points at infinity in the physical plane:

$$\left. \begin{aligned} x_1 - ix_2 &= -e^{-i\phi} \left(\frac{1}{\gamma} \frac{\partial \psi}{\partial \phi} + i \frac{\partial \psi}{\partial \gamma} \right) \rightarrow \frac{K_{III}^2 \gamma_0^2 e^{-2i\phi}}{2\pi\tau_0^2 \gamma^2} \quad \text{as } \gamma \rightarrow 0 \\ \text{or} \quad \psi &\rightarrow -\frac{K_{III}^2 \gamma_0^2 \sin \phi}{2\pi\tau_0^2 \gamma} \quad \text{as } \gamma \rightarrow 0 \end{aligned} \right\} \quad (198)$$

If we now assume a solution for ψ in the form of $\sin \phi$ times a function of γ , we automatically satisfy boundary conditions on the map of the crack surfaces and the problem reduces to determining the function

Lines of constant strain magnitude in the plastic region are circles with radius $R(\gamma)$ and centers located a distance $X(\gamma)$ ahead of the crack tip on the x_1 axis. The principal shear direction angle ϕ at any point on a constant strain circle is one half the angle made with the x_1 axis by a line from the center of the circle to that point. The elastic-plastic boundary is also a circle with center at $X(\gamma_0)$ and radius $R(\gamma_0) = K_{III}^2/2\pi\tau_0^2$; this radius is independent of the stress-strain relation in the hardening range. Lines of constant strain magnitude in the elastic region remain circular but are now concentric with the elastic-plastic boundary. Stresses in the elastic region may be obtained from the latter set of Eqs. (201) as

$$\sigma_{32} + i\sigma_{31} = \frac{K_{III}}{\{2\pi[z - X(\gamma_0)]\}^{1/2}} \quad (202)$$

and it is again seen that the effect of yielding is to shift the elastic singularity ahead as if the crack tip were at the center of the plastic zone. Strains along the line directly ahead of the crack are obtained by setting $\phi = 0$ in Eqs. (201). The result in the plastic region is

$$x_1 = \frac{\gamma_0 K_{III}^2}{\pi\tau_0} \int_{\gamma_{32}(x_1, 0)}^{\infty} \frac{du}{u^2\tau(u)} \quad (203)$$

As an example, consider a stress-strain relation exhibiting hardening according to a power law

$$\tau = \tau_0(\gamma/\gamma_0) \quad \text{for } \gamma < \gamma_0, \quad \tau = \tau_0(\gamma/\gamma_0)^N \quad \text{for } \gamma > \gamma_0 \quad (204)$$

$N = 0$ describes perfect plasticity and $N = 1$ describes perfect elasticity. The radius and center location of a constant strain circle in the plastic region is

$$R(\gamma) = \frac{K_{III}^2}{2\pi\tau_0^2} \left(\frac{\gamma_0}{\gamma}\right)^{1+N}, \quad X(\gamma) = \frac{1-N}{1+N} R(\gamma) \quad (205)$$

The plastic zone extends a distance $R(\gamma_0) + X(\gamma_0) = K_{III}^2/(1+N)\pi\tau_0^2$ ahead of the crack tip and a distance $R(\gamma_0) - X(\gamma_0) = NK_{III}^2/(1+N)\pi\tau_0^2$ behind. Strains directly ahead of the crack in the plastic region are

$$\gamma_{32}(x_1, 0) = \gamma_0 \left[\frac{K_{III}^2}{(1+N)\pi\tau_0^2 x_1} \right]^{1/(1+N)} \quad (206)$$

7. Complete Solution for Strain Hardening

Following Rice (1967c), the strain-hardening elastic-plastic solution is sketched here for an edge crack of depth a in a semi-infinite plane (Fig. 19a) subject to a uniform remote shear stress τ_∞ which does not

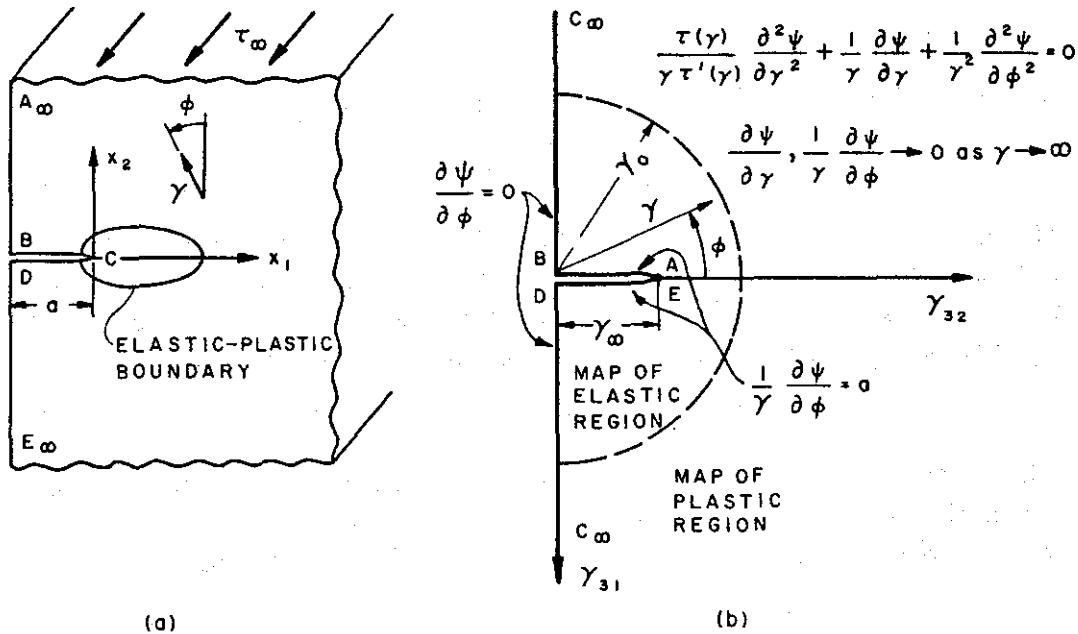


FIG. 19. Formulation of the edge crack problem for a work-hardening elastic-plastic material subjected to antiplane strain. (a) Physical plane. (b) Map of physical plane into strain plane, with corresponding points as labeled and with boundary conditions as shown.

exceed the initial yield stress. The map of this configuration into the strain plane appears in Fig. 19b with corresponding points labeled and with boundary conditions (resulting from Eqs. (193) or (195) indicated. The differential Eq. (196) is Laplace's equation in the elastic region ($\gamma < \gamma_0$) and its solution can be represented as the imaginary part of a harmonic function, say

$$\psi = -\gamma_0 \text{Im} \left[\int F(\xi) d\xi \right] \quad \text{where} \quad \xi = \frac{\gamma}{\gamma_0} e^{i\phi} = \frac{\gamma_{32} - i\gamma_{31}}{\gamma_0} \quad (207)$$

Physical coordinates in the elastic region $|\xi| < 1$ are then

$$x_1 - ix_2 = F(\xi) \quad (208)$$

as in Eq. (175). Symmetry considerations require $F(\xi)$ to be real on the real axis ahead of the slit so that $\bar{F}(\xi) = F(\xi)$. In view of the vanishing normal derivative on the γ_{31} axis, an image half plane with identical boundary conditions may be introduced in the region $\gamma_{32} < 0$, so that

we now have a slit extending from $-s < \xi < +s$ where s is the dimensionless remote stress or strain

$$s = \tau_\infty/\tau_0 = \gamma_\infty/\gamma_0 \quad (209)$$

The boundary condition $x_1 = -a$ on the slit becomes

$$-2a = 2 \operatorname{Re}[F(t)] = F(t) + \overline{F(t)} = [F(t)]^+ + [F(t)]^- \quad (210)$$

Here, t denotes points along the slit and $+$, $-$ refer to upper and lower surfaces of the slit. We have considered similar Hilbert equations in Sect. II,C, III,A, and III,B. Its general solution, which satisfies also the vanishing normal derivative on the γ_{31} axis, may be written as

$$F(\xi) = -a[1 + \xi g(\xi)(\xi^2 - s^2)^{-1/2}] \quad (211)$$

where $g(\xi)$ is analytic within the unit circle and has a Taylor expansion containing only even powers of ξ with real coefficients. The solution for ψ in the plastic region ($\gamma > \gamma_0$) can be written in the form

$$\psi = \sum_{k=1}^{\infty} D_k f_k(\gamma) \sin[(2k-1)\phi] \quad (212)$$

which automatically satisfies the boundary condition on the γ_{31} axis. In order to satisfy the governing equation for ψ and conditions at infinity, the set of functions $f_k(\gamma)$ are chosen so that

$$\frac{\tau(\gamma)}{\gamma\tau'(\gamma)} f_k''(\gamma) + \frac{1}{\gamma} f_k'(\gamma) - \frac{(2k-1)^2}{\gamma^2} f_k(\gamma) = 0 \quad (213)$$

with $f_k(\gamma_0) = 1$ and $f_k'(\infty) = 0$.

We now have two solutions for ψ , one containing the unknown Taylor coefficients of $g(\xi)$ and the other containing the unknown constants D_k . These are determined by requiring that both solutions give the same values of the physical coordinates on the elastic-plastic boundary ($\gamma = \gamma_0$), or, equivalently, that first derivatives of ψ be continuous. An infinite system of linear equations results. If the unknown constants are each, in turn, expanded in powers of s , a recursive method of solution may be developed. The resulting formulas are given by Rice (1967c), along with a solution for the constants D_k accurate to within an error of order s^{12} , and with extensive numerical tabulations for materials hardening according to the power law of Eq. (205). Figure 20 shows some of the final results in graphical form for power law hardening with $N = 0.1$ and 0.3 . The position of the elastic-plastic boundary (lower right quartiles of figures) and strain distribution in the plastic

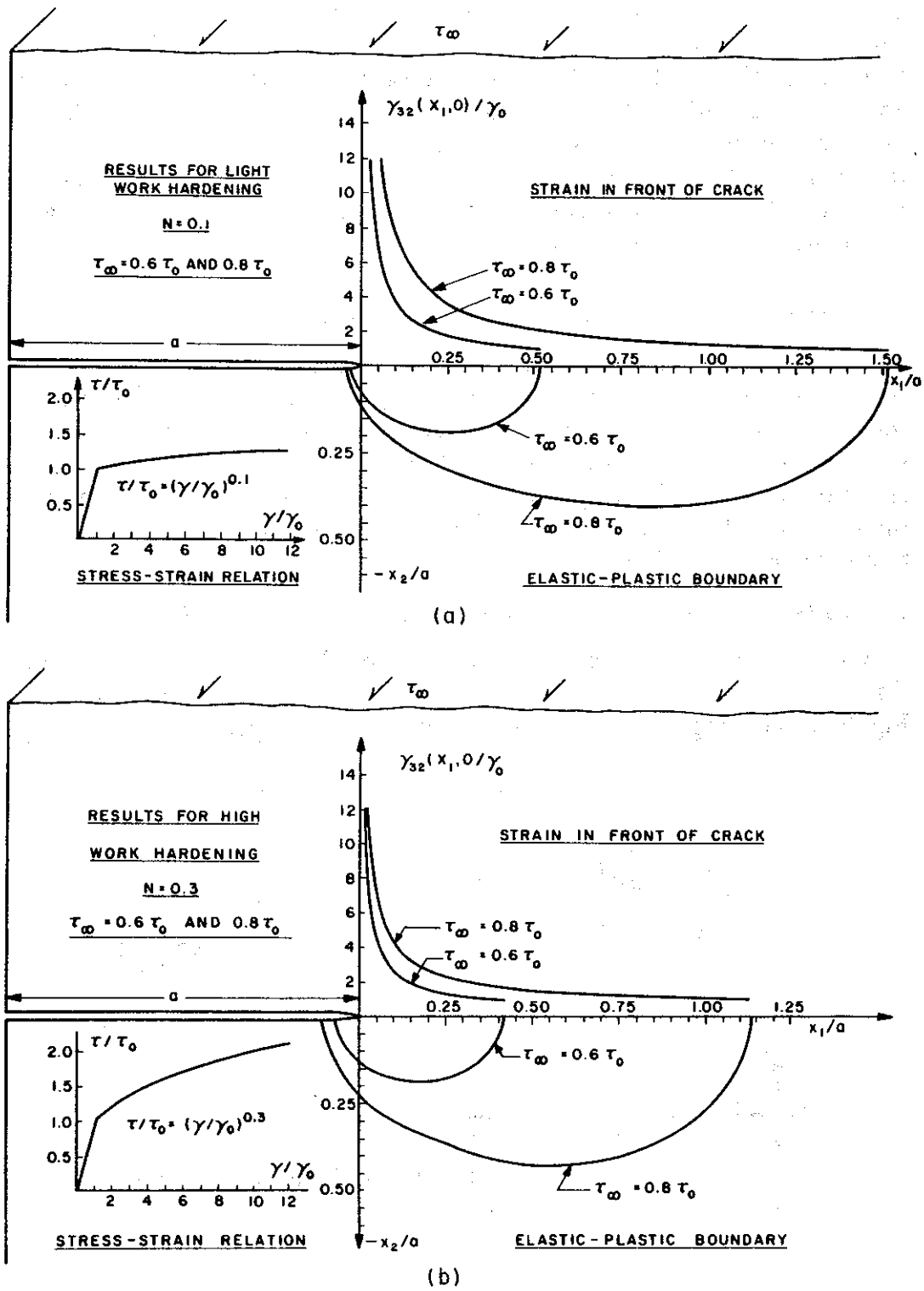


FIG. 20. Results of large-scale yielding solutions for power law hardening materials. (a) $N = 0.1$, (b) $N = 0.3$.

zone ahead of the crack tip (upper right quartiles) are shown for two remote stress levels, $\tau_\infty = 0.6\tau_0$ and $0.8\tau_0$. These stress levels serve to indicate the transition from the circular small-scale yielding plastic zones to the highly elongated zones appearing as general yield levels are approached. The variation in strain-hardening exponents from 0.1 to 0.3 is seen to significantly affect the plastic zone size at a given stress level. Further comparisons show that the higher exponent of 0.3 leads to results about as close to perfect elasticity as to perfect plasticity.

C. CRACKS IN ELASTIC-PLASTIC TENSILE FIELDS

The important elastic-plastic problems of cracks subjected to mode I tensile loadings are not as well treated as desirable for applications to fracture prediction. Some progress has been made with a simple model for fully developed plane stress yielding in thin sheets and with an approximate analysis of plane strain yielding based on the slip line theory. As will be seen, the path-independent integral J is an effective tool for analysis in these cases.

1. Dugdale-Barenblatt Yield Model and Plane Stress Plasticity

A model for plane stress yielding, proposed by Dugdale (1960) and similar to the Barenblatt (1962) cohesive force model, is shown in Fig. 21a. Yielding is assumed to be confined to a narrow zone directly

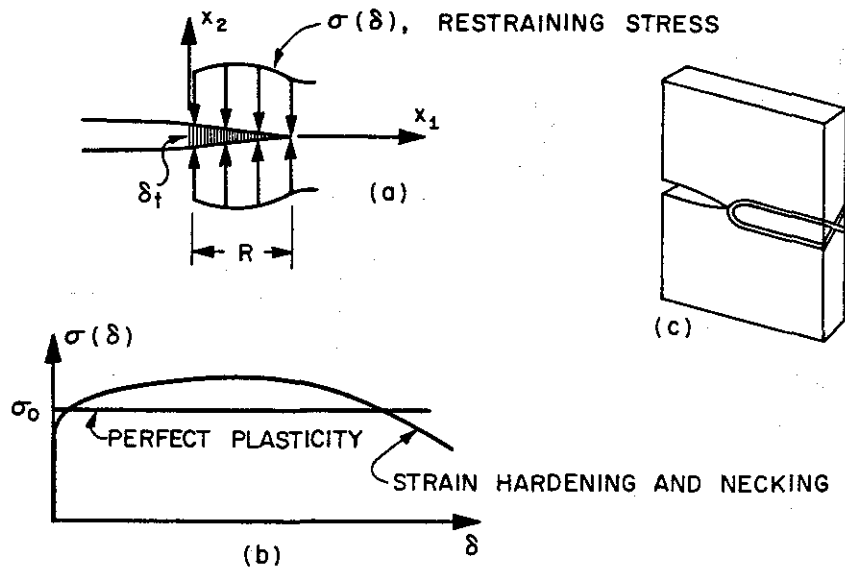


FIG. 21. Dugdale-Barenblatt model for plane stress yielding. (a) Yielding viewed as confined to a narrow zone in front of crack where stresses oppose separation of extended crack surfaces. (b) Restraining stress versus separation distance. (c) Physical justification in terms of through-the-thickness slip in fully developed plane stress yielding.

ahead of the crack tip (at $x_1 = 0$), and the model is analyzed by viewing the effect of yielding as making the crack longer by an amount equal to the plastic zone size R , with cohesive stresses in the plastic zone acting on the extended crack surface so as to restrain the opening. Both the applied load and the restraining stresses create inverse square root singularities at the outer tip of the plastic zone, but these singularities are of opposite sign and the zone size is chosen so that they cancel and bounded stresses result at the outer tip. As shown in Fig. 21b, the restraining stress may be a function of separation distance $\delta = u_2^+(x_1, 0) - u_2^-(x_1, 0)$, or may be taken as constant at a yield stress σ_0 in the case of perfect plasticity for which several complete solutions are available. Rosenfield *et al.* (1966) have shown the particular relevance of this model to fully developed plane stress yielding in thin sheets, through revealing plastic zones by etching techniques. A somewhat idealized schematic view of their observations is shown in Fig. 21c. Plastic flow consists of two intersecting shear bands through the sheet thickness at 45° angles. Yielding is then localized to a narrow region of height roughly equal to the sheet thickness. The average plastic extensional strain is approximately

$$\bar{\epsilon}^p = \delta/h \tag{214}$$

where δ is separation distance and h is sheet thickness.

Just as in the discussion of the Barenblatt cohesive model for elastic brittle fracture, Fig. 8 and Eq. (136), the separation distance δ_t at the crack tip (or crack opening displacement) may be solved for in terms of the restraining stress-separation distance curve and the value of the path-independent integral J . Thus

$$J = \int_0^{\delta_t} \sigma(\delta) d\delta = h \int_0^{\delta_t/h} \sigma(\bar{\epsilon}^p) d\bar{\epsilon}^p \tag{215}$$

the latter form applying for plane stress with the approximation of Eq. (214) and where $\sigma(\bar{\epsilon}^p)$ is the stress-strain relation. It was shown in Sect. IV,A that the path-independent integral has the same value as for linear elasticity in the boundary-layer style, small-scale yielding solutions. Thus, using the plane stress value of J , the crack opening displacement in the small-scale yielding solution is obtained from

$$\frac{K_I^2}{E} = \int_0^{\delta_t} \sigma(\delta) d\delta = h \int_0^{\delta_t/h} \sigma(\bar{\epsilon}^p) d\bar{\epsilon}^p \tag{216}$$

As an example, for linear strain hardening at a constant tangent modulus,

$$\sigma(\bar{\epsilon}^p) = \sigma_0 + E_{\tan} \bar{\epsilon}^p \tag{217}$$

substitution into Eqs. (215) and (216) results in the crack opening displacement

$$\delta_t = \frac{\sigma_0 h}{E_{\tan}} \left[\left(1 + \frac{2E_{\tan} J}{h\sigma_0^2} \right)^{1/2} - 1 \right] \quad (218)$$

$$\delta_t = \frac{\sigma_0 h}{E_{\tan}} \left[\left(1 + 2 \frac{E_{\tan}}{E} \frac{K_I^2}{h\sigma_0^2} \right)^{1/2} - 1 \right]$$

with the latter form applying for small-scale yielding. In the case of perfect plasticity ($E_{\tan} = 0$), these become

$$\delta_t = J/\sigma_0, \quad \delta_t = K_I^2/E\sigma_0 \quad (219)$$

2. Perfectly Plastic Solutions to the Dugdale–Barenblatt Model

The methods of solution for elastic crack problems (Sects. III, A, B, and C) are readily extended to the Dugdale–Barenblatt model, in the special case of perfect plasticity with constant cohesive stress σ_0 . For small-scale yielding, we view the crack as semi-infinite and add together a solution which correctly gives the asymptotically approached inverse square-root singularity of Eqs. (78), but which leaves the extended crack surfaces in the plastic zone tractionfree, and a solution for a semi-infinite crack with restraining stresses $\sigma_{22}(x_1, 0) = \sigma_0$ acting in the cohesive zone. The latter solution is obtained from the general solution of Eq. (98). Thus, the complex stress functions entering into the analysis of inplane deformations, as defined by Eqs. (20)–(22) and (70), are

$$\phi'(z) = \Omega'(z) = \frac{K_I(z-R)^{-1/2}}{2(2\pi)^{1/2}} + \frac{\sigma_0(z-R)^{-1/2}}{2\pi} \int_0^R \frac{(R-t)^{1/2}}{t-z} dt \quad (220)$$

for the crack tip at $x_1 = 0$, as in Fig. 21a. The plastic zone size is determined from the boundedness condition, which means that the coefficient of $(z-R)^{-1/2}$ must vanish at $z = R$. Thus

$$\frac{K_I}{2(2\pi)^{1/2}} + \frac{\sigma_0}{2\pi} \int_0^R \frac{(R-t)^{1/2}}{t-R} dt = 0 \quad \text{or} \quad R = \frac{\pi}{8} \frac{K_I^2}{\sigma_0^2} \quad (221)$$

In terms of the plastic zone size R , Eq. (220) leads to the stress functions

$$\phi'(z) = \Omega'(z) = \frac{\sigma_0}{\pi} \arctan \left[\left(\frac{R}{z-R} \right)^{1/2} \right] \quad (222)$$

Computing displacements from Eq. (22), one finds for the separation distance δ in the cohesive zone

$$\delta = \frac{(\kappa+1)\sigma_0 R}{\pi G} \left[\xi - \frac{x_1}{2R} \log \left(\frac{1+\xi}{1-\xi} \right) \right], \quad \text{where} \quad \xi = (1 - x_1/R)^{1/2} \quad (223)$$

Choosing the plane stress value of $\kappa = (3 - \nu)/(1 + \nu)$, this is seen to agree at $x_1 = 0$ with the crack opening displacement, as given by Eq. (219).

The same method may be applied to treat the crack of length $2a$ subjected to a uniform remote stress field $(\sigma_{22})_\infty = \sigma_\infty$, as shown in Fig. 5. Equation (94), written for a crack of length $2(a + R)$, is the starting point. Adding a constant term to this superposition solution to account for the remotely applied stress,

$$\phi'(z) = \Omega'(z) = \frac{\sigma_\infty}{2} - \frac{[z^2 - (a + R)^2]^{-1/2}}{2\pi} \int_{-(a+R)}^{+(a+R)} p_2(t)[(a + R)^2 - t^2]^{1/2} \frac{dt}{t - z} \quad (224)$$

where $p_2(t) = \sigma_\infty$ for $|t| < a$ and $p_2(t) = \sigma_\infty - \sigma_0$ for $a < |t| < a + R$. The boundedness condition at $z = \pm(a + R)$ leads to the plastic zone size

$$R = a[\sec(\pi\sigma_\infty/2\sigma_0) - 1] \quad (225)$$

and the corresponding crack opening displacement is (Rice, 1966a)

$$\delta_t = \frac{(\kappa + 1) \sigma_0 a}{\pi G} \log \left[\sec \left(\frac{\pi\sigma_\infty}{2\sigma_0} \right) \right] \quad (226)$$

These two results are plotted in the dimensionless forms

$$\frac{R}{a} \quad \text{and} \quad \frac{\pi G \delta_t}{(\kappa + 1) \sigma_0 a}$$

as a function of the ratio of applied stress to yield stress, in Fig. 22. Recalling that $K_I = \sigma_\infty(\pi a)^{1/2}$, the small-scale yielding solution of Eqs. ((221) and (223) or (219)) shows both dimensionless forms to equal $\pi^2 \sigma_\infty^2 / 8 \sigma_0^2$, the dashed-line result of Fig. 22. Again, the range of accuracy of the small-scale yielding approximation may be judged from the graphs.

The Dugdale-Barenblatt model has been analyzed for various other configurations. Bilby and Swinden (1965) and Smith (1966) have shown that, for the infinite periodic array of collinear cracks (Fig. 6), the plastic zone size is

$$R = a\{(2b/\pi a) \arcsin[\sin(\pi a/2b) \sec(\pi\sigma_\infty/2\sigma_0)] - 1\} \quad (227)$$

and the crack opening displacement is given by

$$\delta_t = \frac{(\kappa + 1) \sigma_0 b \sin \alpha}{\pi^2 G} \int_\mu^{\pi/2} \frac{\cos \lambda}{(1 - \sin^2 \alpha \sin^2 \lambda)^{1/2}} \log \left[\frac{\sin(\lambda + \mu)}{\sin(\lambda - \mu)} \right] d\lambda \quad (228)$$

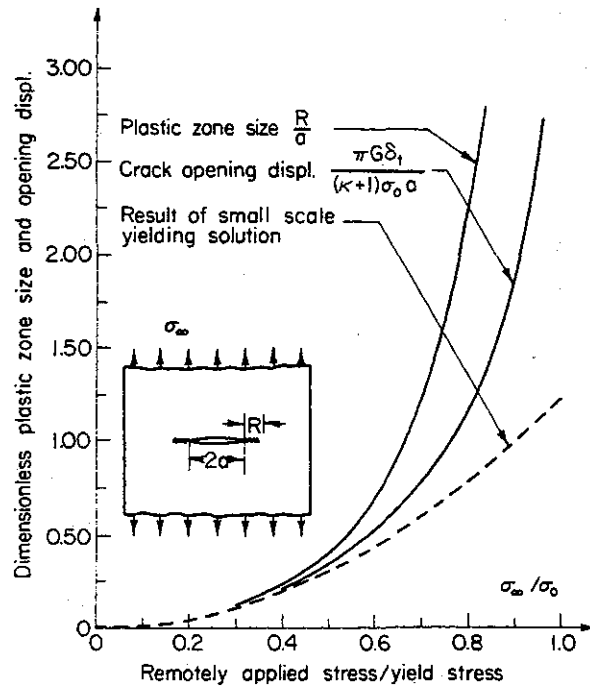


FIG. 22. Variation of plastic zone size and crack opening displacement with applied stress. Dashed line is result of small-scale yielding approximation. Perfectly plastic Dugdale-Barenblatt model.

where $\alpha = \pi(a + R)/2b$ and $\mu = \pi(1 - \sigma_\infty/\sigma_0)/2$. Some numerical results have been given. Other two-dimensional problems for this model and similar mode II and III models are discussed by Bilby *et al.* (1963), Smith (1966), Goodier and Field (1963) (who also give a steady state dynamic solution), and Rice (1966a). Keer and Mura (1966) treat the penny-shaped crack of radius a subjected to a remote uniform tensile stress field σ_∞ . Now, of course, the interpretation of the model in terms of a plane stress yielding mode (Fig. 21c) must be dropped. The boundedness condition serving to determine the plastic zone size may be written directly from Eq. (102) for a crack of radius $(a + R)$:

$$\sigma_\infty \int_0^a \frac{r dr}{[(a + R)^2 - r^2]^{1/2}} + (\sigma_\infty - \sigma_0) \int_a^{a+R} \frac{r dr}{[(a + R)^2 - r^2]^{1/2}} = 0 \quad (229)$$

or $R = a\{[1 - (\sigma_\infty/\sigma_0)^2]^{-1/2} - 1\}$. The crack opening displacement is

$$\delta_t = \frac{4(1 - \nu)\sigma_0 a}{\pi G} \left\{ 1 - \left[1 - \left(\frac{\sigma_\infty}{\sigma_0} \right)^2 \right]^{1/2} \right\} \quad (230)$$

Both of these reduce to the small-scale yielding results of Eqs. (221) and (223), provided the plane strain value of κ is chosen, on noting that $K_I = 2\sigma_\infty(a/\pi)^{1/2}$. In contrast to the two-dimensional problem of

a crack of length $2a$ in an infinite body, the crack opening displacement approaches a finite limit at the general yielding stress for the penny-shaped crack.

Some writers prefer an alternate terminology for the Dugdale-Barenblatt model, referring to it as a continuous array of dislocations distributed on a plane. Yielding on a macroscopic scale at a crack tip involves very complicated dislocation networks and any simple description at the physical dislocation level in terms of a linear array is inappropriate. Thus, the term "continuous dislocation array" should here be interpreted in a mathematical sense as the use of a Green's function in elasticity (as in the last part of Sect. III,C) to describe displacement discontinuities, rather than in a physical sense. Nevertheless, the dislocation array as a starting point in analysis provides a powerful technique allowing full use of the theory of singular integral equations. The direct physical interpretation is less objectionable for single crystalline bodies. Continuum plasticity solutions then involve discrete slip planes corresponding in direction to slip planes in the crystal (Rice, 1967b), and these solutions can be interpreted in terms of the pileup along available slip planes of dislocations forced into the material by the blunting of the crack tip.

3. *Slip Line Field in Perfectly Plastic Plane Strain*

Consider a crack in a plane strain deformation field and let us assume for the present that the material under consideration exhibits elastic as well as plastic incompressibility and that the plastic zone completely surrounds the crack tip. We shall relax these assumptions shortly. Incompressibility permits full use of the plane strain slip line theory discussed in Sect. II,D, and the zone surrounding the tip allows construction of at least a portion of the stress field, as illustrated in Fig. 23. An approximate solution may then be obtained as by Rice (1967a) in application of the J integral. The traction-free crack surface boundary condition determines a constant stress state in the largest isosceles right triangle (A in Fig. 23) which may be fit into the plastic region:

$$\sigma_{11} = 2\tau_0, \quad \sigma_{12} = \sigma_{22} = 0 \quad (\text{region A}) \quad (231)$$

Now, any β line (notation of Sect. II,D) emanating from the crack surface and crossing the x_1 axis in front of the crack must decrease its shear angle by $\pi/2$ so that a hydrostatic stress elevation by $2\tau_0(\pi/2)$ results uniformly on the x_1 axis, determining a constant stress state in the diamond-shaped region B

$$\sigma_{11} = \pi\tau_0, \quad \sigma_{22} = (2 + \pi)\tau_0, \quad \sigma_{12} = 0 \quad (\text{region B}) \quad (232)$$

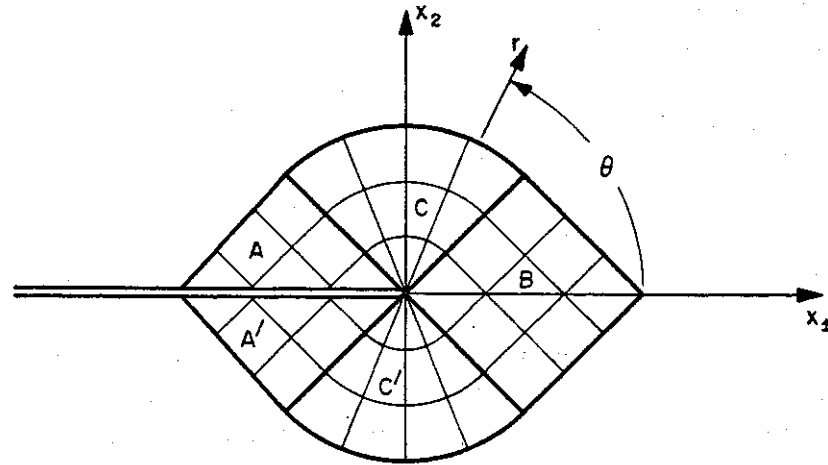


FIG. 23. Construction of plane strain slip line field in yielded region surrounding the tip of a crack in an incompressible perfectly plastic material.

A centered fan C must join two such constant stress state regions (Prager and Hodge, 1951). Radial lines in a polar coordinate system are α lines in the fan, and the shear angle is θ . Thus

$$\sigma_{rr} = \sigma_{\theta\theta} = (1 + 3\pi/2) \tau_0 - 2\tau_0\theta, \quad \sigma_{r\theta} = \tau_0 \quad (\text{region C}) \quad (233)$$

We employ a deformation theory to discuss strains, so as to permit full use of the path-independent energy integral. Adapting Eq. (39) to the incompressible perfectly plastic case, the associated energy density is

$$W = \frac{1}{2}G\gamma^2 \quad \text{for } \gamma < \gamma_0 \quad \text{and} \quad W = \tau_0(\gamma - \gamma_0/2) \quad \text{for } \gamma > \gamma_0 \quad (234)$$

where $\gamma = (2\epsilon_{ij}\epsilon_{ij})^{1/2}$ and $\epsilon_{ii} = 0$. Severe strain concentrations can occur only when slip lines focus, as in the fan. There, the vanishing of ϵ_{rr} and $\epsilon_{\theta\theta}$ imply that

$$u_r = f'(\theta), \quad u_\theta = -f(\theta) + g(r) \quad (235)$$

Similar relations apply to displacement rates in a proper incremental theory, from Eqs. (46), and these would integrate into the above equations if stresses remained constant at each point from the time it was first enveloped by the plastic region. This case is approached for small values of r , so that Eqs. (235) apply at least very near the crack tip in an incremental solution. The "engineering" shear strain in the fan is representable as

$$\gamma_{r\theta} = \frac{1}{r} \frac{\partial u_r}{\partial \theta} + \frac{\partial u_\theta}{\partial r} - \frac{u_\theta}{r} = \frac{f''(\theta) + f(\theta)}{r} + g'(r) - \frac{g(r)}{r} \quad (236)$$

We now examine expressions for displacements and strains very near the crack tip. The displacement may arbitrarily be chosen as zero when the crack tip is approached along the positive x_1 axis in region B, and, since strains are bounded in this region, u_r and u_θ vanish at $r = 0$ on the boundary between B and C. Thus

$$g(0) = 0, \quad g'(0) \text{ is bounded,} \quad \text{and} \quad f(\pi/4) = f'(\pi/4) = 0 \quad (237)$$

Now, let us define a function $R(\theta)$ so that

$$\gamma_0 R(\theta) = f''(\theta) + f(\theta) \quad (238)$$

Then, very near the crack tip, Eq. (236) becomes

$$\gamma_{r\theta} = \gamma_0 [R(\theta)/r] \quad (239)$$

similar in form to the antiplane strain result of Eq. (171). This equation would apply throughout the fan if $g(r)$ were a linear function of r . We shall henceforth refer to $R(\theta)$ as the distance to the elastic-plastic boundary, remembering that it is only an approximate indication. Displacements and energy density very near the crack tip are then

$$u_r = f'(\theta), \quad u_\theta = -f(\theta), \quad W = \tau_0 \gamma_0 [R(\theta)/r] \quad (240)$$

The energy line integral J of Eq. (60) may be evaluated on a circle of radius r surrounding the crack tip, and path independence permits us to let $r \rightarrow 0$. No contribution is then made by the constant state regions A and B of Fig. 23 in view of strain boundedness, and the entire contribution to J comes from the centered fan. Employing the stress field of Eqs. (233) and the small r forms of Eqs. (240), Eq. (60) results in (Rice, 1967a)

$$J = 2\tau_0 \gamma_0 \int_{\pi/4}^{3\pi/4} R(\theta) [\cos \theta + (1 + 3\pi/2 - 2\theta) \sin \theta] d\theta \quad (241)$$

This relation may also be expressed in terms of displacements. On converting from polar to Cartesian coordinates and employing Eqs. (240) and (238), one finds that, near the crack tip,

$$du_2/d\theta = \gamma_0 R(\theta) \sin \theta, \quad du_1/d\theta = \gamma_0 R(\theta) \cos \theta \quad (242)$$

Thus

$$J = 2\tau_0 \int_{\pi/4}^{3\pi/4} \frac{du_2}{d\theta} [\text{ctn } \theta + (1 + 3\pi/2 - 2\theta)] d\theta \quad (243)$$

Presuming J is known as a function of the applied load (as for small-scale yielding, Sect. IV,A, when it has the linear elastic value), the two

expressions in terms of $R(\theta)$ and $du_2/d\theta$ may be employed to obtain approximate estimates of the plastic zone size and opening displacement. First, let us review our starting assumptions of incompressible elastic behavior and of a plastic zone surrounding the crack tip. The results finally obtained for J are based on the deformation field very near the crack tip strain singularity. Since slip line theory is valid in regions of large plastic strain even with compressible elastic behavior, the incompressibility assumption can be dropped. While a plastic zone surrounding the crack tip validates the stress field of Eqs. (231)–(233), it is not the only circumstance under which the centered fan would result. In particular, the elastic-plastic boundary could cut sharply into the crack tip in regions A and B of Fig. 23, with the stress fields of Eqs. (231) and (232) approached as one nears the crack tip in elastic material. A result of precisely this sort occurs in the antiplane strain elastic-plastic solution. There, had we constructed the α lines of Sect. II,D on the assumption that plastic flow surrounded the tip, a centered fan would result ahead of the tip in the region $x_1 > 0$, and constant stress regions would result adjacent to crack surfaces in the region $x_1 < 0$. But exact solutions lead to an elastic-plastic boundary encompassing points in the fan region and cutting in toward the crack tip along the boundary of the fan and constant stress regions, as in Fig. 12.

4. Plane Strain Crack Opening Displacement and Plastic Zone Size

The remaining steps to get from the integrated averages of Eqs. (241) and (243) to specific results are necessarily approximate. Note that $u_2 = \delta_t/2$ at $\theta = 3\pi/4$, where δ_t is the crack opening displacement. As an approximation, let us assume that $du_2/d\theta$ is a symmetrical function about $\theta = \pi/2$. From Eq. (242), this is equivalent to assuming $R(\theta)$, the approximate plastic zone dimension, is symmetric with respect to the x_2 axis, $R(\pi/2 - \psi) = R(\pi/2 + \psi)$. The bracketed term in the integrand of Eq. (243) consists of a constant symmetric part, $1 + \pi/2$, and an antisymmetric part. The latter does not contribute to the accuracy of the symmetry assumption, and Eq. (243) leads to

$$J \approx 2(1 + \pi/2) \tau_0 \int_{\pi/4}^{3\pi/4} \frac{du_2}{d\theta} d\theta = (1 + \pi/2) \tau_0 \delta_t \quad (244)$$

or

$$\delta_t \approx \frac{J}{(1 + \pi/2) \tau_0}, \quad \delta_t \approx \frac{(1 - \nu^2) K_I^2}{(1 + \pi/2) E \tau_0}$$

The second expression applies for small-scale yielding. Comparing with the Dugdale–Barenblatt plane stress prediction Eq. (214) for the same stress-intensity factor and with $\nu = 0.3$, the plane strain opening

displacement is 61% of the plane stress value for a Mises material ($\sigma_0 = \sqrt{3}\tau_0$) and 70% for a Tresca material ($\sigma_0 = 2\tau_0$). A lower bound on the plane strain opening displacement may be obtained by noting that $du_2/d\theta \geq 0$ in the fan by Eq. (242), since $R(\theta) \geq 0$. Thus, $u_2 \leq \delta_t/2$ for all θ in the fan. First integrating Eq. (243) by parts and then applying this inequality, one obtains

$$\delta_t \geq \frac{J}{2(1 + \pi/2)\tau_0} \quad (245)$$

the lower bound being one-half of the above approximate result.

Experience with the antiplane strain case and with the Dugdale-Barenblatt model has shown that the plastic zone shape and maximum dimension is much more sensitive to stress level in the large-scale yielding range than is the opening displacement (Figs. 14, 15, and 22). Thus, no functional form assumed for $R(\theta)$ that is independent of stress level could lead to accurate results. For small-scale yielding, let us assume

$$R(\theta) \approx R_0 \cos[2(\theta - \pi/2)] \quad (246)$$

where R_0 is the maximum value, occurring at $\theta = \pi/2$, and thus an approximate indication of the maximum plastic zone dimension. This is an example of an elastic-plastic boundary cutting into the crack tip along the fan boundaries, as discussed above, for $R(\pi/4) = R(3\pi/4) = 0$. The approximate estimate of the small-scale yielding-zone size results upon substitution into Eq. (241),

$$R_0 \approx \frac{3J}{4\sqrt{2}(1 + \pi/2)\tau_0\gamma_0} = \frac{3(1 - \nu)}{8\sqrt{2}(1 + \pi/2)} \frac{K_I^2}{\tau_0^2} \quad (247)$$

Comparing with the plane stress zone dimension of Eq. (221) for $\nu = 0.3$, the plane strain estimate is 55% of the plane stress value for a Mises material and 73% for a Tresca material. Etching observations by Hahn and Rosenfield (1966) suggest a figure in the neighborhood of 50% and also reveal an elastic-plastic boundary which appears to cut in toward the crack tip as assumed here, although details are not clear very near the tip. A lower bound on the maximum value of the function $R(\theta)$ may be obtained by employing the inequality $R_{\max} \geq R(\theta)$ in Eq. (241), resulting in

$$R_{\max} \geq \frac{J}{2\sqrt{2}(1 + \pi/2)\tau_0\gamma_0} \quad (248)$$

This lower bound is two-thirds of the above approximate estimate of the maximum zone dimension for small-scale yielding.

A guess as to the change in shape of the plane strain elastic-plastic boundary with stress level is shown, in Fig. 24a, for the edge crack in a semi-infinite plane subjected to a remote tensile field. The smallest curve typifies the localized plastic zone expected for small-scale yielding. At stress levels approaching general yielding, the plastic zone would

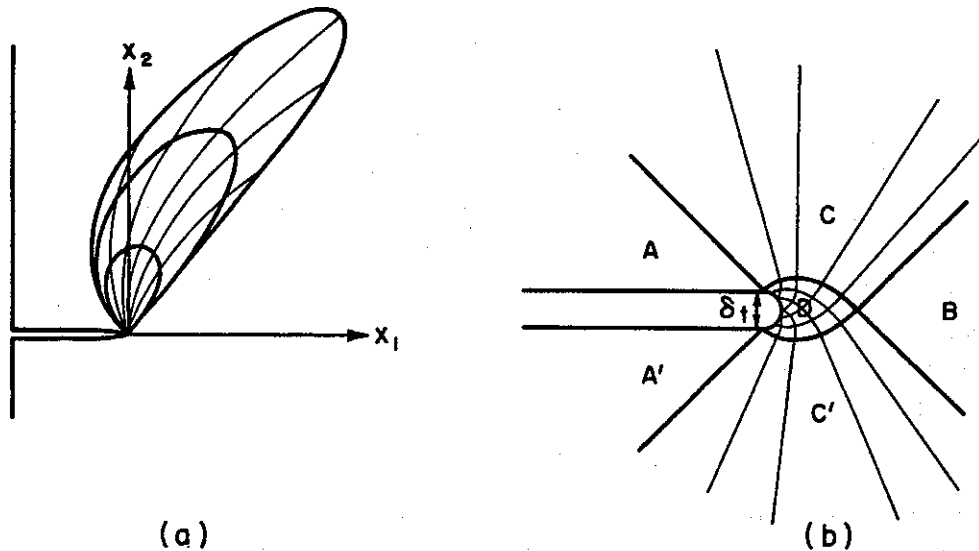


FIG. 24. Further features of perfectly plastic plane strain yielding. (a) Conjectured growth of plastic zone and curvature of slip line field for large-scale yielding near edge crack in half plane. (b) Blunting of the crack tip by plastic deformation causes the fans C, C' to become noncentered and to focus into a region D ahead of the tip, resulting in large strains.

elongate considerably, as suggested by the largest curve. Far from the crack tip at the outer extremity of this zone, one would expect the stress state to vary little from yield in simple tension $\sigma_{22} = 2\tau_0$ and $\sigma_{11} = \sigma_{12} = 0$. Thus, α lines toward the extremity of the zone should have a shear angle in the neighborhood of $\pi/4$. The only radial α slip line of the near tip centered fan which would give this simple tension stress state when bent so that its shear angle equals $\pi/4$ is the α line initially coinciding with the x_2 direction, as may be shown from Eqs. (45). One therefore expects that, for large-scale yielding, only α lines in the neighborhood of the initially vertical radial line in the fan will extend to the outer portions of the plastic zone, whereas other α lines originating in the fan will become extinct by contact with the elastic-plastic boundary, as shown. The validation of these guesses must await complete plane strain elastic-plastic solutions.

Note that the hypothetical elastic-plastic boundaries of Fig. 24a show no plastic flow in front of the crack. Also, as noted in connection with

Fig. 23, even if the plastic zone does extend in front of the crack, large plastic strains cannot occur in the constant stress region there. The way very intense deformations may actually occur is shown in Fig. 24b. Presuming, for simplicity of illustration, that the crack opening creates a semicircular blunted tip of diameter δ_t , a very different picture results on a small scale of the order of the opening displacement. The fan C now becomes noncentered and its straight α lines focus into the exponential spiral (Hill, 1950) slip line field adjacent to the blunted crack tip, resulting in a small region D of intense deformation over a length $1.9\delta_t$. The crack opening is on the order of the initial yield strain times a linear dimension of the plastic zone, so Fig. 24b is essentially Fig. 23 magnified in linear dimensions by a large factor of order one over the initial yield strain. Since the blunted region is small, an effective procedure would be to perform an incremental analysis of blunting by regarding the constant displacement rate along each straight α line of the noncentered fan to be given by the rate of increase of displacement $u_r = u_r(\theta)$ of our present analysis, with the shear angle ϕ of the noncentered α lines replacing the polar coordinate θ (and shear angle for centered α lines). For example, near crack tip displacements in the centered fan resulting from the approximate elastic-plastic boundary of Eqs. (246) and (241) may be found from Eqs. (238), (237), and (240), and, when expressed in terms of crack opening displacement Eq. (244), are

$$\begin{aligned} u_r &= (\delta_t/2\sqrt{2})[\cos(\theta - \pi/4) - \cos(2\theta - \pi/2)] \\ u_\theta &= -(\delta_t/4\sqrt{2})[2 \sin(\theta - \pi/4) - \sin(2\theta - \pi/2)] \end{aligned} \quad (249)$$

Thus, for the analysis of blunting, the displacement rate $du_r/d\delta_t$, as a function of θ , is set equal to $du_\alpha/d\delta_t$, as a function of ϕ , in the noncentered fan

$$du_\alpha/d\delta_t = (1/2\sqrt{2})[\cos(\phi - \pi/4) - \cos(2\phi - \pi/2)] \quad (250)$$

This gives the boundary condition on the β line between the noncentered fan and the region affected by blunting, and deformations in the blunted region may, in principle, be determined from Eqs. (46). The calculation is somewhat involved and has not yet been carried out, although a similar problem has been treated by Wang (1953).

5. Power Law Hardening in Plane Strain

Applications of the path-independent integral technique to determining the structure of near crack tip singularities in plane strain are discussed by Rice and Rosengren (1968) and Hutchinson (1968) (who

also considers two-dimensional plane stress). Employing a circle of radius r centered at the tip to evaluate the path integral,

$$J/r = \int_{-\pi}^{+\pi} \{W[\epsilon(r, \theta)] \cos \theta - \mathbf{T}(r, \theta) \cdot \partial \mathbf{u} / \partial x_1(r, \theta)\} d\theta \quad (251)$$

It is thus clear that the bracketed integrand exhibits, at least in angular average, a $1/r$ singularity as $r \rightarrow 0$. Since all terms in the integrand are of order stress times strain, one is tempted to conclude

$$\sigma_{ij} \epsilon_{ij} \rightarrow \frac{\text{a function of } \theta}{r} \quad \text{as } r \rightarrow 0 \quad (252)$$

Now consider the plane straining of an incompressible elastic-plastic material with the power law relation of Eq. (204) applying in the strain-hardening range between the principal inplane shear stress and strain. The $1/r$ singularity and satisfaction of stress-strain relations then requires asymptotic near tip behavior of the form

$$\sigma_{ij} \rightarrow r^{-N/(1+N)} \Sigma_{ij}(\theta); \quad \epsilon_{ij} \rightarrow r^{-1/(1+N)} E_{ij}(\theta) \quad (253)$$

Solutions may be found for the functions of θ in such a way that equilibrium, compatibility, stress-strain relations, and tractionfree crack

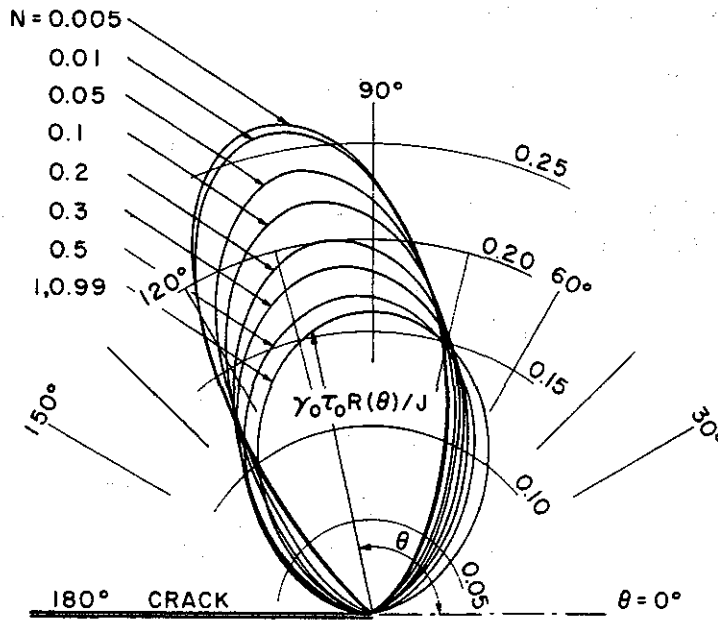


FIG. 25. Plane strain of an incompressible power law hardening material. Geometrical shape of constant equivalent shear lines very near the crack tip, and distance $R(\theta)$ to the approximate elastic-plastic boundary (as predicted from singular term only) (Rice and Rosengren, 1968).

surface boundary conditions are satisfied; in fact, one may show that boundary conditions may be satisfied in solutions of this form only when the powers of r are as in Eqs. (253).

The corresponding asymptotic structure of equivalent shears is

$$\begin{aligned} \tau &= (\frac{1}{2} s_{ij} s_{ij})^{1/2} \rightarrow \tau_0 [R(\theta)/r]^{N/(1+N)} \\ \gamma &= (2 \epsilon_{ij} \epsilon_{ij})^{1/2} \rightarrow \gamma_0 [R(\theta)/r]^{1/(1+N)} \end{aligned} \tag{254}$$

Here, $R(\theta)$ gives the geometrical shape of constant equivalent shear lines near the tip and, as an approximation, is the distance to the elastic-plastic boundary. The functions of θ in the above equations are determined only to within a multiplicative constant by the governing equa-

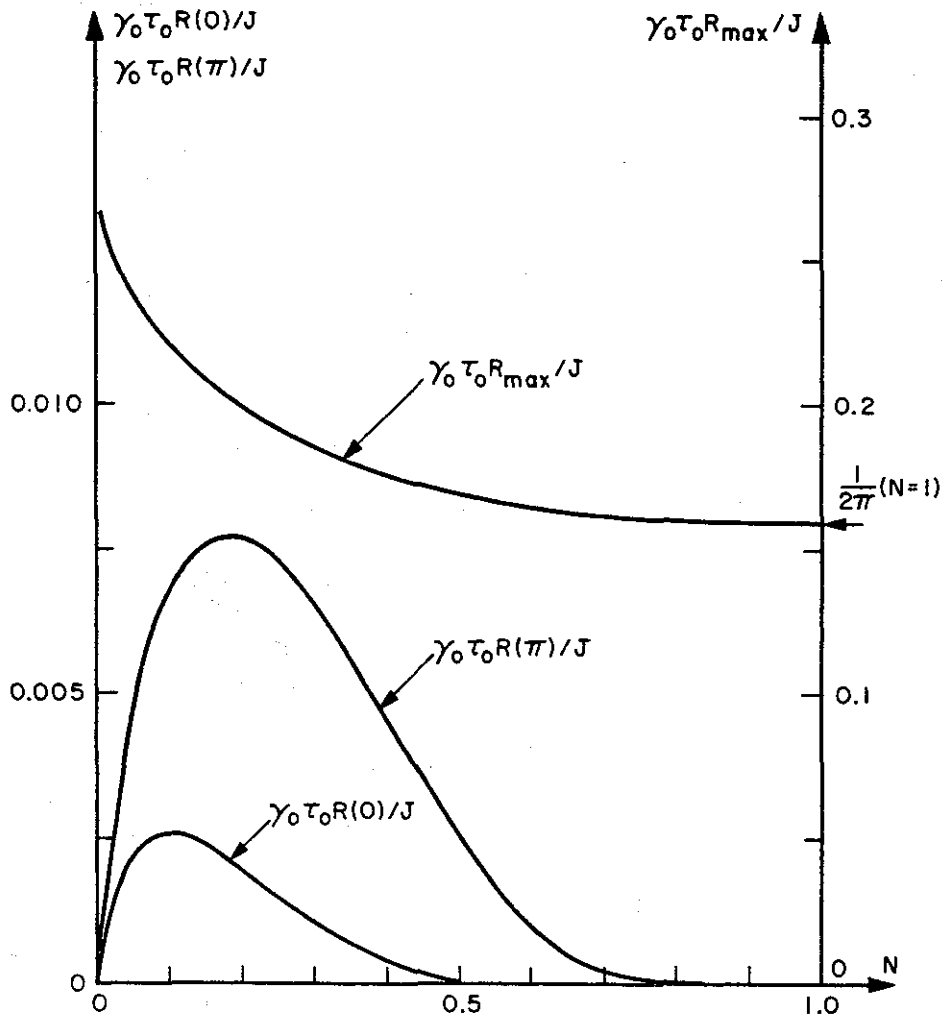


FIG. 26. Distance which approximate elastic-plastic boundary extends ahead, $R(0)$, and behind, $R(\pi)$, the crack tip. Also, maximum size of approximate plastic zone, R_{max} . Plane strain of power law hardening material (Rice and Rosengren, 1968).

tions, but this constant may be expressed in terms of J by substitution of the solution into the path integral. Results for $R(\theta)$ are shown in nondimensional form in Fig. 25 for a range of values of N . Although not clear from this figure, the curve $r = R(\theta)$ actually extends a small distance in front of and behind the crack tip, except when N is zero (perfect plasticity) or unity (linear elasticity). Resulting values for $R(0)$ and $R(\pi)$, as well as the maximum value achieved by $R(\theta)$, are shown as a function of N in Fig. 26. Figure 27 shows the variation of the ratio of the mean normal stress $p = (\sigma_{11} + \sigma_{22})/2$ to the equivalent shear stress τ . This ratio is a function of θ only, and the slip line theory

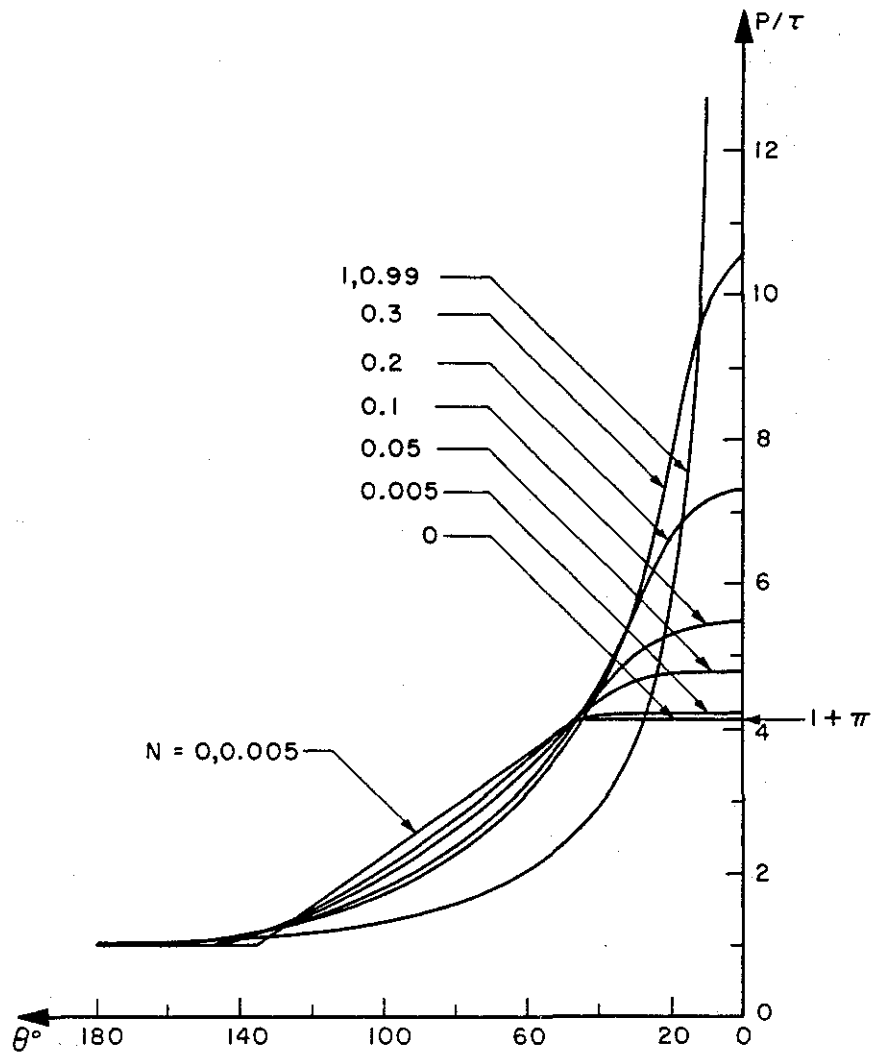


FIG. 27. Variation of the ratio of mean normal stress, $p = (\sigma_{11} + \sigma_{22})/2$, to equivalent shear stress, τ , as a function of orientation angle for several hardening exponents. Plane strain (Rice and Rosengren, 1968).

prediction of Eqs. (231)–(233) is seen to be approached for small values of N . One noteworthy feature of this figure is the rapid rise with hardening exponent of the ratio of maximum tensile stress directly ahead of the crack, $\sigma_{\max} = p + \tau$, to the equivalent uniaxial tensile stress, 2τ (under plane strain conditions). For example, $\sigma_{\max}/2\tau = 1 + \pi/2 = 2.57$ when $N = 0$, as expected from the slip line theory [Eq. (232)], but the stress ratio increases to 3.36 when $N = 0.1$, 4.21 when $N = 0.2$, and 5.85 when $N = 0.3$. The incompressibility assumption becomes questionable at such high mean stresses, and more exact figures must await further analyses.

We have seen the utility of the path-independent energy integral in treating plasticity problems, both in plane stress and plane strain. One difficulty is that only its value for small-scale yielding (Sect. IV,A) is known. We shall see in Sect. IV,E on notch strain concentrations, however, that known exact and approximate elastic-plastic solutions may be employed to estimate its value in the large-scale yielding range and, thus, to extend the range of usefulness of formulas in this section giving results in terms of J .

D. ELASTIC-PLASTIC ANALYSIS OF EXTENDING CRACKS AND FRACTURE INSTABILITY

Incremental plastic stress-strain relations (Sect. II,D) are path dependent, so that strain fields which result from monotonic loading of stationary cracks, as in the last section, will not, in general, be the correct fields for quasistatically extending cracks. This important difference has been emphasized by McClintock (1958, 1965) and McClintock and Irwin (1965), who have shown through an analysis of the antiplane strain case that the stress required for unstable crack extension can greatly exceed the stress which first initiates crack extension in ductile materials.

1. Steady-State Crack Extension in Antiplane Strain

Incremental plastic stress-strain relations for the antiplane case may be written from Sect. II,D as

$$\dot{\gamma} = \dot{\tau}/G + A\tau \quad (255)$$

where A is a nonnegative undetermined proportionality factor for plastic strain rates, where the dot denotes differentiation with respect to any monotonically increasing quantity, and where the shear stress vector τ and strain vector γ are given in Cartesian form by

$$\tau = \sigma_{31}\mathbf{i}_1 + \sigma_{32}\mathbf{i}_2, \quad \gamma = \gamma_{31}\mathbf{i}_1 + \gamma_{32}\mathbf{i}_2 = \nabla u_3 \quad (256)$$

We begin by seeking the strain distribution in the plastic zone for hypothetical steady-state conditions in which the elastic-plastic boundary is imagined to remain fixed in shape and size and to move along with the extending crack, so that the solution depends only on moving coordinates x_1, x_2 with moving origin always at the crack tip as in Fig. 12. We shall here let the dot denote differentiation with respect to crack length, which is the same as the negative of the derivative with respect to x_1 . Equilibrium and the yield condition again result in a centered fan of α lines ahead of the crack, as in Fig. 12, and the stress state is $\tau = \tau_0 \mathbf{i}_\theta$. Thus Eq. (255) becomes

$$-\nabla \frac{\partial u_3}{\partial x_1} = -\frac{\tau_0}{G} \frac{\partial \mathbf{i}_\theta}{\partial x_1} + A\tau_0 \mathbf{i}_\theta = -\gamma_0 \frac{\sin \theta}{r} \mathbf{i}_r + A\tau_0 \mathbf{i}_\theta \quad (257)$$

On equating radial components on both sides and integrating in r , noting that $\partial u_3 / \partial x_1 = \gamma_{31} = -\gamma_0 \sin \theta$ on the elastic-plastic boundary,

$$\begin{aligned} \frac{\partial}{\partial r} \left(\frac{\partial u_3}{\partial x_1} \right) &= \gamma_0 \frac{\sin \theta}{r} \\ \frac{\partial u_3}{\partial x_1} &= \gamma_{31} = -\gamma_0 \sin \theta \left[1 + \log \frac{R(\theta)}{r} \right] \end{aligned} \quad (258)$$

Differentiation with respect to x_2 results in

$$\frac{\partial \gamma_{32}}{\partial x_1} = \frac{\gamma_0}{r} \left\{ \sin^2 \theta - \cos^2 \theta \left[1 + \log \frac{R(\theta)}{r} \right] - \sin \theta \cos \theta \frac{R'(\theta)}{R(\theta)} \right\} \quad (259)$$

and γ_{32} is determined by integrating in the x_1 direction from the elastic-plastic boundary, noting that $\gamma_{32} = \gamma_0 \cos \theta$ on the boundary. The general computation is difficult, but, on the line ahead of the crack, there results

$$\gamma_{32}(x_1, 0) = \gamma_0 \left\{ 1 + \log(R_0/x_1) + \frac{1}{2} [\log(R_0/x_1)]^2 \right\} \quad (260)$$

For comparison, the monotonic loading solution of Sect. IV,A leads to a different strain singularity

$$\gamma_{32}(x_1, 0) = \gamma_0 (R_0/x_1) \quad (261)$$

Choosing as a fracture criterion the achievement of a critical plastic strain γ_f^p at a fixed microstructural distance ρ_s ahead of the crack (McClintock and Irwin, 1965), the plastic zone required for steady-state quasi-static extension of the crack is obtained from Eq. (260) as

$$(R_0)_{\text{steady state}} = \rho_s \exp \{ [2(\gamma_f^p/\gamma_0) + 1]^{1/2} - 1 \} \quad (262)$$

whereas, for the initiation of crack extension in monotonic loading, Eq. (261),

$$(R_0)_{\text{initiation}} = \rho_s[(\gamma_f^p/\gamma_0) + 1] \quad (263)$$

The ratio of the steady-state extension plastic zone size to the zone size for initiation of extension rises rapidly with ductility; this ratio is 1.04 when $\gamma_f^p = \gamma_0$, 3 when $\gamma_f^p = 10\gamma_0$, 18 when $\gamma_f^p = 25\gamma_0$, 169 when $\gamma_f^p = 50\gamma_0$, and 5100 when $\gamma_f^p = 100\gamma_0$. As seen below, instability sets in before attainment of the steady-state plastic zone size for typical crack configurations, but the zone size for initiation is considerably exceeded at instability in ductile materials.

2. Quasistatic Initiation and Growth of Cracks in Antiplane Strain

We consider here the general antiplane strain problem where both the crack length and the size and shape of the elastic-plastic boundary change with time, and obtain expressions for strain rates within the plastic zone. Then, adopting the fracture criterion of a critical strain at some fixed distance ahead of the crack, an integral equation is derived for the manner in which the plastic zone size must vary with increase in crack length in order to meet the fracture criterion. When specific crack configurations are considered, such as an edge crack in a semi-infinite plane, it is found that increasing load is at first required for an increase in crack length, but, ultimately, the load must stop increasing and then decrease in order to meet the fracture criterion, resulting in an instability marking the onset of catastrophic crack extension. The starting point is again Eq. (255), but now we take the x_1, x_2 coordinate system fixed in the material, call l a measure of crack length, and introduce a moving polar coordinate system with origin at the crack tip, as in Fig. 28. Noting again that $\tau = \tau_0 \mathbf{i}_\theta$ in the centered fan region

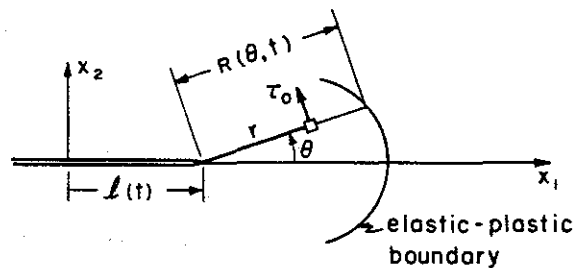


FIG. 28. Combined crack growth and plastic zone enlargement in the antiplane straining of a perfectly plastic material; $l(t)$ and $R(\theta, t)$ denote crack length and plastic zone shape, respectively, at time t .

ahead of the crack and letting the dot in Eq. (255) denote differentiation with respect to time t at a fixed material point, there results

$$\begin{aligned}\dot{\gamma} &= \nabla \frac{\partial u_3(x_1, x_2, t)}{\partial t} = \dot{\tau}/G + \Lambda\tau \\ &= -\gamma_0 \frac{\sin \theta}{r} \frac{dl}{dt} \mathbf{i}_r + \Lambda\tau_0 \mathbf{i}_\theta\end{aligned}\quad (264)$$

Equating radial components in the moving polar coordinate system and integrating in r ,

$$\frac{\partial}{\partial r} \left[\frac{\partial u_3(x_1, x_2, t)}{\partial t} \right] = -\gamma_0 \frac{\sin \theta}{r} \frac{dl}{dt}$$

or

$$\frac{\partial u_3}{\partial t} = \gamma_0 \sin \theta \left[\log \frac{R(\theta, t)}{r} \right] \frac{dl}{dt} + \left(\frac{\partial u_3}{\partial t} \right)_{B(\theta)}$$

where $R(\theta, t)$ denotes the position of the elastic-plastic boundary at time t and $(\partial u_3/\partial t)_{B(\theta)}$ denotes the velocity at the point $B(\theta)$ on the boundary at angle θ . To compute this velocity, first note from Fig. 28 that if x_{1B} , x_{2B} are coordinates of the point $B(\theta)$ defined from the distance to the boundary at angle θ at any time t ,

$$\left. \begin{aligned}x_{1B} &= l(t) + R(\theta, t) \cos \theta, & x_{2B} &= R(\theta, t) \sin \theta, \\ \text{and} & & u_3(x_{1B}, x_{2B}, t) &= \gamma_0 \int_0^\theta R(\alpha, t) d\alpha\end{aligned} \right\} \quad (266)$$

the latter equation resulting from $\gamma \equiv \nabla u_3 = \gamma_0 \mathbf{i}_\theta$ on the boundary. Now, letting d/dt denote a total time derivative at a fixed angle θ and introducing an equality with "transport" terms

$$\begin{aligned}\frac{du_3(x_{1B}, x_{2B}, t)}{dt} &= \gamma_0 \int_0^\theta \frac{\partial R(\alpha, t)}{\partial t} d\alpha \\ &= \left(\frac{\partial u_3}{\partial t} \right)_{B(\theta)} + \left(\frac{\partial u_3}{\partial x_1} \right)_{B(\theta)} \frac{dx_{1B}}{dt} + \left(\frac{\partial u_3}{\partial x_2} \right)_{B(\theta)} \frac{dx_{2B}}{dt} \\ &= \left(\frac{\partial u_3}{\partial t} \right)_{B(\theta)} + (-\gamma_0 \sin \theta) \left[\frac{dl}{dt} + \frac{\partial R(\theta, t)}{\partial t} \cos \theta \right] \\ &\quad + (\gamma_0 \cos \theta) \left[\frac{\partial R(\theta, t)}{\partial t} \sin \theta \right]\end{aligned}\quad (267)$$

The velocity at the boundary may be found from this equation, and, on substitution into Eq. (265),

$$\frac{\partial u_3}{\partial t} = \gamma_0 \sin \theta \left[1 + \log \frac{R(\theta, t)}{r} \right] \frac{dl(t)}{dt} + \gamma_0 \int_0^\theta \frac{\partial R(\alpha, t)}{\partial t} d\alpha \quad (268)$$

Strain rates are determined from $\dot{\gamma} = \nabla(\partial u_3/\partial t)$, and along the line ahead of the crack this results in

$$\frac{\partial \gamma_{32}(x_1, 0, t)}{\partial t} = \frac{\gamma_0}{x_1 - l(t)} \left\{ \left[1 + \log \frac{R_0(t)}{x_1 - l(t)} \right] \frac{dl(t)}{dt} + \frac{dR_0(t)}{dt} \right\} \quad (269)$$

where we have written $R_0(t) = R(0, t)$ for the extent of the plastic zone ahead of the crack. Note that the resulting strain rate is a simple linear combination of the steady-state solution (compare Eq. (259) for $\theta = 0$ with the terms multiplying dl/dt) and the monotonic loading solution. An explicit formula for the strain is obtained by integrating from the first time $t^*(x_1)$ at which the point with coordinate x_1 enters the plastic zone to the current time t

$$\gamma_{32}(x_1, 0, t) = \gamma_0 + \int_{t^*(x_1)}^t \frac{\partial \gamma_{32}(x_1, 0, \tau)}{\partial \tau} d\tau \quad (270)$$

where $l(t^*) + R_0(t^*) = x_1$. The path dependence is evident, for both the integrand and lower limit depend on the previous history of crack length and plastic zone size.

We now employ the fracture criterion of a critical plastic strain at distance ρ_s ahead of the crack, $\gamma_{32}[l(t) + \rho_s, 0, t] = \gamma_0 + \gamma_f^p$ to determine how the plastic zone size would have to vary with increasing crack length to maintain a quasistatic extension of the crack. From Eq. (270),

$$\gamma_f^p = \int_{t^*[l(t)+\rho_s]}^t \frac{\partial \gamma_{32}[l(t) + \rho_s, 0, \tau]}{\partial \tau} d\tau \quad (271)$$

As clear from the time-independent nature of plastic stress-strain relations, natural time may be replaced with any monotonically increasing parameter. We choose crack length as the parameter and measure l (Fig. 28) from zero at the initial crack length before extension begins, so that l is the quasistatic change in length of the crack due to plastic deformation. Also, the notation $R_0^f(l)$ will indicate the plastic zone size when the crack has extended by a distance l , and we define $R_0^f(0)$ as the zone size for initiation of Eq. (263)

$$R_0^f(0) = \rho_s(1 + \gamma_f^p/\gamma_0) \quad (272)$$

Then, after replacing natural time by crack extension in Eq. (271) and integrating by parts to remove the derivative of plastic zone size in Eq. (269), the resulting zone size required to quasistatically extend the crack a distance l satisfies the integral equation

$$R_0^f(l) = R_0^f(0) + \rho_s \int_{l^*}^l \left[\frac{R_0^f(x)}{\rho_s + l - x} - \log \frac{R_0^f(x)}{\rho_s + l - x} - 1 \right] \frac{dx}{\rho_s + l - x} \quad (273)$$

where

$$l^* = 0 \quad \text{if } \rho_s + l \leq R_0^f(0)$$

and

$$l^* + R_0^f(l^*) = \rho_s + l \quad \text{if } \rho_s + l \geq R_0^f(0)$$

The nonlinearity has prohibited exact solutions, but it is an easy matter to show that the initial slope is

$$\left[\frac{dR_0^f(l)}{dl} \right]_{l=0} = \frac{R_0^f(0)}{\rho_s} - \log \frac{R_0^f(0)}{\rho_s} - 1 = \gamma_p^f/\gamma_0 - \log(1 + \gamma_p^f/\gamma_0) \quad (274)$$

and when $l \rightarrow \infty$ the solution is asymptotic to the plastic zone size of Eq. (262) for the steady-state problem.

3. Fracture Instability

The plastic zone size for monotonic loading has been determined for edge and internal cracks in finite or infinite width planes at all stress levels up to general yielding (Sect. IV,B, Fig. 14, and Rice, 1966b). Also, for small-scale yielding, the plastic zone size may be expressed in terms of the elastic stress intensity factor as in Eq. (181). Let us generally denote these solutions as

$$R_0 = R_0(Q, a) \quad (275)$$

where Q denotes the applied load and a denotes crack length. While the form of strain singularities may be determined for extending cracks as above, no complete solutions have been obtained and it is an easy matter to show that the elastic-plastic boundary for monotonic loading cannot be the boundary for an extending crack under the same load and at the same crack length. The difficulty is that the plastic work rate would turn negative at values of the angle θ in Fig. 12 around 45° . Nevertheless, overall equilibrium considerations would suggest that monotonic loading solutions are reasonable estimates of the extent of yielding in front of an extending crack, and we here use Eq. (275) for this purpose. Let a_0 be the initial crack length. Then, crack extension is initiated at a value of the applied load satisfying

$$R_0(Q, a_0) = R_0^f(0) \quad (276)$$

as defined by Eq. (272). Stable crack extension under increasing load then begins, such that when the crack has extended an amount l the load is given by

$$R_0(Q, a_0 + l) = R_0^f(l) \quad (277)$$

the right side being the solution of the integral Eq. (273). Differentiation of both sides with respect to l leads to

$$\frac{\partial R_0(Q, a_0 + l)}{\partial Q} \frac{dQ}{dl} + \frac{\partial R_0(Q, a_0 + l)}{\partial a} = \frac{dR_0^f(l)}{dl} \tag{278}$$

and the instability point is reached when no further load increase is required to maintain quasistatic crack extension, $dQ/dl = 0$

$$\frac{\partial R_0(Q, a_0 + l)}{\partial a} = \frac{dR_0^f(l)}{dl} \tag{279}$$

Thus, the load at instability and the amount of prior stable crack extension are given by the simultaneous solution of this equation and Eq. (277). The procedure is shown in Fig. 29 where the plastic zone size $R_0^f(l)$

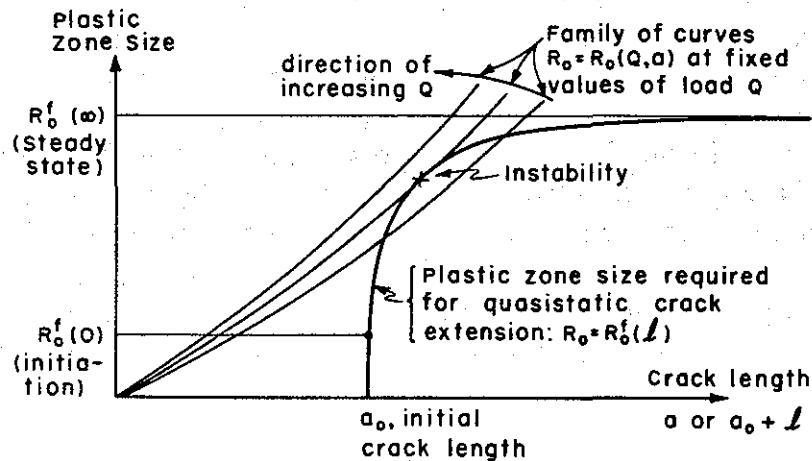


FIG. 29. Graphical representation of conditions determining fracture instability. The point of tangency indicates the load, and corresponding amount of stable growth beyond which a load drop would be required to maintain quasistatic crack extension.

for quasistatic extension, a universal curve for a given material and condition, is shown by the heavy line with initiation and steady-state extension values labeled. The family of light lines originating at the origin represent the variation of plastic zone size with crack length at fixed values of the applied load Q . It is seen that the instability load, simultaneously satisfying Eqs. (277) and (279), corresponds to the member of this family which tangentially touches the plastic zone size curve for quasistatic extension, and the amount of stable crack growth is determined by the point of tangential contact.

The curve family for plastic zone size at constant load is a family of straight lines for a crack in an infinite body, but has curvature of the

type shown in Fig. 29 for the edge of central crack in a finite-width plane. A few observations on fracture strength may be made immediately from this figure. For a given initial crack length, the plastic zone size (or stress-intensity factor for small-scale yielding) at fracture depends on plane width because the curvature does. For a given plane width, the zone size (or stress-intensity factor) is larger at fracture for the longer initial crack lengths, and more stable growth occurs for the longer lengths. A similar analysis of crack instability has been employed in elastic fracture mechanics, as discussed in the work of Krafft *et al.* (1961) and Srawley and Brown (1965). These writers employ a figure identical to Fig. 29, but plot a family of Irwin energy-release rates at constant loads (replacing the family R_0 at constant loads) and introduce a "resistance curve" which varies with crack extension (replacing the R_0^f curve). Since R_0 is proportional to K_{III}^2 for small-scale yielding and thus to the energy rate, this method is equivalent to the analysis of instability based on the elastic-plastic extending crack solutions. This equivalence has apparently never been noted in the literature, possibly because our presentation of the elastic-plastic instability criterion here and its representation in Fig. 29 differs markedly from the way it was introduced and employed by McClintock.

Analytical representations of stable growth and instability are quite difficult, but a simple approximation may be employed to predict instability. First note that, when expressed in terms of the plastic zone size $R_0(Q, a)$ for a specific crack configuration, the fracture criterion of Eq. (271) is

$$\begin{aligned} \gamma_f^p/\gamma_0 = \int_{a^*}^a \left\{ \frac{\partial R_0[Q(x), x]}{\partial Q} \frac{dQ(x)}{dx} + \frac{\partial R_0[Q(x), x]}{\partial x} \right. \\ \left. + \log \frac{R_0[Q(x), x]}{\rho_s + a - x} + 1 \right\} \frac{dx}{\rho_s + a - x} \end{aligned} \quad (280)$$

where $a^* + R_0[Q(a^*), a^*] = a + \rho_s$. Here, we have replaced time by crack length, and have written a formula valid when the currently fracturing point is outside the plastic zone for initiation of extension. The first two terms in the integrand come from the total time derivative of plastic zone size in Eq. (269), and the notation $Q(x)$ denotes the unknown applied load as a function of crack length. This equation, together with a similar equation for the fracturing point inside the plastic zone, form a nonlinear integral equation for the applied load required for extension. Now let a denote the crack length at instability. Then dQ/dx vanishes at the upper limit. Since almost the entire contribution to the integral comes from values of x near the upper limit for any

reasonable ductility, we can neglect the first term of the integrand and everywhere replace the plastic zone size by its value at instability, $R_0(Q, a)$, where here Q denotes the load at instability. Thus

$$\frac{\gamma_f^p}{\gamma_0} \approx \int_{a+\rho_s-R_0(Q,a)}^a \left\{ \frac{\partial R_0(Q, a)}{\partial a} + \log \frac{R_0(Q, a)}{\rho_s + a - x} + 1 \right\} \frac{dx}{\rho_s + a - x} \quad (281)$$

and the resulting relation between load and crack length at instability is

$$R_0(Q, a) \approx \rho_s \exp \left\{ \left(2 \frac{\gamma_f^p}{\gamma_0} + \left[1 + \frac{\partial R_0(Q, a)}{\partial a} \right]^2 \right)^{1/2} - \left[1 + \frac{\partial R_0(Q, a)}{\partial a} \right] \right\} \quad (282)$$

This equation was first given by McClintock and Irwin (1965) for the special case of an edge crack in a semi-infinite plane, in which case $\partial R_0/\partial a$ depends only on the remotely applied stress, Eq. (186). Its use is limited in that it depends on the crack length at instability which may not be found in terms of the initial crack length unless the quasistatic extension zone $R_0^f(l)$ is known or, equivalently, the integral Eq. (280) is solved.

The three dashed curves in Fig. 30 show resulting fracture stresses as a function of crack length at instability for values of fracture ductility γ_f^p equal to γ_0 , $10\gamma_0$, and $100\gamma_0$. These are plots of Eq. (282) for the edge crack in an infinite body, and τ_∞^f/τ_0 is given in terms of a/ρ_s on a log-log scale so that the minus one-half slope at low stress levels corresponds to the result anticipated from elastic fracture mechanics. The solid curves show computations by McClintock of slow growth to instability from various initial crack lengths. Equation (282) is seen to be highly accurate in locating the instabilities.

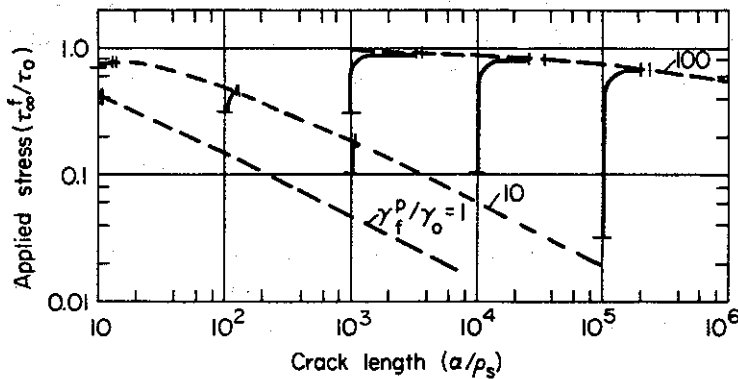


FIG. 30. Instability fracture criterion for edge crack of depth a in a half plane. Solid lines show growth from initial crack length to instability. Dashed lines represent approximate relation between load and crack length at instability, as developed in text (McClintock and Irwin, 1965).

4. Steady-State Crack Extension in Plane Strain

The form of the crack tip singularity for steady-state crack extension in perfectly plastic plane strain may be deduced just as for antiplane strain. Let x_1, x_2 be a moving system of coordinates always at the crack tip, as in Fig. 23. The deviatoric stress diadic \mathbf{s} in the centered fan is

$$\mathbf{s} = \tau_0(\mathbf{i}_r\mathbf{i}_\theta + \mathbf{i}_\theta\mathbf{i}_r) \quad (283)$$

and incremental stress-strain relations for an incompressible elastic-plastic material are

$$\begin{aligned} \dot{\epsilon} &= \dot{\mathbf{s}}/2G + \Lambda\mathbf{s} = -\frac{1}{2G} \frac{\partial \mathbf{s}}{\partial x_1} + \Lambda\mathbf{s} \\ &= \gamma_0 \frac{\sin \theta}{r} (\mathbf{i}_\theta\mathbf{i}_\theta - \mathbf{i}_r\mathbf{i}_r) + \Lambda\tau_0(\mathbf{i}_r\mathbf{i}_\theta + \mathbf{i}_\theta\mathbf{i}_r) \end{aligned} \quad (284)$$

where the dot denotes differentiation with respect to crack length and thus $-\partial/\partial x_1$ in the steady-state solution. $\dot{\epsilon}$ is the symmetric part of $\nabla \dot{\mathbf{u}}$, where the velocity vector is

$$\begin{aligned} \dot{\mathbf{u}} &= -\frac{\partial \mathbf{u}}{\partial x_1} = -\mathbf{i}_1 \frac{\partial u_1}{\partial x_1} - \mathbf{i}_2 \frac{\partial u_2}{\partial x_1} \\ &= \mathbf{i}_1 \frac{\partial u_2}{\partial x_2} - \mathbf{i}_2 \frac{\partial u_2}{\partial x_1} \quad (\text{by incompressibility}) \\ &= -\mathbf{i}_3 \times \nabla u_2 = \mathbf{i}_r \frac{1}{r} \frac{\partial u_2}{\partial \theta} - \mathbf{i}_\theta \frac{\partial u_2}{\partial r} \end{aligned} \quad (285)$$

The strain rate in polar coordinates may be computed in terms of the polar velocity representation above. Then equating either rr or $\theta\theta$ components in Eq. (284) leads to the single equation

$$\dot{\epsilon}_{rr} = -\dot{\epsilon}_{\theta\theta} = \frac{\partial}{\partial r} \left[\frac{1}{r} \frac{\partial u_2}{\partial \theta} \right] = -\gamma_0 \frac{\sin \theta}{r} \quad (286)$$

Integrating twice subject to the conditions $u_2 = 0$ and $\partial u_2/\partial r$ bounded at $r = 0$ and $\theta = \pi/4$ (since strains are nonsingular in the constant state region ahead of the crack tip) leads to

$$u_2 = \gamma_0(2^{-1/2} - \cos \theta) r \log(R_0/r) + rF(\theta) + G(r) \quad (287)$$

Here, R_0 is a pertinent constant with length dimensions, say, the maximum size of the plastic zone. $F(\theta)$ and $G(r)$ are undetermined functions from the integration, with $G(0) = G'(0) = 0$. The displace-

ment component u_1 may be obtained from incompressibility. Limiting attention to terms which will result in nonvanishing strains near the crack tip (that is, neglecting $G(r)$ in Eq. (287), and requiring $u_1 = 0$ and $\partial u_1/\partial r$ bounded at $\theta = \pi/4$ and $r = 0$, the resulting expression has the form

$$u_1 = \frac{\gamma_0}{\sqrt{2}} \sin \theta \log \left[\frac{(1 + \sqrt{2}) \sin \theta}{1 + \cos \theta} \right] r \log \frac{R_0}{r} + rH(\theta) \quad (288)$$

$H(\theta)$ is given by a very lengthy expression in terms of $F(\theta)$ above and θ after writing the incompressibility condition in polar coordinates.

We shall not here pursue the solution beyond this point, but some of its principal features are clear. Strain components very near the crack tip in the centered fan exhibit a logarithmic singularity of the form

$$\epsilon_{ij} = f_{ij}(\theta) \log(R_0/r) + g_{ij}(\theta) \quad (289)$$

in the steady-state extension solution, as compared with a $1/r$ singularity for monotonic loading of a stationary crack. This same difference resulted in the antiplane strain case. Also, the displacements are zero at the crack tip, so that the discrete opening displacement of the monotonic solution no longer results. Nevertheless, the $r \log r$ dependence would create a blunted tip since $\partial u_2/\partial r$ is infinite at $\theta = 3\pi/4$. While the general features of the antiplane strain problem are seen to be also present in the plane strain case, it is not clear that stable growth actually occurs (prior to pop-in) in this case. McClintock and Irwin (1965) note the detection of slow growth by recording ink, but stress corrosion may well be the cause. Results by Broek (1967) on aluminum alloys and some as yet unpublished work on silicon iron and a medium-strength steel by W. G. Clark and E. T. Wessel of Westinghouse Electric Corporation suggest that slow growth prior to pop-in diminishes to an undetectable amount as idealized plane strain conditions are increasingly approached. These latter workers failed to detect growth through an acoustical technique sensitive to 0.001 inch for cases of large plate thickness relative to plastic zone size, so it may be presumed that growth is limited to the rather small extension involved in the blunting of the crack tip by plastic deformation.

5. Stable Crack Extension under Tensile Loadings

Stable crack extension under tensile loadings is observed when plane stress conditions prevail, and after a plane strain pop-in when the first crack extension under constrained conditions does not mark an instability. In addition to the growth effects anticipated from the

incremental nature of plastic stress-strain relations, the situation is further complicated by a geometry change of the fracture surface with the development of partial or complete shear lips corresponding to a through-the-thickness slip mode of deformation. No analysis of growing cracks in plane stress has yet been attempted.

Essentially, growth effects occur because of the advance of a crack into plastically deformed material. The effect is most easily seen in the fully plastic deformation of a rigid-plastic (or nearly so) material under imposed boundary displacements. The small further advance of a crack results in no additional deformation in this extreme case, and the new crack tip region may be strained only by the further imposition of boundary displacements. This may be contrasted with a nonlinear elastic material having similar uniaxial monotonic tension behavior, for which the advance of a crack would cause the strain field to readjust so that a large concentration remains at the tip. The important feature in elastic-plastic problems would appear to be a plastic strain concentration directly ahead of the tip with progressively larger strains as the tip is approached. This is a feature of the antiplane strain problem where growth effects have been seen to be important; it is not a feature of the plane strain problem, and perhaps this is the reason for limited observed stable growth in this case. Two-dimensional plane stress solutions, as by Swedlow *et al.* (1966) and Hutchinson (1968), do reveal a highly strained region extending in front of the crack tip, so that growth effects may be anticipated from a proper analysis of this case.

E. ELASTIC-PLASTIC STRAIN CONCENTRATIONS AT SMOOTH-ENDED NOTCHES

Strain concentrations at smooth-ended notch tips serve to initiate cracking and subsequent extension. Elastic stress concentrations are discussed in Sect. III,G, and elastic-plastic problems are taken up here.

1. *Antiplane Strain*

Smooth-ended notches as well as cracks are more readily analyzed for antiplane strain loadings. In fact, as Neuber (1961) and Rice (1967b) have noted, the crack solution also generates the solution for a family of smooth-ended notches. The tractionfree notch surface boundary condition is that the stress vector $\tau = \sigma_{31}\mathbf{i}_1 + \sigma_{32}\mathbf{i}_2$ be tangent to the boundary, so that stress trajectories of the crack solution locate notch boundaries. Letting ϕ be the counterclockwise angle between the x_2 axis and the stress vector, trajectories are given by (Figs. 10 and 19a)

$$dx_1 + \tan \phi dx_2 = 0 \quad (290)$$

Recalling from Eqs. (195) that physical coordinates are expressed in terms of the principal shear strain γ and direction ϕ in the strain-hardening crack solution, this becomes a differential equation for γ as a function of ϕ along a trajectory, and, after employing the differential Eq. (196),

$$\frac{d\gamma}{d\phi} = \frac{\tau(\gamma) \frac{\partial^2 \psi(\gamma, \phi)}{\partial \gamma^2}}{\tau'(\gamma) \frac{\partial}{\partial \gamma} \left[\frac{1}{\gamma} \frac{\partial \psi(\gamma, \phi)}{\partial \phi} \right]} \quad (291)$$

Initial conditions may be written as $\gamma = \gamma_{\max}$ when $\phi = 0$, so that γ_{\max} is the maximum concentrated strain at the tip of a notch formed by a trajectory. Once γ is determined as a function of ϕ , physical coordinates of the notch boundary are given parametrically in terms of the shear angle by Eqs. (195). The resulting notch root radius of curvature, $r_t(0)$ in the notation of Fig. 10, is then

$$r_t(0) = \left[\frac{\partial^2 \psi}{\partial \gamma \partial \phi} - \frac{1}{\gamma} \frac{\partial \psi}{\partial \phi} \right]_{\phi=0, \gamma=\gamma_{\max}} \quad (292)$$

Employing the small-scale yielding crack solution of Eqs. (199), one finds that trajectories are governed by

$$d\gamma/d\phi = -\gamma \tan \phi, \quad \text{or} \quad \gamma = \gamma_{\max} \cos \phi \quad (293)$$

independently of the stress-strain relation, and that the notch root radius is

$$r_t(0) = \frac{K_{III}^2}{\pi \tau_0^2} \frac{\gamma_0 \tau_0}{\gamma_{\max} \tau(\gamma_{\max})} \quad (294)$$

Thus, for a given root radius, the product of stress and strain and the tip does not depend on the form of the stress-strain relation in the strain hardening range (Neuber, 1961). It must be remembered, however, that the result applies only for small-scale yielding and also that the detailed shape of the notches under consideration does depend on the stress-strain relation. For example, from Eqs. (201) and (293), stress trajectories of the small-scale yielding crack solution are parabolas for a linear elastic material, and are arcs of circles when passing through the yield zone of a perfectly plastic material, connecting to parabolas at the elastic-plastic boundary. A more complicated dependence between root radius and maximum strain results for large-scale yielding, and there is a strong dependence on the stress-strain relation.

2. Smooth-Ended Notches in Tension

Considering a flat-surfaced notch in a two-dimensional deformation field (Figs. 2 and 10) and employing a deformation plasticity theory so that an energy density may be defined, the path-independent integral J of Sect. II,E may be evaluated along the curved notch tip Γ_t

$$J = \int_{\Gamma_t} W dx_2 = \int_{-\pi/2}^{+\pi/2} W[\epsilon(\phi)] r_t(\phi) \cos \phi d\phi \quad (295)$$

Here, $\epsilon(\phi)$ is the surface extensional strain at a tangent angle ϕ in Fig. 10. Recall that J has its linear elastic value for small-scale yielding and also that narrow notches lead to expressions for J differing negligibly from those for cracks. We shall subsequently give approximations for the large-scale yielding range. Following Rice (1967a), approximations to the maximum concentrated strain are obtained by assuming a dependence of surface strain on ϕ , containing an unknown constant, and finding the constant through the above equality. Let us assume that surface strains on the notch tip are compatible with the homogeneous deformation of an imagined inclusion with zero elastic modulus, as in Sect. II,G. When the notch is narrow, only the ϵ_{22}^v component of the void strain is expected to be large and surface strains are then approximated as in Eq. (160). Thus

$$J \approx \int_{-\pi/2}^{+\pi/2} W(\epsilon_{\max} \cos^2 \phi) r_t(\phi) \cos \phi d\phi \quad (296)$$

For perfectly plastic behavior, surface stress-strain relations may be idealized to

$$\sigma = (\sigma_0/\epsilon_0) \epsilon \quad \text{for } 0 < \epsilon < \epsilon_0 \quad \text{and} \quad \sigma = \sigma_0 \quad \text{for } \epsilon > \epsilon_0 \quad (297)$$

with σ_0, ϵ_0 the yield stress and initial yield strain. Computing the associated energy density $W(\epsilon)$ and evaluating Eq. (296) for the special case of a semicircular tip, $r_t(\phi) = r_t = a$ constant, there results

$$\left(\frac{\epsilon_{\max}}{\epsilon_0}\right)^2 - \left(\frac{\epsilon_0}{\epsilon_{\max}}\right)^{1/2} \left(\frac{\epsilon_{\max}}{\epsilon_0} - 1\right)^{5/2} \approx \frac{15J}{8\sigma_0\epsilon_0 r_t} = \frac{15K_I^2}{8\sigma_0^2 r_t} \quad (298)$$

whenever the maximum strain computed by this formula exceeds the initial yield strain. The expression of J in terms of the stress-intensity factor applies for small-scale yielding in either plane stress or plane strain (with $\epsilon_0 = (1 - \nu^2)\sigma_0/E$ in the latter case). This result is shown by the solid curve in Fig. 31, with $\epsilon_{\max}/\epsilon_0$ plotted in terms of the square root of the terms on the right. Note that the dimensionless loading

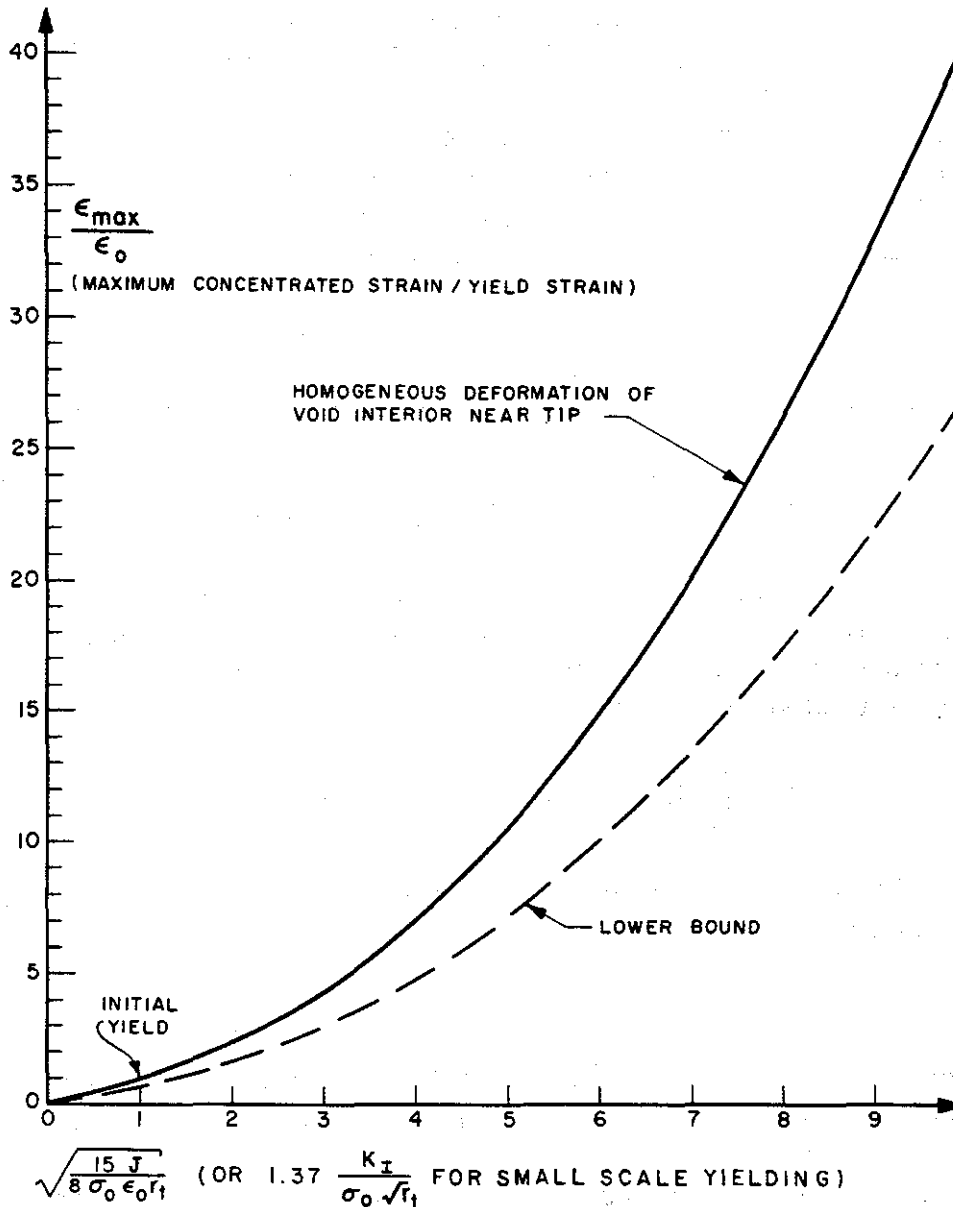


FIG. 31. Approximate estimate and lower bound to strain concentration at the tip of a flat surfaced notch with semicircular tip in an elastic perfectly plastic material (Rice, 1967a).

is linear with the applied load on the notched body for small-scale yielding, and that it has the value unity at initial yield, connecting with the linear elastic result of Eq. (161). Expanding the above equation in a series and neglecting all terms which vanish for $\epsilon_{\max}/\epsilon_0 \gg 1$, there results

$$\epsilon_{\max} \approx \frac{3}{4}\epsilon_0[1 + (J/\sigma_0\epsilon_0 r_t)]; \quad \epsilon_{\max} \approx \frac{3}{4}\epsilon_0[1 + (K_I^2/\sigma_0^2 r_t)] \quad (299)$$

This equation predicts a maximum concentrated strain 15% too high, in comparison to Eq. (298), at initial yield, but the discrepancy becomes imperceptible at loads greater than three times the initial yield load.

Strain hardening poses no fundamental difficulty with our present method; one simply enters the appropriate form of the energy density into Eq. (296). For example, with a power law stress-strain relation on the notch surface in the hardening range,

$$\sigma = \sigma_0(\epsilon/\epsilon_0)^N \quad \text{for } \epsilon > \epsilon_0 \quad (300)$$

the insertion of the associated energy density into Eq. (296) leads to

$$\epsilon_{\max} \approx \epsilon_0 \left[\frac{(N + \frac{1}{2})(N + \frac{3}{2}) \Gamma(N + \frac{1}{2})}{\Gamma(\frac{1}{2}) \Gamma(N + 1)} \frac{J}{\sigma_0 \epsilon_0 r_t} \right]^{1/(1+N)} \quad (301)$$

Here, terms of order $\sigma_0 \epsilon_0$ have been neglected in the energy density, as appropriate for $\epsilon_{\max}/\epsilon_0 \gg 1$. The equality between J and the integrated energy density also leads to a lower bound on the maximum concentrated strain at a flat surfaced notch tip

$$J = \int_{r_t} W dx_2 \leq W(\epsilon_{\max}) \int_{r_t} dx_2 = 2hW(\epsilon_{\max}) \quad (302)$$

where $2h$ is the notch thickness, as in Fig. 10. For a perfectly plastic material and semicircular root, this becomes

$$\epsilon_{\max} \geq \frac{1}{2}\epsilon_0 [1 + (J/\sigma_0 \epsilon_0 r_t)] \quad (303)$$

whenever the right side of the inequality exceeds ϵ_0 . This lower bound, along with the lower bound in the preyield region (Eq. (163)) is shown by the dashed curve in Fig. 31.

Perfectly plastic yielding in plane strain results in an exponential spiral slip line field ahead of a semicircular notch tip (much as in Fig. 24b), but this slip line field will not, in general, make up the entire plastic zone, nor will it necessarily encompass the entire semicircular tip. Stresses acting within the spiral region are

$$\sigma_{\theta\theta} = \sigma_{rr} + 2\tau_0 = 2\tau_0 [1 + \log(r/r_t)], \quad \sigma_{r\theta} = 0 \quad (304)$$

where r is measured from the notch tip center of curvature. The maximum normal stress which may be achieved is $(1 + \pi/2)(2\tau_0)$, and this results at $r = r_t e^{\pi/2}$ when the spiral region completely envelopes the semicircular tip, as in Fig. 24b. Equation (295) applies also to a

V notch with a semicircular tip, but now the maximum stress achievable in the spiral region is

$$\sigma_{\max} = (1 + \frac{1}{2}\pi - \alpha)(2\tau_0) \quad (305)$$

where 2α is the angle of the V notch.

3. Path-Independent Integral for Large-Scale Yielding

Many of the approximate or exact results on elastic-plastic problems have been given in terms of the path-independent energy integral J . Its value is known exactly only in the small-scale yielding limit (Sect. IV,A), in which case it has the same value as for the corresponding linear elastic problem. The interpretation of J in terms of an overall energy comparison for notches of neighboring size, as in Sect. II,E, suggests a method for approximating its value in the large-scale yielding range. For example, suppose a simplified elastic-plastic model is analyzed for yielding near a notch. Even though the solution may be wrong in detail, we may confidently expect the model to predict a gross feature of the solution such as the energy variation. Thus, large-scale yielding range estimates of J may be obtained from simplified models which can be analyzed, and then we may ignore the model and go on to use the approximate value of J in the various formulas of this and prior sections.

One such approximate estimate of J is obtainable from the perfectly plastic Dugdale-Barenblatt model. The crack opening displacement is given by Eq. (226) for the crack of length $2a$ in an infinite plane subjected to the remote tensile stress σ_∞ . But J is expressible directly in terms of the opening displacement, as in Eq. (219). Thus

$$J = \frac{(\kappa + 1) \sigma_0^2 a}{\pi G} \log \left[\sec \left(\frac{\pi \sigma_\infty}{2\sigma_0} \right) \right] \quad (306)$$

On the other hand, the linear elastic (or small-scale yielding) value of J for this configuration is

$$J_{\text{lin}} = \frac{(\kappa + 1)}{8G} K_I^2 = \frac{\pi(\kappa + 1) \sigma_\infty^2 a}{8G} \quad (307)$$

Thus

$$\frac{J}{J_{\text{lin}}} = \frac{2 \log[\sec(\pi\sigma_\infty/2\sigma_0)]}{(\pi\sigma_\infty/2\sigma_0)^2} \quad (308)$$

This ratio is shown as a function of the applied stress by the solid line in Fig. 32. Large-scale yielding estimates may also be based on the

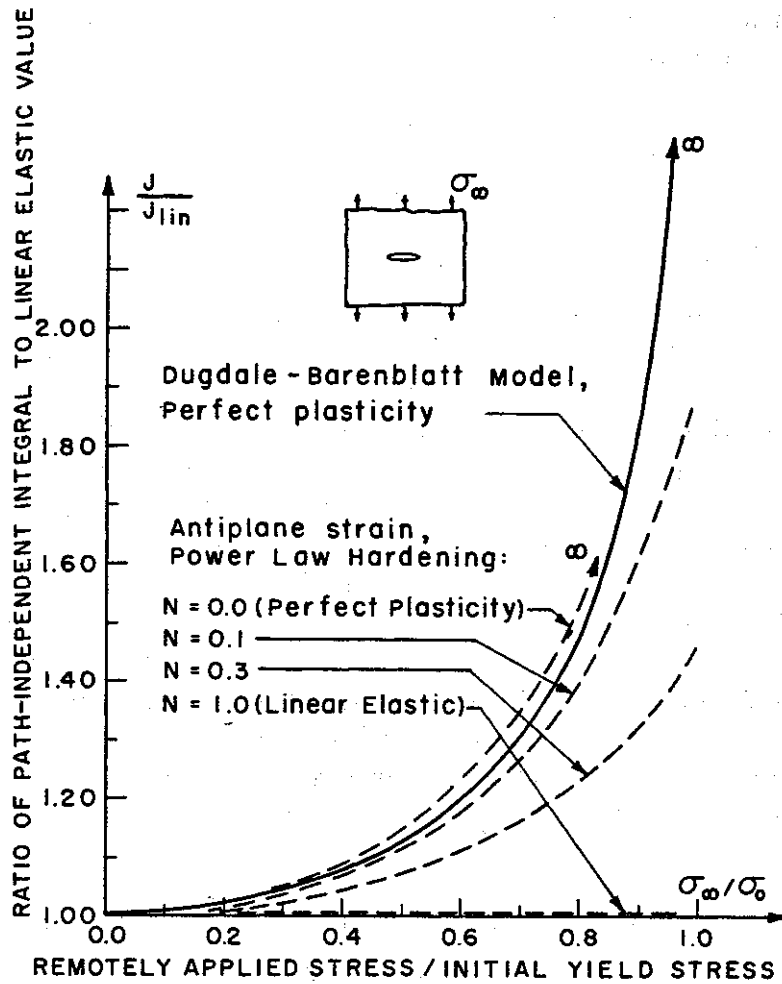


FIG. 32. The path-independent energy line integral differs significantly from its linear elastic value in the large-scale yielding range. Approximate estimates of the deviation may be obtained from simple models, as shown.

antiplane strain solutions. For this mode of deformation, Eq. (60) defining J becomes

$$J = \int_{\Gamma} \left\{ \left[\int_0^{\gamma} \tau(u) du \right] dx_2 - \gamma \tau(\gamma) \sin \phi [\cos \phi dx_1 + \sin \phi dx_2] \right\} \quad (309)$$

Here, the notation of the strain-hardening formulation in Sect. IV, B has been adopted; ϕ is the principal shear angle as measured counterclockwise from the x_2 direction. The path Γ may be chosen at will as any surrounding the crack tip. We take it to coincide with the elastic-plastic boundary. Since $\gamma = \gamma_0 = \text{constant}$ on Γ , the first term in the integrand is a constant times dx_2 , and thus contributes zero to the integral. Now x_1 and x_2 may be expressed parametrically in terms

of the shear angle from Eqs. (195), and the variable of integration may be chosen as ϕ , resulting in

$$J = \tau_0 \gamma_0 \int_{-\pi/2}^{+\pi/2} \sin \phi \left[\frac{1}{\gamma} \frac{\partial^2 \psi(\gamma, \phi)}{\partial \phi^2} + \frac{\partial \psi(\gamma, \phi)}{\partial \gamma} \right]_{\gamma=\gamma_0} d\phi \quad (310)$$

Substituting for ϕ from the series solution of Eqs. (212) and (213), one finds that only the first term of the series contributes as all other terms contain trigonometric functions orthogonal to $\sin \phi$, and

$$J = -\pi D_1 \left(2\gamma_0 \int_{\gamma_0}^{\infty} \frac{du}{u^2 \tau(u)} \right)^{-1} \quad (311)$$

D_1 (which is always negative) has been given in series form by Rice (1967c) for the crack of length $2a$ in an infinite plane subjected to a remote antiplane shear stress τ_∞ (or equivalently, the edge crack of length a). The result for J then becomes

$$J = J_{lin} \left\{ 1 + \frac{1}{2} C_1 s^2 + \frac{1}{4} C_1^2 s^4 + \frac{1}{8} \left(\frac{3}{4} C_2 + C_1^3 \right) s^6 + \frac{1}{16} \left(\frac{3}{2} C_2 C_1 + C_1^4 \right) s^8 + \frac{1}{32} \left(\frac{5}{4} C_3 + \frac{5}{4} C_2 C_1^2 + C_1^5 \right) s^{10} + \dots \right\} \quad (312)$$

where

$$J_{lin} = \frac{\pi \tau_\infty^2 a}{2G}, \quad s = \frac{\tau_\infty}{\tau_0}, \quad \text{and} \quad C_k = \frac{(2k-1) + f'_k(\gamma_0)}{(2k-1) - f'_k(\gamma_0)}$$

The functions $f_k(\gamma)$ are solutions to Eqs. (213). Resulting values of J/J_{lin} are shown by the dashed curves of Fig. 32 for the special case of power law hardening, with $N = 0$ (perfect plasticity), $N = 0.1$, $N = 0.3$, and $N = 1$ (linear elasticity, for which $C_k = 0$ and $J = J_{lin}$). Here the shear stress ratio τ_∞/τ_0 has been replaced by σ_∞/σ_0 , and computations were performed after adding four more terms to the above series, according to the recursive formulas of Rice (1967c), so that the error is order s^{20} . The perfectly plastic result appears not to differ significantly from the Dugdale result in tension. But a small amount of strain hardening ($N = 0.1$) greatly alters J near the general yielding level and removes the singularity at limit load in the perfectly plastic cases. Within an order of accuracy probably comparable to the difference between the Dugdale and antiplane perfect plasticity results, these curves (and similar results for other stress-strain relations and other crack configurations) may be employed to approximate J in the large-scale yielding range.

F. LIMIT ANALYSIS OF NOTCHED BODIES

Small-scale yielding near cracks and notches allows the simplicity of a one-parameter representation of local deformation fields. No similar single parameter exists in the large-scale yielding range for nonhardening materials. This is readily seen by a perusal of perfectly plastic limit load solutions for notched bodies as discussed by McClintock and Irwin (1965) and Drucker (1963). The governing theorems are discussed in Sect. II, D. Single edge notched and internally notched bodies in plane strain (Fig. 33) result in no hydrostatic stress elevation at limit load. Flow fields consisting of sliding off at 45° result in a net section stress of $2\tau_0$, the simple tension yield stress under plane strain conditions. Evidently, this stress field can be extended in the internal notch case in a manner which does not violate equilibrium or yield, and also in the single edge notch case with appropriate remote loadings, so that the actual net stress at limit load is $2\tau_0$.

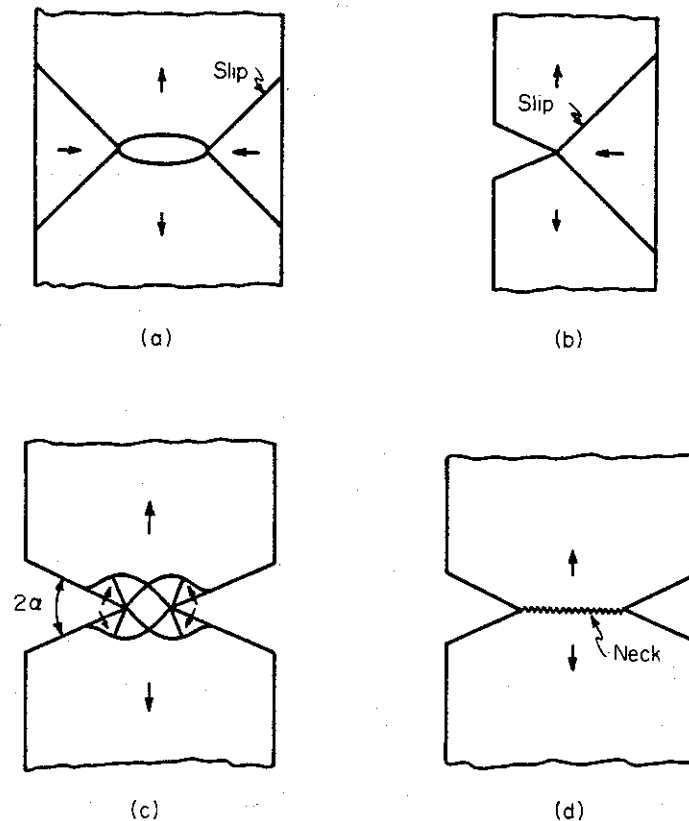


FIG. 33. Limit fields for notched bodies. Internal notch (a) and single edge notch (b) in plane strain or in plane stress of a Tresca material, $\sigma_{\text{net}} = 2\tau_0$. For Mises material in plane stress, $\sigma_{\text{net}} = \sqrt{3}\tau_0$ and flow field consists of local necks at $\pm 35^\circ$ with notch line. Deep double edge notches (c) in plane strain, $\sigma_{\text{net}} = (2 + \pi - 2\alpha)\tau_0$. Double edge notches (d) in plane stress, $\sigma_{\text{net}} = 2\tau_0$ for either Tresca or Mises material.

An entirely different field results for the double edge notch case. The flow field consisting of constant stress regions joined by centered fans leads to a net stress of $(2 + \pi - 2\alpha)\tau_0$, where 2α is the total angle of the notch. An equilibrium stress field may be found for sufficiently large ratios of notch depth to unnotched thickness, completing this solution. The great differences in local stress and strain state show that no single parameter can replace the stress-intensity factor to correlate fracture in the large-scale yielding range. The form of large-scale elastic-plastic yielding near a crack has been conjectured in Fig. 24a for situations before intersection of the boundary and a free surface or specimen centerline in the double edge notch case. For consistency with 45° slip in the single edge or internal notch cases, the initially vertical slip line would have a radius of curvature that decreased toward zero as the boundary approached the free surface. This means that unloading must occur at points near the tip as limit conditions are approached.

Plane stress conditions lead to no significant hydrostatic stress elevations. For example, the plane stress double edge notch specimen in Fig. 33 carries a net stress of $2\tau_0$ when a flow field involving through the thickness necking is assumed. This is only slightly above the uniaxial yield of $\sqrt{3}\tau_0$ for a Mises material, and is equal to the uniaxial yield for a Tresca material.

G. FRACTURE MECHANISMS IN DUCTILE MATERIALS

Thus far, we have dealt with the analysis of fracture at the usual continuum level. Excepting the case of elastic brittle fracture (Sect. III,E), specific fracture mechanisms have not yet been considered. We deal here with the analysis of some microstructural mechanisms of separation in ductile materials.

1. *Dislocation Pileups and Blocked Slip Bands*

The inhomogeneity of plastic flow at the dislocation level can result in severe stress concentrations even though macroscopic averages of stress over several dislocation arrays are limited to a value in the neighborhood of the yield stress or somewhat higher by geometric constraint and strain hardening. Several dislocation models for the nucleation of cracks are reviewed by Low (1963), who also cites evidence for plastic deformation as a precursor to fracture in even the most brittle of cleavage failures. Following Eshelby *et al.* (1951), we consider here the pileup of n edge dislocations on a common slip plane, the first dislocation being locked at a barrier, such as a grain boundary or hard

inclusion. Suppose the pileup is along the negative x_1 axis, with $x_1 = t_1, t_2, \dots, t_n$ denoting positions of the n cores, and that the locked dislocation is at the origin so that $t_1 = 0$. The array is subjected to a remote uniform shear stress $(\sigma_{12})_\infty = \tau_\infty$. The stress field of an isolated dislocation is given by the first of Eqs. (112), and, for plane strain conditions, the shear stress at points along the slip plane is

$$\sigma_{12}(t, 0) = \tau_\infty + \frac{Eb}{4\pi(1-\nu^2)} \sum_{i=1}^n \frac{1}{t-t_i} \quad (313)$$

Supposing that, for equilibrium, the shear stress (in addition to the symmetric self stress) on each dislocation is equal to a friction stress τ_0 , locations t_2, t_3, \dots, t_n of the $n-1$ free dislocations are given by

$$\tau_0 = \tau_\infty + \frac{Eb}{4\pi(1-\nu^2)} \sum_{\substack{i=1 \\ i \neq j}}^n \frac{1}{t_j - t_i}, \quad j = 2, 3, \dots, n \quad (314)$$

The stress on the locked dislocation at $t_1 = 0$ is found by a simple calculation

$$\begin{aligned} \tau_1 &= \tau_\infty - \frac{Eb}{4\pi(1-\nu^2)} \sum_{i=2}^n \frac{1}{t_i} \\ &= \tau_\infty - \frac{Eb}{4\pi(1-\nu^2)} \sum_{j=2}^n \sum_{\substack{i=1 \\ i \neq j}}^n \frac{1}{t_j - t_i} \\ &= \tau_\infty - (n-1)(\tau_0 - \tau_\infty) \end{aligned}$$

therefore

$$\tau_1 = \tau_0 + n(\tau_\infty - \tau_0) \quad (315)$$

so that the stress tending to move the locked dislocation is concentrated in proportion to the number of dislocations in the pileup. The direct solution of the equilibrium Eqs. (314) has been carried out by Eshelby *et al.* (1951) who also gave asymptotic results for large n .

Large n results may be obtained directly by introducing a continuous dislocation array and writing Eq. (314) as a singular integral equation with Cauchy kernel and solving according to the methods of Sect. II, C. It is simpler, however, to note that the continuous dislocation array may be represented as a crack subjected to inplane shear loadings. To conform with the notation of Sect. III, B on plane elastic crack problems, consider the pileup to extend from $-a$ to $+a$ on the x_1 axis. An applied shear stress $\sigma_{12} = \tau_\infty$ acts at infinity and a friction stress $\sigma_{12} = \tau_0$ acts along the slit. In addition to satisfying stress boundary

conditions and the condition of zero normal displacement discontinuity across the slit, the net Burgers vector of the slip band is specified as B . For example, $B = nb$ for the array of n dislocations considered above. Then the complex stress functions of Eqs. (21), (22), and (70) which solve the problem are given through a modification of Eq. (94) to account for the Burgers vector. There results

$$\phi'(z) = -\Omega'(z) = -\frac{i}{2} \left[(\tau_\infty - \tau_0) z + \frac{EB}{4\pi(1-\nu^2)} \right] (z^2 - a^2)^{-1/2} - \frac{i}{2} \tau_0 \quad (316)$$

Resulting stresses near the end of the pileup at $x_1 = a$ are the same as for mode II crack problems [Eqs. (80) and (81)] with

$$K_{II} = \left[(\tau_\infty - \tau_0) + \frac{EB}{4\pi(1-\nu^2)a} \right] (\pi a)^{1/2} \quad (317)$$

Not all the parameters entering this equation are independent. For the pileup of n dislocations considered above, the stress must be bounded at the far end $x_1 = -a$ in the continuous distribution representation. Thus

$$B = nb = \frac{4(1-\nu^2)}{E} (\tau_\infty - \tau_0) a, \quad \text{and} \quad K_{II} = 2(\tau_\infty - \tau_0)(\pi a)^{1/2} \quad (318)$$

Solving for the number of dislocations accompanying a pileup of total length $2a$ and inserting into Eq. (315), one may show that the stress on the locked dislocation is given by

$$\tau_1 b = (1-\nu^2) K_{II}^2 / E \quad (319)$$

It is interesting to note that the right-hand side is the energy release rate for the equivalent elastic crack problem.

Equations (316) and (317) also solve the problem of a slip band blocked at both ends with zero net Burgers vector

$$B = 0 \quad \text{and} \quad K_{II} = (\tau_\infty - \tau_0)(\pi a)^{1/2} \quad (320)$$

While the connection with a linear dislocation array is clear, these results may also be taken as a general model of stress concentration at the end of any inhomogeneous band of slip deformation, even though the geometry of participating dislocations is much more complicated than the simple linear array. Identifying the slip band length as proportional to a mean grain diameter d in polycrystalline materials, one is then led to Petch-type relations of the form

$$\tau_\infty = \tau_0 + (\text{constant}/d^{1/2}) \quad (321)$$

for either crack nucleation or continued slip in neighboring grains. Adopting the linear dislocation array viewpoint, Stroh (1957) has suggested a value of the constant descriptive of crack nucleation, basing his calculations on a Griffith-type energy balance. Although the concept of inhomogeneous plastic deformation on the microscale serving as a source of stress concentration is general, the specific type of analysis considered here is most appropriate for very low temperature cleavage initiated in the beginning stages of plastic deformation.

2. Ductile Void Growth and Coalescence

A common fracture mechanism in materials which do not cleave is the ductile growth and coalescence of holes, as shown by the studies of Gurland and Plateau (1963), Rogers (1960), and Puttick (1959). The early cracking of impurity inclusions can serve as the origin of these voids, but it is not known if all such voids originate from inclusions. Some understanding of the role of stress state in void growth is gained through the analysis of simple models. Following McClintock and Argon (1966), we consider here an infinitely long circular cylindrical hole of radius r_0 and with axis in the x_3 direction. The material is idealized as rigid-perfectly plastic and of the Mises type. A uniform strain rate $\dot{\epsilon}_{33}$ is imposed on the material and we seek an expression for the rate of hole growth \dot{r}_0 as a function of the current radius r_0 and the stress state at infinity. Introducing polar coordinates r, θ in the x_1x_2 plane and letting \dot{u}_r be the radial velocity, incompressibility requires that

$$(\partial \dot{u}_r / \partial r) + (\dot{u}_r / r) + \dot{\epsilon}_{33} = 0 \quad (322)$$

Thus, in terms of the rate of hole growth \dot{r}_0

$$\begin{aligned} u_r &= -\frac{1}{2}\dot{\epsilon}_{33} \left(r - \frac{r_0^2}{r} \right) + \dot{r}_0 \left(\frac{r_0}{r} \right) \\ \dot{\epsilon}_{rr} &= -\frac{1}{2}\dot{\epsilon}_{33} - \left(\frac{1}{2}\dot{\epsilon}_{33} + \frac{\dot{r}_0}{r_0} \right) \frac{r_0^2}{r^2} \\ \dot{\epsilon}_{\theta\theta} &= -\frac{1}{2}\dot{\epsilon}_{33} + \left(\frac{1}{2}\dot{\epsilon}_{33} + \frac{\dot{r}_0}{r_0} \right) \frac{r_0^2}{r^2} \\ \dot{\epsilon}_{r\theta} &= \dot{\epsilon}_{r3} = \dot{\epsilon}_{\theta3} = 0 \end{aligned} \quad (323)$$

The stress equilibrium equation for the radial direction is

$$\frac{\partial \sigma_{rr}}{\partial r} + \frac{\sigma_{rr} - \sigma_{\theta\theta}}{r} = 0 \quad (324)$$

and from the Mises flow rule (Sect. II,D)

$$\sigma_{rr} - \sigma_{\theta\theta} = s_{rr} - s_{\theta\theta} = \sqrt{2}\tau_0 \frac{\dot{\epsilon}_{rr} - \dot{\epsilon}_{\theta\theta}}{(\dot{\epsilon}_{ij}\dot{\epsilon}_{ij})^{1/2}} \quad (325)$$

where τ_0 is the yield stress in shear. Integrating the equilibrium equation from the hole boundary to infinity and letting $(\sigma_{rr})_\infty$ be the remotely applied stress in the radial direction,

$$(\sigma_{rr})_\infty = \sqrt{2}\tau_0 \int_{r_0}^{\infty} \frac{\dot{\epsilon}_{\theta\theta} - \dot{\epsilon}_{rr}}{(\dot{\epsilon}_{ij}\dot{\epsilon}_{ij})^{1/2}} dr \quad (326)$$

After substituting from the expressions for strain rates above and integrating, one obtains for the rate of growth

$$\dot{r}_0/r_0 = \frac{1}{2}\dot{\epsilon}_{33}\{\sqrt{3} \sinh[(\sigma_{rr})_\infty/\tau_0] - 1\} \quad (327)$$

The hyperbolic sine leads to an exponential amplification of the void strain rate \dot{r}_0/r_0 over the imposed strain rate $\dot{\epsilon}_{33}$ for large values of the remote stress. For example, taking $(\sigma_{rr})_\infty = (1 + \pi)\tau_0$ (the average principal stress directly ahead of a crack in plane strain, Sect. IV,C)

$$\dot{r}_0/r_0 = 26.6\dot{\epsilon}_{33} \quad (328)$$

which would suggest a very rapid enlargement of voids ahead of a crack.

Strain hardening undoubtedly has a strong influence in reducing growth under given stress ratios, as McClintock and Argon (1966) have suggested. At the same time, the hydrostatic-to-deviatoric stress ratio ahead of a crack increases rapidly with hardening (Rice and Rosengren, 1968), so a resolution of the effect of hardening in ductile crack extension requires more study. Blunting further complicates the situation, as the most highly strained region is also the region where geometry changes modify the stress state (Fig. 24b).

V. Recommended Research

As concerns static elasticity, two-dimensional plane problems appear to be well enough understood and standardized so as not to require a great deal of further research. Some studies on convergence and accuracy of boundary collocation (described in Sect. III,C) would, however, be useful, as this method appears to be the most versatile of approximate techniques. A more challenging class of problems includes cracks in thin-walled plate and shell structures, and three-dimensional problems such as the part-through crack in a pressure

vessel wall. Also of interest is a clarification of the actual three-dimensional stress state near a crack in a flat plate subjected to stretching or bending. A plasticity analysis would undoubtedly be more revealing, but such an elastic solution should aid in the interpretation of plane stress and plate bending solutions and should help in extrapolating fracture data from one configuration to others in brittle materials.

Dynamic elastic crack problems require further study. In particular, solutions for stress-wave-type loadings would be useful in the analysis of materials with a rate-dependent fracture toughness. Interactions of cracks with resonant vibrations of structures and dynamic amplification of stress concentrations also merit study, especially in relation to fatigue. Constant-velocity, running crack problems with rather special starting conditions have been analyzed (Sect. III,F), but more general problems involving acceleration from rest, and also arrest, should be attempted. Such solutions would enable a complete formulation of elastic brittle fracture and should also aid the interpretation of running crack results in other brittle materials.

Progress has been made in the understanding of contained plasticity, particularly as involves near crack tip plane strain fields and fully developed plane stress yielding of the Dugdale type, as discussed in Sect. IV,C. Still, no complete and nonapproximate plane strain solutions have been obtained. Also, as has been noted, finite geometry changes at the crack tip must be considered if an accurate description of local conditions is to be available for connection with studies on microstructural mechanisms. The three-dimensional character of "plane stress" yielding in plates poses one of the most important plasticity problems in need of resolution. These three-dimensional features must govern the variation in fracture toughness with sheet thickness and the fraction of shear lip appearing on the fractured surface; loss of transverse constraint, the changing mode of plastic flow from inplane to through-the-thickness slip, and possibilities for localized necking are all involved. Three-dimensional aspects might be responsible for localized Dugdale plane stress plastic zones in some materials and more diffuse patterns of flow in others, although differing yield conditions may also be involved. For example, the stress state in the Dugdale zone turns out to be equal biaxial tension, at least for small-scale yielding, as may be verified from the solutions of Sect. IV,C. A necking type normal displacement discontinuity is admissible with this stress state for a Tresca material, but not for a Mises material.

Stable crack extension preceding instability is to be expected from the incremental and path-dependent nature of plastic stress-strain relations. Such stable growth becomes particularly significant in the

plane stress range, and an analysis paralleling the work by McClintock on antiplane strain would be useful. An additional feature which must be considered here is the changing geometry of the fracture surface. Aside from perfectly plastic limit load calculations, little is known on strain concentrations at cracks or notches in the general yielding range. Such analysis is important for correlating small laboratory specimens with larger structures, since general yielding conditions will often prevail at fracture in the former case. Service failures in the tougher metals may also involve general yielding, and yielding near intersections or other structural discontinuities over regions large compared to flaw sizes is not uncommon.

Time dependence of inelastic behavior is an important feature which must be included in the analysis of fracture for a complete description of transitional and running crack behavior. Mild steel, for example, is known to allow very brittle crack propagation through strain rate elevation of the local flow stress so as to promote cleavage, particularly if plane strain constraint can be achieved. At the same time, localized heating results from plastic flow as near adiabatic conditions are approached at fast rates. An analysis of the combined role of these two features, and possibly inertial considerations, in determining minimum toughness levels for running cracks would be extremely valuable. This would allow determination of conditions for crack arrest, a perhaps more pertinent problem than that of initiation for highly rate-sensitive materials, in view of possibilities for initiation of a running crack in localized regions inadvertently embrittled through fabrication or welding (Mylonas, 1964).

Studies on microstructural mechanisms are necessary to provide fracture criteria for inclusion in continuum solutions. This is particularly so when no single parameter serves to characterize local deformations, as in the large-scale yielding range or when varying transverse constraint is involved, as in plane stress. These studies may concentrate on brittle mechanisms, such as cleavage microcrack initiation and joining, or more ductile mechanisms, such as void initiation and plastic enlargement. Ultimately, a fracture criterion in terms of local average stress and strain history over a small region with characteristic microstructural dimensions is desired. This approach presumes no significant coupling between separation mechanisms and continuum solutions, in the sense that fracture processes will not greatly alter predicted stress and strain fields in regions larger than the characteristic microstructural size. Exceptions will undoubtedly exist, and more complete descriptions of fracture with significant interactions between mechanisms and local deformation fields should be attempted.

VI. Summary

Section II begins with a review of topics in elasticity and plasticity, as well as associated mathematical methods, which are pertinent to later analyses of crack and notch problems. The last section of this part introduced the unifying theme of energy comparisons for neighboring geometries, and led to the path-independent energy line integral. This path independence, and sometimes the relation to energy rates, permitted a variety of subsequent results on notches in linear and nonlinear materials.

The basic results of linear elastic fracture mechanics are outlined in the first section of Section III. All crack problems lead to characteristic inverse square root stress singularities, and the load transmitted to the crack tip region may be conveniently characterized by an Irwin stress-intensity factor when inelastic behavior is confined to a small region near the crack tip. Presuming all other material and environmental variables held constant, low stress fracture behavior may then be correlated in terms of the stress-intensity factor. Some of the simpler two-dimensional elastic crack problems are solved and methods are presented for approximate analysis of the more complicated cases. These include the boundary collocation of stress functions expressed so as to automatically insure stressfree crack surfaces, approximate conformal transformations by polynomials or ratios of polynomials, and representation of cracks as continuous dislocation arrays with subsequent reduction from singular to regular integral equation.

The rate of equilibrium potential energy variation with respect to crack length is directly related to the stress-intensity factor(s). This permits compliance testing, and sometimes simple "strength of materials" style calculations, for determination of stress-intensity factors. Energy variation rates for narrow smooth-ended notches differ negligibly from those for cracks and may be related to surface stresses in a manner permitting approximate estimates of stress-concentration factors.

Two different approaches to elastic-brittle fracture are investigated and are seen to lead to identical predictions of equilibrium crack length and stability behavior. These include the Griffith energy balance and the Barenblatt-type cohesive forces theories. Characteristic dynamic stress singularities are established for constant velocity crack motion. These show the stress field bifurcation noted by Yoffé at speeds in the terminal range observed in brittle materials.

Plasticity effects in fracture are taken up in Section IV. Small-scale yielding notch and crack problems may be formulated in a boundary layer style involving an asymptotic approach to the characteristic

elastic singularity at large distances from the tip. Perfectly plastic and strain hardening crack solutions for the simpler antiplane mode are reviewed first. These shed little light on detailed strain distributions for tensile problems, but some important gross features do appear reasonably in accord with tensile behavior, as McClintock has emphasized. Perfectly plastic plane strain conditions lead to a large hydrostatic stress elevation ahead of a crack and to strain singularities above and below the tip but not directly ahead. Blunting of the tip by plastic deformation is required for large straining directly ahead of the tip, contrary to usual notions. Approximate estimates of opening displacement and plastic zone size are given through application of the energy line integral. Another application of the energy integral suggests a variation of stress times strain inversely proportional to distance from the crack tip, independently of the stress-strain relation. The form of near crack tip plane strain singularities is established for materials hardening according to a power law, and a rapid rise of stress triaxiality with hardening exponent results.

Fully developed plane stress conditions, involving through-the-thickness slip and possible necking, may be analyzed through a Dugdale-type model which envisions yielding confined to a narrow region ahead of crack. More diffuse patterns of plastic flow result from two-dimensional generalized plane stress formulations for Mises materials. One useful application of such simple plasticity models is in clarifying geometry-dependent transitions in fracture strength; plane strain constraint in cracked plates and accompanying stress elevations will be lost when plastic zone dimensions become comparable to or greater than thickness dimensions.

Plastic stress-strain relations are incremental in nature and path dependent. Thus, solutions for advancing cracks may differ significantly from those for stationary cracks. The effect is seen clearly in the antiplane case where continued crack advance is predicted under increasing load, and fracture appears as an instability in the process. It is shown that this instability behavior from McClintock's antiplane analysis can be formulated in terms of a universal resistance curve, much as proposed by Krafft and co-workers. Little progress has been made with analysis of elastic-plastic growth effects in tension; the form of plane strain singularities is established here, but practical problems involving stable growth appear limited to plane stress or mixed mode conditions, and are further complicated by a change in fracture geometry with complete or partial shear lips.

Plastic strain concentrations at smooth-ended notch tips are estimated through the path-independent energy line integral. The integral has

the same value as for linear elasticity when yielding is confined to a small region near a notch tip; its value in the large-scale yielding range may be estimated from simple models, and some examples are given. Perfectly plastic limit analyses indicate the loss of unique crack tip stress-and-strain distributions in the general yielding range, at least for lightly hardening materials. Hydrostatic stress elevations may persist to limit load in configurations such as deep double edge notches in plane strain; they are lost, in many cases, and the deformation field consists of sliding off in shear bands. This suggests that no single parameter can replace the stress-intensity factor as uniquely characterizing local conditions in the large-scale elastic-plastic and general yielding ranges. Specific fracture mechanisms must be considered. Brief treatments are given of mechanisms, including dislocation pileups and blocked slip bands as sources of microcracks, and the large plastic growth of voids. Hydrostatic stress elevation, as in plane strain, is seen to greatly accelerate growth in the latter case.

Some of the more important areas in need of further research include a clarification of three-dimensional features of near crack tip deformations and accompanying plane strain-plane stress transitions, an analysis of dynamic and running crack behavior in rate-sensitive materials, and the combined analysis of near crack tip deformation fields and microstructural separation mechanisms.

It has been learned, since completion of the manuscript, that Dr. J. D. Eshelby has previously discovered an energy line integral identical in special cases to the one introduced here. He refers to it as the energy-momentum tensor, and employs the integral to identify generalized forces on point singularities and inhomogeneities in elastic fields. The work is summarized in the interesting article, *The Continuum Theory of Lattice Defects* (in "Solid State Physics," Volume III, Academic Press, 1956).

Symbols

A	Area of integration	C	Closed curve in complex plane
a	Crack length or half length; ellipse or ellipsoid semi-major axis; point in complex plane	C_{ijkl}	Elastic moduli
		c	Intermediate axis of ellipsoid
		c_d	Dilatational wave speed
		c_s	Shear wave speed
b	Ellipse or ellipsoid semiminor axis; point in complex plane; closed curve in complex plane	E	Young's modulus
		F_i	Body force
		$F(\xi)$	Analytic function of dimensionless complex stress
b, b_i	Dislocation Burgers vector	$f(z)$	Analytic function of z

G	Shear modulus	u, u_i	Displacement
\mathcal{G}	Energy release rate	V	Volume of region; velocity of crack
$g(z)$	Analytic function of z	$W, W(\epsilon_{mn}), W(\epsilon)$	Strain energy density
Im	Imaginary part of	X_1	Coordinate with origin moving with crack tip
i	Unit imaginary number	$X(\gamma)$	Coordinate describing center of constant shear lines
i_j	Unit vector associated with direction j	x	Coordinate with origin moving with crack tip
J	Value of path-independent energy line integral	x_1, x_2, x_3	Cartesian coordinates
J_{lin}	Linear elastic value of J	y_a, y_b	Coordinates employed in dynamic crack solution
K_I, K_{II}, K_{III}	Stress-intensity factors	z	Complex variable $x_1 + ix_2$
K_D	Dynamic stress-intensity factor	$z_1(\xi)$	Conformal mapping function
L	Arc in complex plane	α_d, α_s	Functions of crack velocity and wave speeds
l	Crack length; change in crack length	Γ	Path surrounding notch tip in energy line integral J
N	Strain-hardening exponent	Γ_t	Curved tip of a flat surfaced notch
N_{ij}	Components of unit outward normal to yield surface in stress space	$\Gamma(\dots)$	Gamma function
n, n_i	Unit normal vector to line or surface	γ	Principal shear strain; Mises equivalent shear strain
P	Potential energy	γ, γ_{si}	Antiplane shear strain vector
$P(z)$	Polynomial in z	γ_0	Initial yield strain in shear
p	Mean normal stress	γ_f^p	Plastic shear strain at fracture
$p_i(\dots)$	Prescribed traction along crack surface	δ_{ij}	Kronecker delta
Q	Generalized force	δ_t	Crack opening displacement at tip
q	Generalized displacement	ϵ, ϵ_{ij}	Strain
R, R_0	Maximum plastic zone dimension	ϵ_{max}	Maximum strain at notch root
$R(\theta)$	Distance to elastic-plastic boundary	ϵ_0	Initial yield strain in tension
$R_0^f(l)$	Plastic zone size required for quasistatic crack extension l	θ	Polar coordinate
$R(\gamma)$	Coordinate giving radius of constant shear lines	κ	$3 - 4\nu$ for plane strain; $(3 - \nu)/(1 + \nu)$ for plane stress
Re	Real part of	λ	Proportionality parameter in perfectly plastic stress-strain increment relations
r	Polar coordinate	$\mu_i(\dots)$	Dislocation density for continuous distribution on a plane
\mathbf{r}	Position vector	ν	Poissons ratio
r_t	Notch root radius of curvature	ξ	Complex variable; dimensionless complex antiplane shear stress
$r_t(\phi)$	Radius of curvature along notch surface		
S	Surface of region; surface energy		
s	Dimensionless applied stress		
\mathbf{s}, s_{ij}	Deviatoric stress		
\mathbf{T}, T_i	Surface tractions	ρ	Mass density
t	Time; variable of integration	ρ_s	Characteristic microstructural dimension
U	Airy stress function		

σ, σ_{ij}	Stress	$\phi(z)$	Complex stress function in plane elasticity
σ_0	Yield stress in tension		
$\sigma(\delta)$	Restraining stress opposing separation of surfaces by distance δ	$\chi(z)$	Homogeneous solution to Hilbert arc equation
		Ψ	Shear wave function
τ	Principal shear stress; Mises equivalent shear stress	ψ	Potential function of anti-plane strains
τ_0	Yield stress in shear; friction stress	$\psi(z)$	Complex stress function in plane elasticity
τ_1	Shear stress on locked dislocation	$\Omega(z)$	$z\phi'(z) + \psi(z)$
		ω, ω_{ij}	Rotation
Φ	Dilatational wave function	$\omega(z)$	Complex stress function in antiplane elasticity
ϕ	Principal shear direction; tangent angle to notch surface		

ACKNOWLEDGMENTS

Conclusions presented in this chapter were reached in the course of research sponsored by the Advanced Research Projects Agency under Contract SD-86 with Brown University.

REFERENCES

- ASTM (1960). "Fracture Testing of High Strength Sheet Materials," Bulletin No. 243, pp. 29-40. ASTM, Philadelphia.
- Argyris, J. H. (1965). In "Matrix Methods in Structural Mechanics" (J. S. Przemieniecki, ed.), Technical Report No. AFFDL-TR-66-80. Air Force Flight Dynamics Laboratory, Wright-Patterson Air Base, Dayton, Ohio.
- Baker, B. R. (1962). *J. Appl. Mech.* **29**, 449.
- Barenblatt, G. I. (1962). *Advan. Appl. Mech.* **7**,
- Bilby, B. A., and Swinden, K. H. (1965). *Proc. Roy. Soc. (London) Ser. A* **285**, 23-33.
- Bilby, B. A., Cottrell, A. H., and Swinden, K. H. (1963). *Proc. Roy. Soc. (London) Ser. A* **272**, 304.
- Bishop, J. F. W., and Hill, R. (1951). *Phil. Mag.* **42**, 414-427.
- Bowie, O. L. (1956). "Analysis of an Infinite Plate Containing Radial Cracks Originating From the Boundary of an Internal Circular Hole." *J. Math. and Phys.* **35**.
- Bowie, O. L. (1964). *J. Appl. Mech.* **31**, 208.
- Bowie, O. L., and Neal, D. M. (1967). "The Effective Crack Length of an Edge Notch in a Semi-Infinite Sheet Under Tension." *Intern. J. Fracture Mech.* (To be published.)
- Broberg, K. B. (1960). *Arkiv Fysik* **18**, 159.
- Broek, D. (1967). "Conditions for Slow Crack Growth." *Intern. J. Fracture Mech.* (To be published.)
- Budiansky, B. (1959). *J. Appl. Mech.* **26**, 259-264.
- Bueckner, H. F. (1958). *Trans. ASME* **80**, 1225-1229.
- Bueckner, H. F. (1960). In "Boundary Value Problems in Differential Equations" (R. Langer, ed.), pp. 215-230. University of Wisconsin Press, Madison.
- Churchill, R. V. (1960). "Complex Variables and Applications." McGraw-Hill, New York.
- Cottrell, B. (1964). *J. Appl. Mech.* **31**, 12-16.
- Cottrell, A. H. (1953). "Dislocations and Plastic Flow in Crystals." Oxford (Clarendon) Press, Oxford.

- Craggs, J. W. (1960). *J. Mech. Phys. Solids* 8, 66-76.
- Drucker, D. C. (1951). In "Proceedings of the 1st National Congress for Applied Mechanics," pp. 487-491. ASME, New York.
- Drucker, D. C. (1960). In "Structural Mechanics: Proceedings of the 1st Symposium on Naval Structural Mechanics 1958" (J. N. Goodier and N. J. Hoff, eds.), pp. 407-455. Pergamon, New York.
- Drucker, D. C. (1963). In "Fracture of Solids" (D. C. Drucker and J. J. Gilman, eds.), pp. 3-50. Wiley, New York.
- Drucker, D. C. (1964). *J. Mecan.* 3, 235-249.
- Dugdale, D. S. (1960). *J. Mech. Phys. Solids* 8, 100-104.
- Eftis, J., and Krafft, J. M. (1965). *Trans. ASME Ser. D, J. Basic Eng.* 87, 257-263.
- Eshelby, J. D. (1957). *Proc. Roy. Soc. (London) Ser. A* 241, 376-396.
- Eshelby, J. D., Frank, F. C. and Nabarro, F. R. N. (1951). *Phil. Mag.* 7, 351.
- Goodier, J. N., and Field, F. A. (1963). In "Fracture of Solids" (D. C. Drucker and J. J. Gilman, eds.), pp. 103-118. Wiley, New York.
- Green, A. E., and Zerna, W. (1954). "Theoretical Elasticity." Oxford (Clarendon) Press, Oxford.
- Grief, R., and Sanders, J. L. (1965). *J. Appl. Mech.* 32, 59-66.
- Griffith, A. A. (1920). *Phil. Trans. Roy. Soc. London, Ser. A* 221, 163-198.
- Gross, B., and Srawley, J. E. (1965a). "Stress Intensity Factors for Single Edge Notch Specimens in Bending or Combined Bending and Tension," NASA TN D-2603.
- Gross, B., and Srawley, J. E. (1965b). "Stress Intensity Factors for Three Point Bend Specimens by Boundary Collocation," NASA TN D-3092.
- Gross, B., Srawley, J. E., and Brown, W. F. (1964). "Stress Intensity Factors for a Single Edge Notch Tensile Specimen by Boundary Collocation of a Stress Function," NASA TN D-2395.
- Gurland, J., and Plateau, J. (1963). *ASM Trans. Quart.* 56, 442-454.
- Hahn, G. T., and Rosenfield, A. R. (1966). "Experimental Determination of Plastic Constraint Ahead of a Sharp Crack under Plane Strain Conditions," Report No. SSC-180. Ship Structure Committee, Department of the Navy, Washington, D.C.
- Hill, R. (1950). "Mathematical Theory of Plasticity." Oxford (Clarendon Press), Oxford.
- Hult, J. A., and McClintock, F. A. (1956). In "Proceedings of the 9th International Congress of Applied Mechanics, Brussels," Vol. 8, pp. 51-58.
- Hutchinson, J. W. (1968). *J. Mech. Phys. Solids.* 16, 13-31.
- Ilyushin, A. A. (1961). *Appl. Math. Mech. (USSR)* 25, 503-507.
- Irwin, G. R. (1957). *J. Appl. Mech.* 24, 361-364.
- Irwin, G. R. (1958). In "Handbuch der Physik," Vol. 6, pp. 551-590. Springer, Berlin.
- Irwin, G. R. (1960). In "Structural Mechanics: Proceedings of the 1st Symposium on Naval Structural Mechanics, 1958" (J. N. Goodier and N. J. Hoff, eds.), pp. 557-591. Pergamon, New York.
- Irwin, G. R. (1962). *J. Appl. Mech.* 29, 651-654.
- Irwin, G. R., and Koskinen, M. F. (1963). *Trans. ASME* 85D, 593-594.
- Johnson, H. H., and Willner, A. M. (1965). *Appl. Mater. Res.*, January, 34-40.
- Kassir, M. K., and Sih, G. C. (1966). *J. Appl. Mech.* 33, 601-611.
- Keer, L. M., and Mura, T. (1966). In "Proceedings of the 1st International Conference on Fracture, Sendai, 1965" (T. Yokobori, T. Kawasaki, and J. L. Swedlow, eds.), Vol. I, 99-116. Japanese Society for Strength and Fracture of Materials, Tokyo.
- Knowles, J. K., and Wang, N. M. (1960). "On the Bending of an Elastic Plate Containing a Crack," Caltech GALCIT SM 60-11. California Institute of Technology, Pasadena, Calif.

- Kobayashi, A. S., Cherepy, R. B., and Kinsel, W. C. (1964). *Trans. ASME Ser. D, J. Basic Eng.* **86**, 681-684.
- Koiter, W. T. (1959). *Ingenieur Archiv* **28**, 168-172.
- Koiter, W. T. (1965). *J. Appl. Mech.* **32**, 237. (Discussion of "Rectangular Tensile Sheet With Symmetric Edge Cracks" by O. L. Bowie.)
- Kolsky, H. (1953). "Stress Waves in Solids." Oxford (Clarendon) Press, Oxford.
- Krafft, J. M., Sullivan, A. M., and Boyle, R. W. (1961). "Effect of Dimensions on Fast Fracture Instability of Notched Sheets." In "Proceedings of the Crack Propagation Symposium." Cranfield College of Aeronautics, Cranfield, England.
- Low, J. R. (1963). *Progr. Mater. Sci.* **12** (1), 1-96.
- McClintock, F. A. (1958). *J. Appl. Mech.* **25**, 582.
- McClintock, F. A. (1965). "Effect of Root Radius, Stress, Crack Growth, and Rate on Fracture Instability." *Proc. Roy. Soc. (London) Ser. A* **285**.
- McClintock, F. A., and Argon, A. S. (1966). "Mechanical Behavior of Materials." Addison-Wesley, Reading, Massachusetts.
- McClintock, F. A., and Irwin, G. R. (1965). In "Fracture Toughness Testing and Its Applications." STP 381, pp. 84-113. ASTM, Philadelphia.
- Muskhelishvili, N. I. (1953a). "Singular Integral Equations" (J. R. M. Radok, trans.). Noordhoff, Groningen, Holland.
- Muskhelishvili, N. I. (1953b). "Some Basic Problems in the Mathematical Theory of Elasticity" (J. R. M. Radok, trans.). Noordhoff, Groningen, Holland.
- Mylonas, C. (1964). In "Proceedings of the 11th International Congress on Applied Mechanics, Munich," pp. 652-660.
- Neuber, H. (1937). "Kerbspannungslehre." Springer, Berlin.
- Neuber, H. (1961). *J. Appl. Mech.* **28**, 544-550.
- Orowan, E. (1952). In "Fatigue and Fracture of Metals" (W.M. Murray, ed.), pp. 139-167. Wiley, New York.
- Paris, P. C. (1964). In "Fatigue—An Interdisciplinary Approach" (J. J. Burke, N. L. Reed, and V. Weiss, eds.), pp. 107-132. Syracuse University Press, Syracuse, New York.
- Paris, P. C., and Sih, G. C. (1965). In "Fracture Toughness Testing and Its Applications," STP 381, pp. 30-76. ASTM, Philadelphia.
- Peterson, R. E. (1953). "Stress Concentration Design Factors." Wiley, New York.
- Prager, W., and Hodge, P. G. (1951). "Theory of Perfectly Plastic Solids." Wiley, New York.
- Puttick, K. E. (1959). *Phil. Mag.* **4**, 964-969.
- Rice, J. R. (1966a). In "Proceedings of the 1st International Conference on Fracture, Sendai, 1965" (T. Yokobori, T. Kawasaki, and J. L. Swedlow, eds.), Vol. I, pp. 283-308. Japanese Society for Strength and Fracture of Materials, Tokyo.
- Rice, J. R. (1966b). *Intern. J. Fracture Mech.* **2**, 426-447.
- Rice, J. R. (1967a). "A Path Independent Integral and the Approximate Analysis of Strain Concentration by Notches and Cracks," *J. Appl. Mech.* (To be published.)
- Rice, J. R. (1967b). "The Mechanics of Crack Tip Deformation and Extension by Fatigue." In "Symposium on Fatigue Crack Growth," STP 415. ASTM, Philadelphia.
- Rice, J. R. (1967c). *J. Appl. Mech.* **34**, 287-298.
- Rice, J. R., and Drucker, D. C. (1967). *Intern. J. Fracture Mech.* **3** (1), 19-28.
- Rice, J. R., and Rosengren, G. F. (1968). *J. Mech. Phys. Solids.* **16**, 1-12.
- Rice, J. R., and Sih, G. C. (1965). *J. Appl. Mech.* **32**, 418-423.
- Rogers, H. C. (1960). *Trans. Met. Soc. AIME* **218**, 498-506.
- Rosenfield, A. R., Dai, P. K., and Hahn, G. T. (1966). In "Proceedings of the 1st International Conference on Fracture, Sendai, 1965" (T. Yokobori, T. Kawasaki, and

- J. L. Swedlow, eds.), Vol. I, pp. 223-257. Japanese Society for Strength and Fracture of Materials, Tokyo.
- Sadowsky, M. A., and Sternberg, E. (1949). *J. Appl. Mech.* **16**, 149-157.
- Sanders, J. L. (1960). *J. Appl. Mech.* **27**, 352.
- Savin, G. (1961). "Stress Concentration around Holes." Pergamon, New York.
- Schardin, H. (1959). In "Fracture" (B. L. Averbach, D. K. Felbeck, G. T. Hahn, and D. A. Thomas, eds.), pp. 297-330. Wiley, New York.
- Sih, G. C., Paris, P. C., and Erdogan, F. (1962). *J. Appl. Mech.* **29**, 306-312.
- Smith, E. (1966). In "Proceedings of the 1st International on Fracture, Sendai, 1965" (T. Yokobori, T. Kawasaki, and J. L. Swedlow, eds.), Vol. I, pp. 133-152, Japanese Society for Strength and Fracture of Materials, Tokyo.
- Sneddon, I. N. (1946). *Proc. Roy. Soc. (London) Ser. A* **187**, 229-260.
- Sokolnikoff, I. S. (1956). "Mathematical Theory of Elasticity." McGraw-Hill, New York.
- Srawley, J. E., and Brown, W. F. (1965). In "Fracture Toughness Testing and Its Applications," STP 381, pp. 133-193. ASTM, Philadelphia.
- Srawley, J. E., Jones, M. H., and Gross, B. (1964). "Experimental Determination of the Dependence of Crack Extension Force on Crack Length for a Single Edge-Notch Tension Specimen," NASA TN D-2396.
- Stroh, A. N. (1957). *Advan. Phys.* **6**, 418. *Adv. Phys.* **6**, 418.
- Swedlow, J. L., Yang, A. H., and Williams, M. L. (1966). In "Proceedings of the 1st International Conference on Fracture, Sendai, 1965" (T. Yokobori, T. Kawasaki, and J. L. Swedlow, eds.), Vol. I, pp. 259-282. Japanese Society for Strength and Fracture of Materials, Tokyo.
- van Bueren, H. G. (1960). "Imperfections in Crystals." North-Holland, Amsterdam.
- Wang, A. J. (1953). *Quart. Appl. Math.* **11**, 427-438.
- Williams, M. L. (1957). *J. Appl. Mech.* **24**, 109.
- Williams, M. L. (1961). *J. Appl. Mech.* **28**, 78.
- Williams, M. L. (1962). *Trans. ASME Ser. D, J. Basic Eng.* **84**, 542-546. (Discussion of "An Experimental Investigation of the Crack Tip Stress Intensity Factor in Plates Under Cylindrical Bending" by F. Erdogan, O. Tuncel, and P. C. Paris.)
- Yoffé, E. H. (1951). *Phil. Mag.* **42**, 739.